The Pennsylvania State University

The Graduate School

THERAPEUTIC GRADE RNA PURIFICATION BY ULTRAFILTRATION

A Dissertation in

Chemical Engineering

by

Jesus Ivan Manzano Garcia

Submitted in Partial Fulfillment
of the Requirements
for the Degree of

Doctor of Philosophy

August 2020

The dissertation of Jesus Ivan Manzano Garcia was reviewed and approved by the following:

Andrew Zydney
Bayard D. Kunkle Chair and Professor of Chemical Engineering
Dissertation Advisor
Chair of Committee

Themis Matsoukas
Professor of Chemical Engineering

Hee Jeung Oh
Assistant Professor of Chemical Engineering

William Hancock
Chair of Intercollege Graduate Program and Professor of Bioengineering

Phillip Salvage
Walter L. Robb Family Chair
Head of the Department

ABSTRACT

Recent advances in the use of nucleic acids (NA) for therapeutic applications, including vaccines, gene therapies, and more recently gene editing, have created a need for the development of appropriate separation processes for the large-scale isolation and purification of these biomolecules. One attractive potential method for NA purification is ultrafiltration using semipermeable membranes both for removal of large molecular weight species (with the RNA collected in the permeate) and for RNA concentration or buffer exchange (with the RNA collected in the retentate). The objective of this dissertation was to evaluate the factors controlling the transport of NA through semipermeable ultrafiltration membranes and to explore the development of membrane-based processes for the purification of therapeutic grade DNA and RNA-based therapeutics.

Experimental data were obtained for RNA transmission through a series of composite regenerated cellulose and polyethersulfone ultrafiltration membranes with different molecular weight cutoffs. Initial studies were performed using dilute solutions of Torula yeast RNA with a range of RNA size and conformation. The data showed significant RNA adsorption to the composite regenerated cellulose membrane; this effect was not seen with the polyethersulfone membranes due to electrostatic repulsion between the negatively-charged RNA and the negatively-charged membrane. Subsequent studies examined the effects of RNA size and tertiary structure using RNA with nucleotide sequences that give rise to specific structural motifs. The hairpin RNA had much higher transmission than the corresponding linear RNA with no Watson-Crick pairing. RNA transmission increased at high NaCl concentrations and in the presence of urea, particularly for the linear RNA.

Ribonucleoprotein (RNP) complexes formed from a single guide RNA and the Cas9 protein can be used for CRISPR-based gene editing. Experiments performed with the guide RNA

and Cas9 alone were used to identify filtration conditions that could provide high selectivity for the removal of excess guide RNA from the RNP. Actual separations were performed using a diafiltration process, providing greater than 90% yield of the desired RNP whith significant removal of the free RNA. These studies also demonstrated the importance of shear-induced aggregation of the Cas9, which led to significant fouling that could complicate the application of this technology for large-scale purification of these RNP products.

Experimental studies were performed to evaluate the effects of polyamines (multivalent cations) and membrane orientation on the ultrafiltration of different DNA isoforms. The addition of small quantities of spermine had a very strong effect on DNA transmission, with the sieving coefficient of the supercoiled plasmid decreasing by more than an order of magnitude upon addition of only micromolar levels due to reduction in elongational flexibility of the DNA. A comparable change in DNA transmission required >20X of the amount of trivalent spermidine. The polyamines significantly increased the selectivity for the separation of DNA from a model protein, but they were unable to provide a significant increase in the selectivity for separating DNA isoforms.

Membranes with gradients in pore size can potentially be used to pre-condition (or pre-stretch) the plasmid into an extended conformation, increasing DNA transmission and reducing membrane fouling. We evaluated the potential of using hollow fiber membranes in the reverse orientation for the separation of the linear and supercoiled isoforms. The supercoiled isoform was selectively retained within the microporous support structure at low filtrate flux but could then be recovered by increasing the flux to increase the elongation of the DNA.

Overall, the results presented in this dissertation provide important new insights into the factors controlling the ultrafiltration behavior of nucleic acids while providing a framework for the design and application use of this unit operation for the purification of RNA and DNA-based therapeutics.

TABLE OF CONTENTS

LIST OF FIGURES

LIST OF TABLES

ACKNOWLEDGEMENTS

First and foremost, I would like to express my greatest admiration and gratitude to my advisor, Dr. Andrew Zydney, whom provided guidance throughout my dissertation and research experience. I could not have imagined having a better advisor and mentor for my Ph.D study. Besides my advisor, I would like to thank the rest of my thesis committee: Dr. Themis Matsoukas, Dr. Hee Jeung Oh and Dr. William Hancock, for their encouragement, insightful comments, and hard questions.

This work was made possible by many hardworking undergraduate students that participated in different projects some as volunteers or NSF-REU recipients. Many thanks to Colton Lagerman, Tara Malone, Tim Roehm, Priscilla Maldonado, Ian Li, Carlos DaSilva, Neil Butler and Matt Csordas. Dr. Howard Salis and Grace Vezeau for their support and assistance in the design and synthesis of the RNA molecules. Financial support was provided by the NSF-CBET Grant 1505592 and the membranes donated by MilliporeSigma. Disclaimer: The findings and conclusions in this thesis do not necessarily reflect the view of NSF.

I thank my fellow labmates at Zydney's lab; Dr. Mahsa Hadidi, Dr. Ying Li, and Dr. Ehsan Espah who welcomed me into the lab and help me getting ensconced and trained. Dr. Parinaz Emami, and Dr. Zhao Li, that accompanied me in enduring many of the challenges of graduate school. Dr. Fatemeh Fallabijan, Dr. Youngbin Baek, Chris Yehl, Mario Jabra, Negin Negati, Neil Taylor, Kait Brickey, Matt Billups, Mirko Minervini, Vikram Sundar, Joshua Peles and Dr. Seon Yeop Jung for making life in lab a fun adventure and pleasant experience.

To my friends at Penn State, Dr. Tyler Culp, Dr. Megan Farrell and Daniel Cetnar for their exceptional friendship, all the joys and wonderful times we passed together. You have become part of my family.

Last but not the least, I would like to thank my family: Cecilia, Ana†, Gaby, Marisa and Enrique for their love, care and guidance. To my parents: Jesus and Olivia I thank you deeply. To my wife Luisana, whose selfless love and support accompany me everyday pushing me to succeed and always pursue my best self. To my son Santiago, you have been the bravest of us all, thank you and wish you all the best in your future endeavors.

Chapter 1

Introduction

The central dogma of molecular biology (Figure 1-1) explains the mechanism of protein production from DNA inside *cellular factories*. Specific sequences of DNA in the genome are copied by enzymes (RNA polymerase) into corresponding single stranded RNA molecules (messenger RNA, mRNA); this process is known as *transcription*. These mRNA molecules serve as direct templates for the production of functional proteins. Special ribonucleoprotein complexes known as ribosomes read the message encoded in mRNA and synthesize specific polypeptides / proteins from the constituent amino acids in a process called *translation*. The amino acid sequence determines how a protein folds and gives it a distinctive form (structure) and chemistry (functionality).

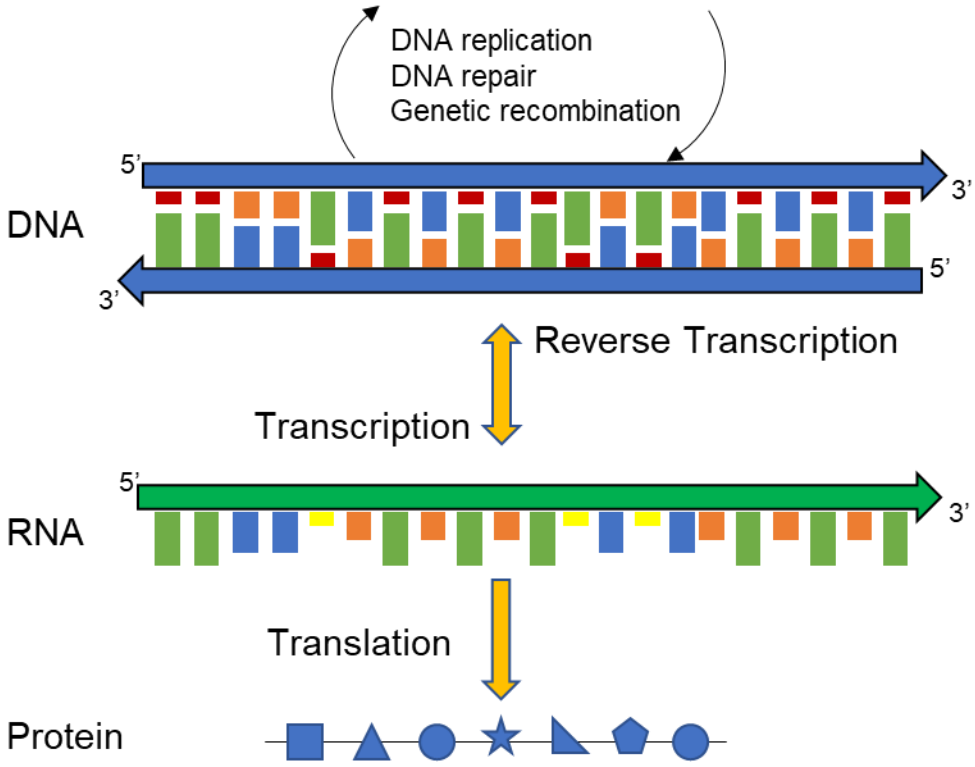

Figure **1-1**: Central dogma of molecular biology for the production of proteins from DNA. Adapted from Alberts et al. (2002)

The processes involved in transcription and translation are repeated thousands of times every second in human cells, making it prone to errors. Many times, misreads and / or typos in the code can occur, although most of these events do not compromise the functionality of the final protein. However, there are instances where just a single letter difference in the genome leads to the creation of toxic proteins, as in the case of prion diseases (Mastrianni 2010), or inactive / defective proteins. For example, the lack of a specific protein due to a missing or defective DNA is the cause of diseases like hemophilia (Hoyer 1994) and various muscular atrophies and dystrophies (Straub and Campbell 1997; Grohmann et al. 2001; Emery 2002; Lunn and Wang 2008).

In some instances, genetic disorders are caused by mutations that are inherited from the parents, like sickle cell disease (Ashley-Koch, Yang, and Olney 2000; Booth, Inusa, and Obaro 2010; Rees, Williams, and Gladwin 2010) or rare inherited blindness (Sohocki et al. 2000). Many other diseases are caused by acquired mutations in a gene (monogenic) or group of genes (multifactorial genetic disorder) that occur during a person's life. Such mutations are not inherited from a parent but occur either randomly or due to some environmental exposure as is the case in many cancers. The U.S. National Institute of Health (NIH, US) enlists 50 genetic, orphan and rare diseases that are currently being investigated by scientists in the National Human Genome Research Institute, and more than 1300 genetic diseases are reported in the NIH Genetics Home Reference website. *https://www.genome.gov/For-Patients-and-Families/Genetic-Disorders* ; https://ghr.nlm.nih.gov/ *both accessed April 1st, 2020.*

1.1 Gene therapies and nucleic acids-based vaccines

As our knowledge of the mechanisms involved in cellular protein synthesis increases, and we better understand how mistakes in the coding occur and cause multiple diseases and disorders, medical treatment has evolved from a symptomatic perspective to the analysis and solution of the root cause of disease. One of the first approaches researchers followed is the introduction of missing genes, and the replacement or override of defective ones. This is achieved by the *in vivo* insertion of a DNA vector that contains the expression code for inducing the correct cellular protein expression. The year 2019 saw the first gene therapy approved against Spinal Muscular Dystrophy in infant patients under the age of two. Zolgensma® is an AAV agent that provides the code for SMN-1 (Survival Motor Neuron 1) gene (Stevens et al. 2020). The absence of the SMN-1, which produces the largest portion of the SMN protein is the root cause for SMD (Mercuri et al. 2018). Several applications are still in development for the use of DNA based therapies as prophylactics and immunotherapy against cancer or autoimmune diseases (Liu 2003; Lopes, Vandermeulen, and Préat 2019). The Introductions in the doctoral theses by David R. Latulippe (2010), Ehsan Espah Borujeni (2015) and Ying Li (2017) provide a broad discussion regarding the advantages and disadvantages of different approaches for the therapeutic usage of DNA molecules. The current discussion is thus focused on the state of the art for RNA as a therapeutic molecule and current approaches for the purification of RNA.

1.2 Nucleic Acids vaccines

Most vaccines against viral diseases are made from viruses grown in a variety of cell lines typically mammalian cells or chicken eggs. It is an extensive process, that can take months to generate the killed or inactivated viruses that will ultimately form the vaccine. In addition to the

long processing times involved in the development of traditional vaccines, which are a particular concern during epidemics and pandemic events, there are biosafety issues involving the manufacture of large quantities of viruses (Merten 2002).

This has generated significant interest in DNA vaccines. In contrast to viruses, plasmid DNA can be produced in microbial hosts, and there is no possibility of disease transmission since the DNA only codes for a small sub-set of the viral proteins. Advances in delivery strategies over the last decade have overcome initial concerns with low antibody induction generated with the first wave of plasmid DNA vaccines (Ferraro et al. 2011b). The use of adjuvants with DNA vaccines has improved the immune response induced by the vaccine alone (Tang and Pietersz 2009), making it an attractive alternative against infections. Veterinary applications have already benefitted from these advances, with the first ever DNA vaccine approved for the treatment of equine West Nile Virus (Ledgerwood et al. 2011). However, despite all of these advantages, no DNA vaccines have been successfully commercialized for human use.

More recently, RNA vaccines have become a new alternative to conventional vaccination (Geall, Mandl, and Ulmer 2013). Here, an RNA molecule, typically synthesized *in vitro* from a DNA template, is injected to the body and enters the cells providing the coding for the production of specific antigens associated with the target infectious organism. These antigens, which are present on surface of the cells associated with the diseases, can trigger an immune response that can provide long-term protection against subsequent infection.

Nucleic acid-based immunization is a safer process since no viral material is needed to produce the desired immunity against infection. Although, the virus is needed to identify the key antigenic proteins and construct the corresponding gene sequence, this would involve very low quantities of virus and none of the actual virus would be administered to patients. Another potential advantage of nucleic acid based vaccines is the greater flexibility and improved economics associated with the biomanufacturing of these nucleotides. It is anticipated that the production

processes for both DNA and RNA based vaccines could be scaled more easily, with much greater standardization as part of a platform process.

1.3 RNA as a therapeutic tool

Nowadays we understand that RNA is more than a simple intermediary between DNA and proteins during protein synthesis. RNA is a dynamic molecule that regulates gene functions in all living organisms. The discovery of RNA interference (RNAi) for gene silencing by Andrew Fire and Craig Mello (Fire et al. 1998) earned the 2006 Nobel Prize in Physiology or Medicine, reigniting interest in RNA-based therapies. Certain cancers, inherited disorders, and other pathologies are directly associated with the overexpression of normal genes. RNA interference (RNAi) presents a new approach for treatment of these diseases by degradation of specific RNA, leading to knockdown of the genetic pathway.

RNAi is a natural process in living organisms used to regulate gene expression. It starts when exogenously introduced double stranded RNA (dsRNA, approx. 100 nucleotides) is processed by the endoribonuclease Dicer into small RNA duplexes (about 21 - 25 nucleotides) with a 3' two nucleotides overhang. These small RNAs interact with RISC (RNA induced silencing complex) where the endonuclease Argonaute 2 (AGO2) is activated and cleaves the passenger strand (sense strand), while the antisense strand remains attached to RISC guiding it to the target mRNA (Lam et al. 2015). Specific domains in the RISC accommodate siRNA, leaving 10 – 12 bases (seed region) open for complementary binding with the target mRNA. Once mRNA is attached to the siRNA, the PIWI domain in AGO2 starts to cleave the mRNA by RNAse H (Gavrilov and Saltzman 2012). The siRNA-RISC complex remains active for weeks, allowing it to target multiple mRNAs and knock down genes in slowly dividing or non-dividing cells for longer periods of time (Wittrup and Lieberman 2015).

In addition to RNA interference, microRNA silencing can also be used to block the translation of specific mRNA into proteins. During microRNA (miRNA) based silencing, primiRNAs (precursors of miRNA) are generated in the nucleus and cut by an RNAse (Drosha) to form a hairpin structured short RNA molecule (approximate 80 nucleotides). Once in the cytoplasm, the hairpin is removed by an endoribonuclease (Dicer) giving a molecule with two complementary sequences (19 – 25 nucleotides/each) similar to siRNA that attaches to RISC (Gavrilov and Saltzman 2012). Unlike siRNA, miRNA is only partially complementary to mRNA. Binding usually occurs at 2 – 7 nucleotides (Seed) of the miRNA 5' end and the 3' UTR region of the target mRNA (Lam et al. 2015), although in some cases a more complementary base pairing can occur triggering mRNA cleavage. Most of the time, gene silencing is caused by translational repression and mRNA degradation by deadenylation, decapping or exonuclease action (Huntzinger and Izaurralde 2011).

Since miRNA is only partially complementary to mRNA, it can target hundreds of mRNAs by inhibiting their translation. This feature may represent a challenge for therapeutic purposes due to potential for off-target knockouts, but it also represents an opportunity for treatment of multigenic pathologies (a single miRNA could potentially inhibit a whole family of mRNAs) (Mack 2007). The majority of clinical trials are currently focused on the use of siRNA due to its high specificity and reduced off target effects. However, Lam et al. (2015) predict an increase in miRNA studies in the coming years due to its ability to target many related mRNAs working together in cellular pathways.

Zhang et al. (2007) have shown that miRNA plays an important role in cancer development, either by the deletion or overexpression of certain miRNAs that regulate the expression of growth factors and other cellular pathways. These abnormal miRNA levels can be used as diagnostic tools for the detection of certain types of cancers. In addition, synthetic miRNA can be introduced to the organism to act as therapeutic molecules by miRNA inhibition (also known

as miRNA reduction) and miRNA replacement. In the first instance, complementary miRNAs are introduced into the organism in order to bind to other miRNA, preventing them from targeting mRNAs that otherwise would trigger tumor expression (Childs-Disney and Disney 2015). Replacement of miRNA consists in the reincorporation of miRNA that was deleted or is currently being underexpressed. These molecules downregulate mRNAs, restoring cellular pathways and providing a desired therapeutic response (Kong et al. 2012; Mack 2007).

While there are different strategies to regulate protein synthesis and gene knockdown in living organisms, the idea that siRNAs can be used to suppress any disease-causing gene, through the appropriate design of a complementary sequence to the target mRNA, makes it extremely attractive for therapeutic purposes. The main drawback with this therapeutic approach is in finding an efficient delivery mechanism of the desired molecule to target a specific system. Different strategies have been followed to overcome these obstacles such as chemical modification, packaging in lipids or nanoparticles, and targeting easily accessible organs such as skin, eyes and mucous. (Wittrup and Lieberman 2015). For example, Alnylam's RNA-based treatment for Transthyretin (TTR) mediated amyloidosis successfully delivered RNA packaged in lipoproteins, which protected the molecules until they reached the liver, activating the defective gene.

RNA can also be used for immunization against infectious disease, similar to the application of plasmid DNA vaccines. One of the advantages of using RNA in place of DNA is that the DNA construct must include sequences that allow the DNA to be replicated in the microbial host in addition to promoters that are functional in the patient. Thus, DNA vaccines are many times larger than RNA vaccines. However, in order to produce an effective immune response, high doses of RNA are required which increases the cost of the vaccine and has caused some companies to lose interest in these technologies. Thus, there is a need to design more cost-effective processes that guarantee the integrity of the RNA molecule while achieving the quality and purity of the final therapeutic required by the regulatory agencies.

1.4 RNA purification

As RNA establishes itself as a new class of therapeutic product, there will be an increase in the number of structural, biophysical and biomedical studies, as well as a growing need for the development and scale-up of purification and isolation processes. One attractive potential method for RNA purification is ultrafiltration using semipermeable membranes. However, there are still considerable uncertainties regarding the key factors governing the ultrafiltration behavior of these ribonucleic acids.

RNA is similar in nature to DNA. They are both constructed of the same building blocks, nucleotides, with uracil (in RNA) replacing thymine (in DNA). They both share a negative charge due to the phosphate groups along their backbones. However, RNA is typically present as a single stranded molecule, whereas DNA typically appears as double stranded. Size is also a key difference; RNA of interest for the pharmaceutical industry is relatively short in size ranging from a few tens to hundreds of nucleotides. Therapeutic DNA, the other hand, typically contains thousands of base pairs. RNA is a highly dynamic molecule, with an ability to display different structures due to intramolecular interactions. However, this high interactivity makes RNA more susceptible to degradation (Arraiano et al. 2010).

Laboratory scale methods for RNA purification such as aqueous two-phase extraction and or gel electrophoresis are typically difficult if not impossible to employ for large-scale commercial separations. Instead, large scale purification of RNA has been successfully performed using a variety of chromatography resins, including both ion exchange (Shanagar 2005; Easton, Shibata, and Lukavsky 2010; Noll et al. 2011) and affinity (Srisawat and Engelke 2002; Martins, Queiroz, and Sousa 2010, 2012; Martins et al. 2012) resins. However, chromatographic separations, especially affinity-based resins, can be expensive and difficult to implement at very large scale.

Ultrafiltration has the potential to play a major role in RNA processing, both for removal of large molecular weight species (with the RNA collected in the permeate) and for RNA concentration or buffer exchange (with the RNA collected in the retentate). Previous studies (Eon-Duval et al. 2003; Nunes et al. 2012, 2014; Manzano et al. 2015) have demonstrated the potential of using tangential flow filtration (TFF) for RNA removal during pDNA processes, but most of these data were obtained with crude RNA mixtures containing RNA with a range of size and structure. New studies are needed to evaluate the potential of using membrane filtration for the purification of RNA-based therapeutic products. Potential advantages of ultrafiltration over other classical downstream operations include cost, linear scaling, and no need for harsh chemicals.

1.5 Dissertation objectives and outline

Given the increased interest in the use of nucleic acids as therapeutic molecules, there is a growing need to generate large quantities of high purity DNA and RNA. Membrane processes have a great potential as unit operations for the large-scale purification of both therapeutic DNA and RNA.

The overall objectives of this dissertation are:

i. Develop a quantitative understanding of the behavior of RNA during ultrafiltration including identification of the key factors governing RNA ultrafiltration.
ii. Determining the role of nucleic acid structure and flexibility in the ultrafiltration behavior of nucleic acids.
iii. Explore potential opportunities for enhanced resolution in nucleic acid separations through the use of small molecule excipients; e.g. polyamines, denaturants, and sodium chloride.

iv. Develop appropriate membrane separation processes for the purification of functional nucleic acid-based therapeutics.

Chapter 2 describes the materials and experimental methods used throughout the different chapters of this dissertation. Additional details that were unique to particular studies are provided at the beginning of each chapter. Detailed protocols for novel experimental approaches are available in the appendices of this dissertation.

Chapter 3 evaluates RNA transmission through a series of composite regenerated cellulose and polyethersulfone ultrafiltration membranes with different molecular weight cutoffs. Results with dilute RNA solutions were strongly influenced by RNA adsorption to the composite regenerated cellulose membrane; this effect was not seen with the polyethersulfone membranes. Data for the polyethersulfone membranes were analyzed using the concentration polarization model, which describes the effects of bulk mass transfer on RNA transmission, in combination with available hydrodynamic models for membrane transport. The results provide important insights into the factors controlling RNA transmission and the potential for using ultrafiltration for the purification of nucleic acid therapeutics.

Chapter 4 assesses the effects of RNA size and tertiary structure on the ultrafiltration behavior over a range of solution conditions (e.g., added salt and urea). Transmission of a hairpin RNA with 70 nucleotides was much greater than that of a linear RNA having the same number of nucleotides, consistent with the smaller size as determined by dynamic light scattering and native gel electrophoresis. RNA transmission increased at high NaCl concentrations and in the presence of urea, particularly for the linear RNA. These results provide new insights into RNA ultrafiltration as well as a framework for the application of ultrafiltration for the purification of RNA therapeutics.

Chapter 5 presents ultrafiltration as a potentially attractive separation process for the purification of a functional ribonucleoprotein complex from free unbound RNA. Similar to the

behavior presented in Chapter 4, RNA transmission increases upon addition of NaCl, providing an attractive opportunity for the separation of the aforementioned molecules. Ultrafiltration data using a variety of membranes with different chemistries and molecular weight cutoffs provide insights into the fouling phenomenon. Shear stress generated by the stirring element in the ultrafiltration device was found to cause protein aggregation that complicates separation as well as affecting the quality of the desired product. Early identification of the challenges presented in this ultrafiltration operation allowed us to design suitable membrane processes for the purification of ribonucleoprotein complexes from free unbound RNA. The robustness of this type of membrane separation provides a framework for the design of similar systems where free RNA is seen as an impurity.

Chapter 6 is an investigation of the effects of polyamines on the ultrafiltration of plasmid DNA. Data were obtained using a wide range of spermine and spermidine concentrations to evaluate DNA transmission through polyethersulfone ultrafiltration membranes. Spermine has a very strong effect on DNA transmission, with the sieving coefficient of the supercoiled plasmid decreasing by more than an order of magnitude upon addition of small quantities of spermine. A comparable change in DNA transmission required 20 times more of the trivalent spermidine. The polyamines were able to significantly increase the selectivity of the separation between DNA and a model protein, but they were unable to provide a significant increase in the selectivity for separating DNA isoforms under the conditions examined in this thesis. The results do demonstrate that both spermine and spermidine can be used to control the extent of DNA transmission / purification during ultrafiltration.

Chapter 7 evaluates the possibility of using non-conventional configurations of commercially available membrane ultrafiltration devices. Ultrafiltration experiments were performed using a reverse orientation in which the DNA solution is fed from the support layer side (bottom) towards the selective membrane skin. This configuration causes elongation of the plasmid

DNA even at very low filtrate fluxes. This work showed that it is possible to exploit differences in elongational flexibility of the different naturally occurring plasmid isoforms for enhanced resolution by relatively small pore size membranes.

Chapter 8 summarizes the major conclusions from this dissertation and presents a series of recommendations for future work. These proposed studies should provide the underlying fundamental insights into the factors controlling nucleic acid ultrafiltration that are required for the successful development of membrane-based processes for the large-scale purification of these increasingly important biotherapeutics.

Chapter 2

Materials and methods

This chapter describes the materials, equipment, and experimental methods used throughout the different chapters of this thesis. Additional details on the specifics of these protocols can be found in the appendices of the dissertation.

2.1 RNA extract and synthetic oligonucleotides

Ribonucleic acids from Torula yeast were obtained from Sigma Aldrich (St Louis, MO). The Torula yeast RNA has a wide range of RNA size and morphology, typical of what might be encountered in the lysate obtained from a specific host organism. The Torula yeast RNA was dissolved in Tris-EDTA (TE) Buffer at pH 7.5, which was obtained by 100-fold dilution of a concentrated stock solution (Sigma Aldrich) with ultrapure water.

RNA molecules with five well-defined sequences (Table 2-1) were synthesized from their respective DNA template (IDT Technologies, San Jose, CA) as described subsequently. Linear-20 and Linear-70 were designed to have minimal internal nucleotide pairing, while Hairpin-70 was designed to have a fully complementary 33-base pair hairpin closed by a tetraloop (consisting of the bases AAUA). Eba39c was developed by inserting the 86 nucleotide-long Eba aptamer domain from the *Erysipelotrichaceae bacterium* NiCo riboswitch within the interior of a 151 nucleotide sequence containing additional structural elements (Furukawa et al. 2015). The analysis of the internal nucleotide pairing is discussed further below. The specific sequences and physical properties of the RNA constructs used in this study are summarized in Table 2-1.

Table **2-1**: Sequence, number of nucleotides, and molecular weight for synthetic RNA.

Name	Number of Nucleotides	MW (kDa)	RNA sequence without T7 promoter
Linear-20	24	7.162	5' - GCACCUCCAAUCACUCACCAACUU - 3'
Linear-70	70	20.951	5' - CCUCCAAUCAGCCCUCCUCACCAACUUAACCUCCUC ACUCACCAACUUAACUCACCAACUUAACCUCCAA - 3'
Hairpin-70	70	21.574	5' - GGCGUUAGGGCUGAUCGUAUCGUAAUCGUAGCCAA UAGGCUACGAUUACGAUACGAUCAGCCCUAACGCC - 3'
sgRNA	124	40.086	5' - GGUACUAAAUAUACAAUCCCUUGUUUUAGAGCUAGA AAUAGCAAGUUAAAAUAAGGCUAGUCCGUUAUCAACUU GAAAAAGUGGCACAAAAGCCAGUCUGGAAACAGGCUGG CUUUUUUUUGCG - 3'
Eba39c	237	73.443	5' - GGAUUAUGCGGUGACCAAGACGUGACAUCGAACUGA GCAGGCAAUGACCAGAGCGGUCAUGCAGCCGGGCUGCG AAAGCGGCAACAGAUGAUUACACGCACAUCUGUGGGACA GUUCAGGUCAUCUAAAUGCCGGUUGUUAUCGACAUCCGG AGAUACCAGCAUCGUCUUGAUGCCCUUGGCAGCUCCGGG CAUUCCUCGCAGGCGCUGGCUAAAAAAAAAAAAAAAAA AAAAAAAA - 3'

Figure 2-1 shows the expected structures of the RNA sequences predicted using RNAfold (http://rna.tbi.univie.ac.at/cgi-bin/RNAWebSuite/RNAfold.cgi) based on minimization of the free energy (Lorenz et al. 2011). These structure predictions assume an aqueous salt solution (1 M NaCl, 20 mM sodium cacodylate, and 0.5 mM Na2EDTA, pH 7.0) at a temperature of 37 °C. Since the experimental studies were performed at room temperature, we also examined the predicted structures at 25 °C. There were no structural differences between the ensembles predicted at 25 and

37 °C except for a small 2% shift with Eba39c. The calculated minimum free energies for Linear-20 and Linear-70 were 0 kcal/mol compared to the reference state, indicating a fully unfolded structural ensemble. In contrast, the algorithm predicts that Hairpin-70 forms a single full RNA duplex with free energy of the thermodynamic ensemble equal to −66 kcal/mol. sgRNA and Eba39c are predicted to have multiple structural motifs, including cloverleafs and hairpins, with an overall minimum free energy of −42 and −78 kcal/mol, respectively.

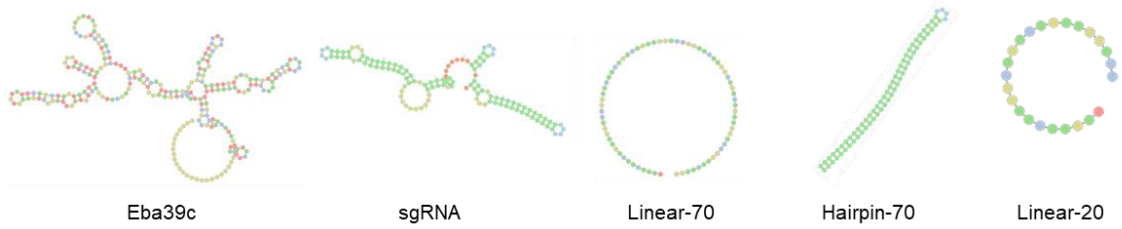

Figure **2-1**: Predicted RNA secondary structure based on minimum free energy using RNAfold webserver

2.1.1 RNA synthesis and purification

DNA templates for each RNA sequence consisted of the T7 promoter sequence, a guanosine nucleoside to promote efficient initiation of transcription, and the appropriate DNA sequence. All DNA was ordered from IDT. Oligo annealing was used to assemble the DNA template for Linear-20, while PCR was used for Linear-70 and Hairpin-70. The DNA templates for Eba39c and sgRNA were prepared from a gBlock fragment and amplified by PCR. T7 RNA polymerase was used for *in vitro* RNA synthesis using the T7 HiScribe Kit (New England Biolabs, Ipswich, MA). Synthesized RNA was purified using phenol:chloroform extraction (Chomczynski and Sacchi 1987, 2006). A detailed protocol for RNA synthesis can be found in *Appendix A.*

2.1.2 RNA characterization

The integrity and purity of the RNA was examined by agarose gel electrophoresis using a 3% agarose TAE (Tris-Acetate-EDTA) gel. 100 ng of RNA in Tris Buffer were loaded into the wells of a 3% agarose gel (Omnipur, EMD Millipore, Billerica, MA) in Tris-Acetate-EDTA buffer (Growcells, Irvine, CA). Samples were run at a constant voltage of 70 V for 1.5 h. GelStar™ (Lonza, Allendale, NJ) nucleic acid stain was used for visualization under blue light.

The RNA concentrations of all stock solutions were determined by UV-vis absorbance at 260 nm using a NanoDrop 1000 Spectrophotometer (Thermo Scientific, Carslbad, CA). All stock solutions were stored at -80°C until needed for filtration experiments and/or further characterization.

2.1.3 RNA quantitation

RNA concentrations in dilute samples (<10 µg/mL) were evaluated by fluorescence intensity, using two different assays from Invitrogen (Carlsbad, CA). The first assay, with an effective concentration range of 0.02 – 0.5 µg/mL, involved mixing 100 µL of RNA with Quant-iT RiboGreen fluorescent dye (cat# R11490) in a 96-well Infinity M2000 microplate reader (Tecan, Hombrechtikon, CH). Samples were mixed on an orbital shaking microplate for 180 s at 25 °C. Fluorescence intensity was measured at an emission wavelength of 485 nm after excitation at 535 nm. Actual RNA concentrations were determined from appropriate calibration curves constructed from the UV absorbance or fluorescence intensity obtained with solutions of known RNA concentration.

A second fluorescence-based assay was used for the quantitation of more concentrated samples ranging from 0.5 – 10 µg/mL. RNA Assay kit (cat# Q10213) was used for concentrations

>0.5 µg/mL. Standards and samples (20 µL volume) were loaded to a 96 well black microplate and mixed with 200 µL of 1X Quant-it BR solution. Fluorescence intensity was evaluated using a Tecan microplate reader at 644/673 nm excitation/emission wavelengths.

2.2 Plasmid DNA

Experiments involving the ultrafiltration of plasmid DNA were conducted using two different size plasmids: gWIZ-GFP a 5,757 bp plasmid that contains the reporter gene for green fluorescent protein (GFP) and pMDY a 9,801 bp plasmid including a 6,840 bp insert of the mouse dystrophin cDNA. Both plasmids are constructed from the pBluescript® II KS+ plasmid vector and are typical of the plasmid size used in gene therapy applications. DNA stock solutions were obtained as the supercoiled isoform from Aldevron (Fargo, ND) in 10 mM Tris 1 mM EDTA, pH 7.5 (TE) buffer. Figure 2-2 shows the vector maps for the gWIZ-GFP (left panel) and the pMDY (right panel) (Latulippe 2010).

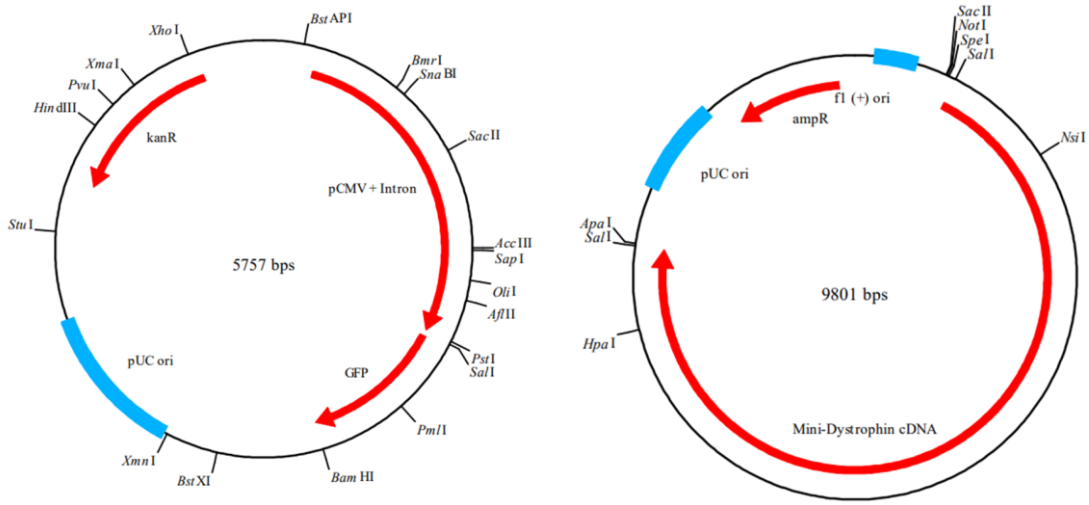

Figure **2-2**: Vector map for the 5.7 kbp gWIZ-GFP (left) and 9.8 kbp pMDY (right) plasmids (adapted from Latulippe, 2010).

2.2.1 Enzymatic digestion of pDNA

Linear and open circular isoforms were prepared by enzymatic digestion of the supercoiled plasmid by appropriate restriction enzymes (New England Biolabs, Ipswich, MA) that recognize a single nucleotide sequence in the DNA. The linear isoform was obtained by double stranded cleavage, whereas the open circular only required a single strand cleave. 25 – 100 µg of supercoiled plasmid were incubated with the appropriate restriction enzyme (Table 2-2) at 37 °C for 3 h. Upon completion of the reaction, samples were purified from the enzymes, salts, and other reaction impurities using the QIAQuick PCR purification kit (Qiagen, Germantown, MD) following the manufacturer's instructions (except for the use of TE buffer in the final elution step).

Table **2-2**: Enzymatic digestion enzymes for pDNA linear and open circular isoforms

Plasmid DNA	Restriction Enzyme	U/µg of pDNA
gWIZ-GFP (Linear)	PaeR7I	1
gWIZ-GFP (Open circular)	Nb.BtsI	2
pMDY (Linear)	KpnI	1 – 2
pMDY (Open circular)	Nt.AlwI	1 – 2

2.2.2 pDNA quantitation

Concentrations of stock pDNA solutions were obtained using a Nanodrop spectrophotometer. Diluted samples were quantified by fluorescence intensity using the PicoGreen assay (Invitrogen, Carlsbad, CA). In this case, 70 µL of DNA sample were mixed with an equal amount of PicoGreen dye (cat# P11496) working solution (200-fold dilution) and loaded in a 96-well Tecan microplate reader (Hombrechtikon, CH). Samples were mixed on an orbital shaking microplate for 180 s at 36 °C. Fluorescence intensity was measured at an emission wavelength of 485 nm after excitation at 535 nm. Actual pDNA concentrations were determined from appropriate calibration curves constructed from the fluorescence intensity obtained with solutions of known pDNA concentration for each of the different isoforms.

2.3 CRISPR associated protein 9 (Cas9)

S. pyogenes Cas9 protein with a 6-His tag was produced in *E. coli* NiCo21 (DE3) cells transformed with the pET-28a-Cas9-Cys plasmid. Cells were grown in a 5 L Sartorius Biostat® B bioreactor at 37 °C in the CSL Behring Fermentation Facility at Penn State. Once an optical density (OD600) value of 0.6-0.8 was achieved, protein expression was induced by addition of 0.2 mM isopropyl β-D-1-thiogalactopyranoside (IPTG) at a reduced temperature of 18 °C. Cells were harvested after overnight induction (12 -16 h) and lysed using a Microfluidics M-110EH-30 microfluidizer at 25000 psi (172 MPa). Lysates were centrifuged at 22000 x g in a Sharples T-1-P tube bowl centrifuge. When not processed immediately, clarified lysates were flash frozen and stored at -80 °C until further purification. Anders and Jinek (Anders and Jinek 2014) showed that clarified lysates, stored under these conditions, are stable for months.

2.3.1 Cas9 purification

Clarified lysates containing the Cas9 protein were purified using nickel affinity chromatography using an AKTA pure FPLC system at a linear velocity of 65 cm/min. A 5 ml HisPur™ Ni-NTA (Thermo Fisher, Carlsbad, CA) column was equilibrated with 3 - 5 column volumes (CV) of 20 mM Tris + 300 mM NaCl at pH 8.0. After equilibration, 30 mL of clarified lysate was injected onto the column using a super loop. Impurities were removed by washing with 5 CV of equilibration buffer + 10 mM imidazole. Elution was achieved using 2 CV of 20 mM Tris + 300 mM NaCl + 250 mM imidazole at pH 8.0. The column was then flushed with 3 CV of elution buffer, washed with DI water, and stored in 30% ethanol at 4°C between uses.

Fractions containing the Cas9 protein were concentrated using Amicon ultraspin concentrators with 100 kDa membranes (Millipore Sigma, Billerica, MA). Imidazole was removed using a 10 kDa Slide-A-Lyzer™ dialysis cassette (Thermo Fisher, Carlsbad, CA) with 20 mM Tris + 300 mM NaCl as the dialysate solution. The dialysate was stored at 4 °C for ultrafiltration experiments. Note Cas9 samples were stored at 4 °C because samples stored at <0 °C precipitated upon warming.

2.3.2 Cas9 quantitation

The concentration of the Cas9 protein was evaluated by a modified Bradford colorimetric assay (Ernst and Zor, 2010; Zor and Selinger, 1996). 100 µL samples and standards were loaded on 96-well clear microplates and incubated with 150 µL of Bradford reagent (Bio-Rad, Hercules, CA) for 15 min at 25 °C. Absorbance was measured at 590 and 450 nm using a Tecan microplate reader, with actual concentrations determined from appropriate calibration curves.

2.4 Ultrafiltration

Ultrafiltration experiments were performed in an Amicon 8010 stirred cell (MilliporeSigma, Billerica, MA) connected to an external solution reservoir pressurized with compressed air. The base of the stirred cell holds a filter disk with diameter of 2.5 cm and effective filtration area of 4.1 cm^2. The system was stirred at 730 rpm using a 17 mm stir bar. All experiments were conducted at room temperature (20 – 24 ºC). Ultracel® composite regenerated cellulose and Biomax® polyethersulfone membranes with different nominal molecular weight cutoffs (MWCO) were provided by MilliporeSigma (Billerica, MA). These membranes are widely used in bioprocessing applications (van Reis and Zydney 2001).

The stirred cell and solution reservoir were initially filled with 10 mM Tris buffer at pH 7.5, with the hydraulic permeability evaluated from data for the filtrate flux (J_v) as a function of the transmembrane pressure (using ΔP between 6 and 90 kPa):

$$L_p = \frac{\mu J_v}{\Delta P} \tag{2-1}$$

where μ is the solution viscosity. Table 2-3 provides a summary of the measured permeability for the different molecular weight cutoff membranes used in this study. The approximate pore sizes for these membranes were evaluated from the measured hydraulic permeability using the Hagen-Poiseuille equation (Latulippe, Ager, and Zydney 2007):

$$r_p = \left(\frac{8\delta_m L_p}{\varepsilon}\right)^{1/2} \tag{2-2}$$

with the membrane thickness (δ_m) estimated as 1.0 μm and the membrane porosity (ε) estimated as 0.5 based on previous results (Hadidi, Buckley, and Zydney 2015). The calculated values of the pore radius (last column in Table 2-3) range from 4.6 nm for the Biomax 50 to 9.7 nm for the Biomax 300 kDa membrane.

Table **2-3**. Permeability and effective pore radius of the different molecular weight cutoff Ultracel and Biomax membranes.

Membrane	L_p (10^{12} m)	r_p (10^9 m)
Biomax 50	1.3 ± 0.1	4.6
Biomax 100	2.1 ± 0.2	5.8
Ultracel 100	2.7 ± 0.2	6.6
Biomax 300	5.9 ± 0.8	9.7

The stirred cell and solution reservoir were then emptied and re-filled with the desired feed solution. Experiments were performed at room temperature over a wide range of filtrate flux by adjusting the air pressurization. The system was allowed to stabilize at each pressure, with sufficient filtrate obtained to wash out the dead volume beneath the membrane. Samples were then obtained from the filtrate, with a retentate sample obtained periodically (by opening the stirred cell). All samples were stored at 4 ºC until analysis.

When noted, filtration experiments were conducted by connecting a peristaltic pump on the permeate side to maintain a constant filtrate flux. In this case, the permeate line was purged with a minimum of 2 ml to wash out the dead volume beneath the membrane. Samples were handled identically to those in the constant pressure experiments.

2.4.1 Concentration polarization analysis

Previous studies of protein ultrafiltration have demonstrated the effects of concentration polarization on the observed sieving coefficient, equal to the solute concentration in the permeate divided by that in the bulk (feed) solution. This includes work by Pujar and Zydney (1994) on the sieving coefficients for bovine serum albumin through polyethersulfone membranes and by Molek and Zydney (2007) on the transmission of α-lactalbumin through regenerated cellulose membranes. We analyzed the increase in RNA transmission with increasing filtrate flux using the concentration polarization model, which accounts for the effects associated with the accumulation of retained RNA at the upstream surface of the membrane (Zydney 1997):

$$S_o = \frac{S_a}{(1 - S_a)exp(-J_v/k_m) + S_a} \tag{2-3}$$

where k_m is the bulk mass transfer coefficient and S_a is the actual sieving coefficient, defined as the ratio of the RNA concentration in the permeate (C_p) to that at the upstream surface of the membrane (C_w). Equation (2-3) can be rearranged in a linearized form as:

$$ln\left[\frac{1}{S_o} - 1\right] = ln\left[\frac{1}{S_a} - 1\right] - \frac{J_v}{k_m} \tag{2-4}$$

Chapter 3

RNA transmission through ultrafiltration membranes; membrane chemistry and flux dependency

The work presented in this chapter is adapted from: Ivan Manzano, Andrew L. Zydney, (2017) Quantitative study of RNA transmission through ultrafiltration membranes, *Journal of Membrane Science*, 544: 272-277. *https://doi.org/10.1016/j.memsci.2017.09.042*

3.1 Introduction

The past two decades have seen growing interest in the development of nucleic acid-based therapies for the treatment of a wide range of genetic disorders as well as for use as novel vaccines (Muralidhara et al. 2016; Ulmer and Geall 2016; Ferraro et al. 2011b). This includes the use of DNA to replace malfunctioning genes, e.g., in the treatment of hemophilia (Lusher et al. 2004), as well as the use of short interfering and micro RNA (siRNA and miRNA) for gene silencing or post-transcriptional regulation of gene expression (Kole, Krainer, and Altman 2012). There are currently more than 200 ongoing clinical studies of RNA-based therapeutics listed on www.clinicaltrials.gov, with even greater numbers of trials of DNA-based therapeutics (Ginn et al. 2013).

Although the development of large-scale processes for the purification of therapeutic proteins like monoclonal antibodies is well-established (Shukla et al. 2007; Kelley 2009), most work on nucleic acid purification has focused on laboratory-scale methods, many of which would be very difficult to employ for commercial manufacturing. This includes the use of agarose gel electrophoresis (AGE) and density gradient centrifugation for the separation of plasmid DNA

isoforms and the fractionation of both RNA and DNA on the basis of size (Viovy 2000; Andersson and Hjorth 1985; H. Zhang, Chen, and Glisin 2003). There is thus a critical need to develop cost-effective processes to ensure the integrity of the final gene therapy agent while achieving the quality and purity requirements needed for clinical applications.

Membrane processes are a potentially attractive alternative for the large-scale purification of nucleic acid-based therapeutics. Ultrafiltration is currently used for the concentration and final formulation of essentially all therapeutic proteins (van Reis and Zydney 2001), and a number of studies have demonstrated the potential of using ultrafiltration for removal of host cell proteins in the purification of monoclonal antibodies and Fab fragments (Castano et al. 2014; Binabaji et al. 2016). Several recent efforts have examined the use of ultrafiltration for the separation of plasmid DNA (pDNA) isoforms to purify the desired supercoiled topology (Borujeni and Zydney 2012; Latulippe and Zydney 2008). However, there have been very few studies of RNA ultrafiltration, either for the purification of RNA therapeutics or for the removal of RNA impurities in the preparation of DNA products. Data obtained by Nunes et al. (Nunes et al. 2012, 2014) showed the feasibility of using ultrafiltration for the removal of RNA impurities in the preparation of pDNA products; however, the data examined a relatively small range of experimental conditions with no results examining the possible effects of interactions between the membrane polymer and the RNA.

The objective of the studies described in this Chapter was to obtain quantitative data for the key factors controlling the ultrafiltration behavior of RNA. Data were obtained with both cellulosic and polyethersulfone ultrafiltration membranes with a range of nominal molecular weight cutoffs. The results clearly demonstrate the importance of both RNA adsorption and size-based sieving on the observed retention characteristics, providing important insights into the potential application of ultrafiltration in the purification of nucleic acid-based biotherapeutics.

3.2 Results and Discussion

3.2.1 Ultracel vs Biomax Membranes

Typical experimental data for the observed RNA sieving coefficient as a function of the bulk (feed) RNA concentration are shown in Figure 3-1 for separate ultrafiltration experiments using 100 kDa nominal molecular weight cutoff Ultracel and Biomax membranes. Each set of experiments was performed using a single membrane disk. Data were obtained at constant transmembrane pressure, corresponding to filtrate flux values of 70 and 120 μm/s for the Ultracel and Biomax membranes, respectively. In each case, the stirred cell was loaded with a fresh RNA solution with the different feed concentrations, with filtrate samples obtained after filtration of approximately 4 mL to wash out any dead volume beneath the membrane and in the exit filtrate line. The sieving coefficient was evaluated as the ratio of the RNA concentration in the permeate (filtrate) solution divided by the RNA concentration in the bulk solution in the stirred cell. The symbols represent the arithmetic average of at least two repeat measurements for each condition, with error bars corresponding to the standard deviation. Error bars are not shown when they are smaller than the size of the symbol for clarity.

The RNA transmission through the Biomax membrane was essentially constant, independent of the feed concentration, with a value of $S_o = 0.51 \pm 0.02$. In contrast, the RNA transmission through the Ultracel membrane increased with increasing feed concentration, going from a value of $S_o < 0.3$ at a feed concentration of 0.6 μg/mL to $S_o > 0.8$ at a feed concentration above 40 μg/mL. Note that there was no measurable change in the permeability of the membrane evaluated before and after the RNA ultrafiltration, with these values differing by less than 10% over the full course of the experiment. There was also no evidence of any RNA damage, with the RNA from the feed, permeate, and retentate samples migrating identically in agarose gel

electrophoresis (Figure 3-2), with similar results obtained with both the Biomax and Ultracel membranes. The diffuse band for the RNA in the agarose gel reflects the heterogeneous mixture of RNA species in the Torula yeast RNA; this is discussed in more detail subsequently.

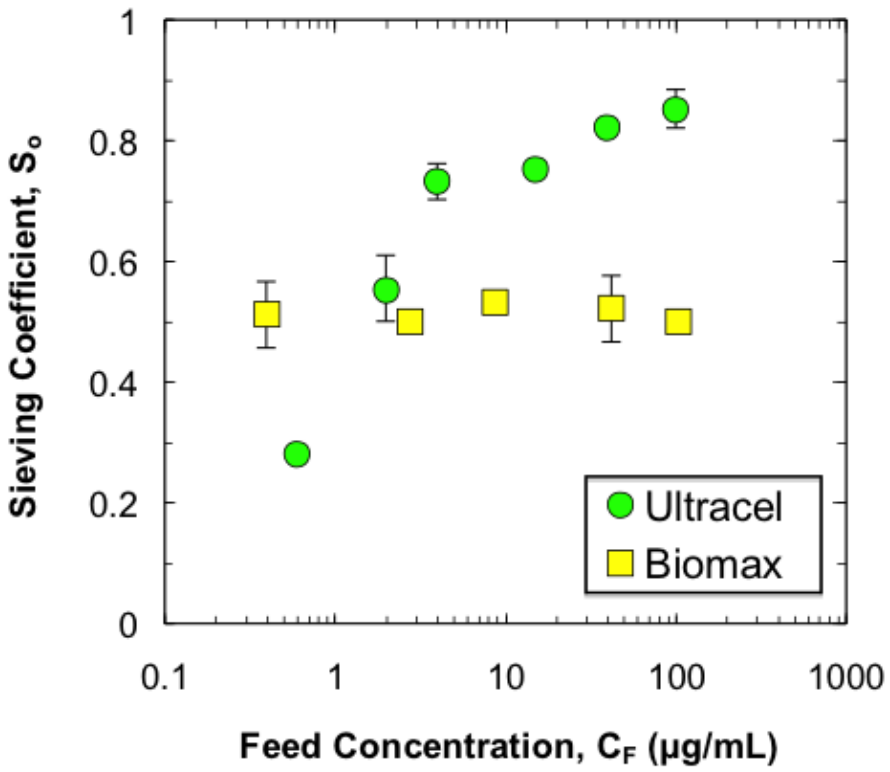

Figure **3-1**: Sieving coefficient as a function of feed concentration for ultrafiltration of the Torula yeast RNA through the 100 kDa Ultracel and Biomax membranes at constant flux of 70 and 120 µm/s, respectively. Error bars represent the standard deviation calculated from duplicate measurements. Error bars are not shown when they were smaller than the size of the symbol.

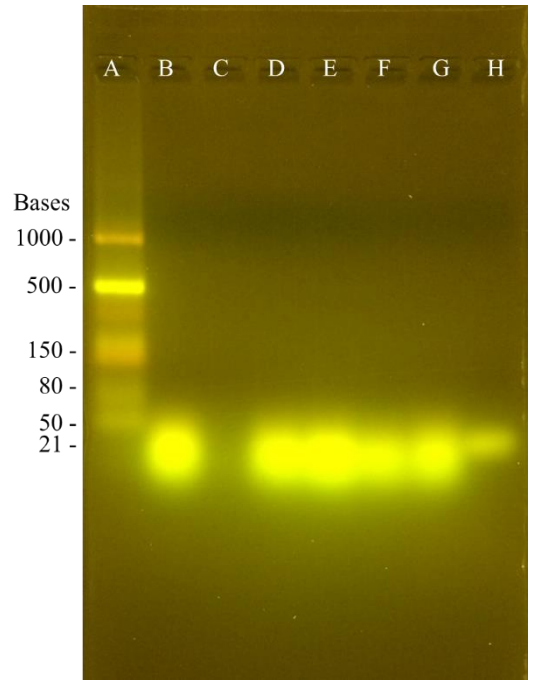

Figure **3-2**: Agarose gel electrophoresis for Torula yeast RNA. Lane A shows RNA molecular weight markers from 50 to 1000 nucleotides (Nt). Lane H is a DNA standard with 21 nucleotides. Lanes B, C, and D are initial feed, permeate, and final retentate samples obtained during filtration through a Biomax 100 kDa membrane at J_v = 30 µm/s. Lanes E, F, and G represent samples obtained at J_v = 120 µm/s.

One possible explanation for the unusual dependence of the RNA sieving coefficient on the feed concentration with the Ultracel membrane is the loss of RNA due to adsorption during passage through the porous membrane, particularly in the more dilute solutions. In order to explore this phenomenon in more detail, two separate ultrafiltration experiments were performed to evaluate the observed sieving coefficient as a function of filtration time (Figure 3-3). In both cases, data were obtained using 0.3 µg/mL solutions of the Torula yeast RNA at a transmembrane pressure of 19 kPa, corresponding to a filtrate flux of J_v = 70 µm/s. RNA transmission through the fresh Ultracel membrane was less than 50% at the start of the experiment, but this increased to a nearly

constant value of $S_o \approx 0.87$ for $t > 10$ min. The Ultracel membrane was then gently rinsed, the stirred cell re-filled with a fresh RNA solution, and a second ultrafiltration experiment was performed. In contrast to the results in the first run, RNA transmission through the "used" membrane remained essentially constant at a value of $S_o = 0.87 \pm 0.03$ throughout the experiment. Exposure of the Ultracel membrane to RNA in the first run likely led to saturation of the adsorption sites within the membrane, with RNA transmission during the second run determined by the intrinsic retention characteristics of the membrane. The lower levels of RNA transmission observed with the fresh membrane, and with the dilute solutions examined in Figure 3-1, are thus a direct result of the loss of transmitted RNA due to adsorption within the porous structure of the Ultracel membrane.

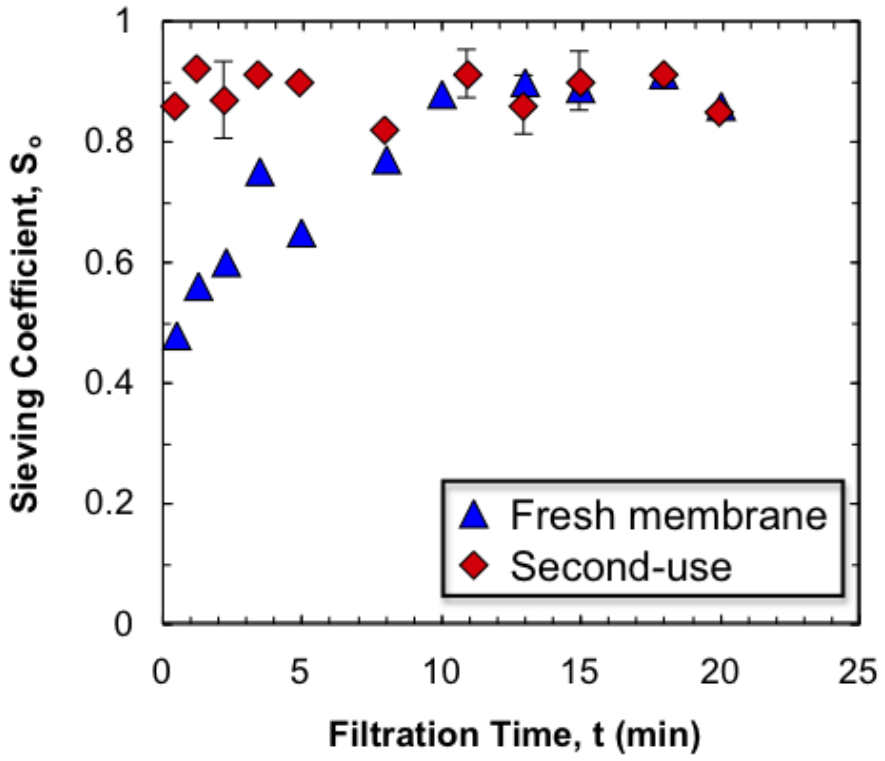

Figure **3-3**: RNA sieving coefficient as a function of time during constant pressure ultrafiltration at 19 kPa ($J_v \approx 70$ µm/s) through a 100 kDa Ultracel membrane. Results are shown for two repeat runs using the same membrane. Error bars represent the standard deviation calculated from duplicate measurements. Error bars are not shown when they were smaller than the symbol size.

Although there have been no previous studies of RNA adsorption to the composite regenerated cellulose Ultracel membranes, RNA adsorption to cellulosic materials is well established. For example, Kitos and Amos (1973) found high levels of adsorption of poly-A RNA to a microcrystalline unmodified cellulose at high ionic strength (500 mM); this binding affinity was lost when the poly-A was coordinated with poly-U in a double helix. Schutz et al. (1972) observed high levels of adsorption of a mixture of eukaryotic mRNA (from rabbit reticulocytes and chicken oviducts) during passage through a cellulose chromatography column. It is also possible that there is RNA adsorption to the polyolefin used as the substructure in the composite Ultracel membranes; the data obtained in this work were insufficient to determine the location of RNA adsorption within the membrane. The lack of adsorption on / within the Biomax polyethersulfone membrane seen in our studies may well be associated with electrostatic repulsion between the negatively-charged RNA and the negatively-charged membrane. The zeta potential of the polyethersulfone membrane is considerably more negative than that of the Ultracel membrane; previous studies report apparent zeta potential values for the Biomax membrane of around -15 mV in a 10 mM KCl solution at pH 7 (Burns and Zydney 2000) compared to -2 mV for the Ultracel membrane at the same conditions (Rohani and Zydney 2009).

3.2.2 Concentration Polarization Effects

The dependence of the RNA transmission on the filtrate flux for the different molecular weight cutoff Biomax membranes is examined in Figure 3-4. The open and filled symbols for the Biomax 50 and 100 kDa membranes are repeat measurements performed using different membrane disks (cut from the same flat sheet) but under otherwise identical conditions. The results from the repeat experiments are in excellent agreement. RNA transmission was greatest with the larger pore

size 300 kDa membrane as expected, with values greater than 0.95 for filtrate flux between 50 and 200 µm/s. In contrast, the observed sieving coefficient through the Biomax 50 and 100 kDa membranes increased significantly with increasing filtrate flux, going from values below 0.02 at very low flux to $S_o > 0.5$ at a flux above 130 µm/s. AGE images of permeate samples obtained at both low and high flux showed identical migration behavior in the gel (Figure 3-2), indicating that there was no irreversible damage to the RNA during the ultrafiltration, even at high values of the filtrate flux.

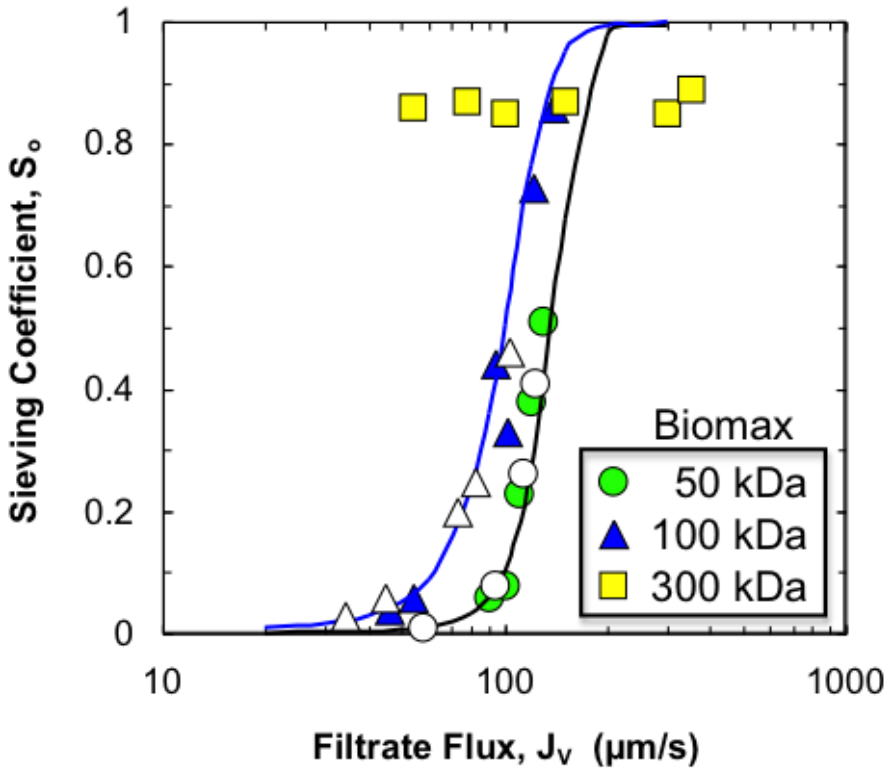

Figure **3-4**: Observed sieving coefficient versus filtrate flux for the Biomax 50, 100, and 300 kDa membranes. Open and filled symbols represent results from repeat experiments performed using different membrane disks with the same molecular weight cutoff. Solid curves are given by the concentration polarization model using the best fit values of the mass transfer coefficient and actual sieving coefficient.

The increase in RNA transmission with increasing filtrate flux could be due to concentration polarization effects (Equation 2-3) associated with the accumulation of retained RNA at the upstream surface of the membrane (Zydney 1997). Previous studies of protein ultrafiltration have demonstrated the effects of concentration polarization on the observed sieving coefficient. This includes work by Pujar and Zydney (1994) on the sieving coefficients for bovine serum albumin (radius of 3.5 nm) through a 100 kD polyethersulfone membrane (OMEGA) and by Molek and Zydney (2007) on the transmission of α-lactalbumin (radius of 2 nm) through a 30 kD Ultracel membrane.

Figure 3-5 shows the sieving coefficient data plotted in the linearized form of the concentration polarization model (Equation 2-4). The data are highly linear when plotted in this manner (r^2 values greater than 0.95), suggesting that the flux dependence of the observed sieving coefficient seen in Figure 3-4 is due to concentration polarization effects in the stirred cell. The slope of the data is equal to $1/k_m$, with an average value of k_m = 17 μm/s for the two sets of data. Also shown for comparison are data for bovine serum albumin (BSA) transmission through an Omega polyethersulfone membrane with 100 kDa nominal molecular weight cutoff obtained by Opong and Zydney (1991) in the same stirred cell at filtrate flux above 7 μm/s; data at lower flux were influenced by transmembrane diffusion causing the actual sieving coefficient to vary with the filtrate flux. The results for BSA are also linear when plotted in this form but with a much steeper slope, corresponding to a smaller value of the mass transfer coefficient, consistent with the larger size (approximately 3.6 nm) and smaller diffusion coefficient for BSA.

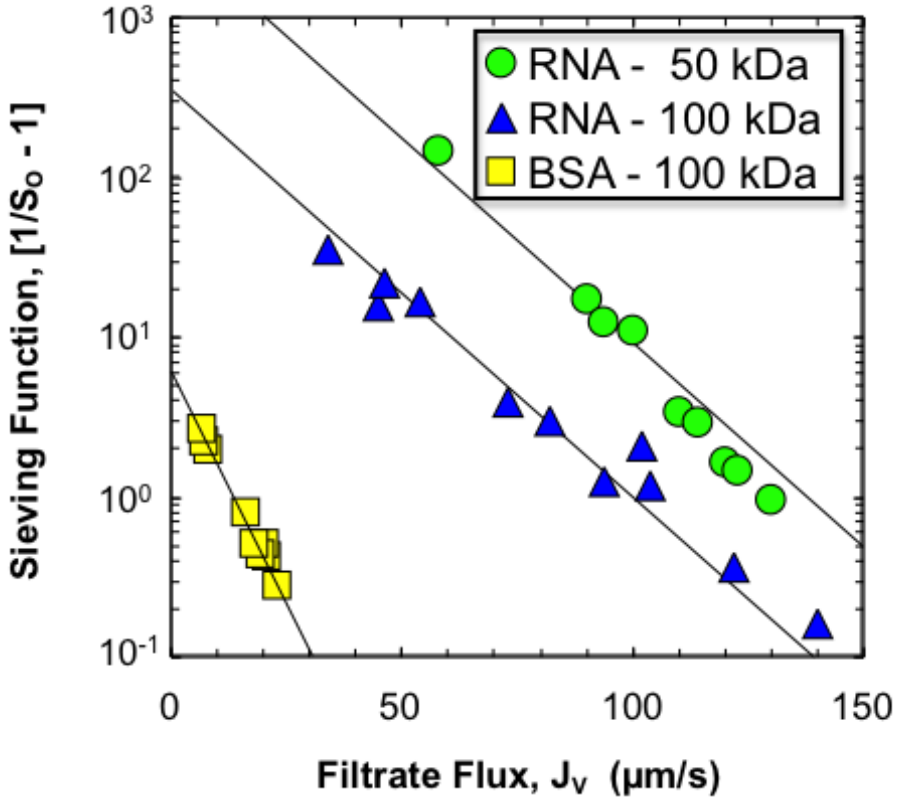

Figure **3-5**: Linearized plot of the sieving function versus the filtrate flux for RNA ultrafiltration through the Biomax 50 and 100 kDa membranes. Results for BSA using an Omega polyethersulfone membrane from Opong and Zydney (1991) are shown for comparison.

The best fit values of the slope and intercept were determined by minimizing the sum of the squared residuals between the model and data using a single (average) value of k_m = 17 µm/s, yielding $S_a = 3.1 \times 10^{-4}$ for the Biomax 50 and $S_a = 2.8 \times 10^{-3}$ for the Biomax 100. Opong and Zydney (1991) evaluated the mass transfer coefficient for BSA solutions in the same stirred cell using the experimental correlation:

$$\frac{k_m r}{D} = 0.23 Re^{0.567} Sc^{0.33} \tag{3-1}$$

where r = 1.25 cm is the radius of the stirred cell, $Re = \omega r^2/\nu$ is the Reynolds number (with ω the stirring speed and ν the kinematic viscosity), and $Sc = \nu/D$ is the Schmidt number. Equation (3-1)

gives k_m = 11 μm/s using a diffusion coefficient of D = 1.52 x 10^{-10} m^2/s based on data for a 20 nucleotide single stranded DNA (Stellwagen and Stellwagen 2002). This is somewhat smaller than that found from the linear regression fits to the data in Figure 3-5, which could reflect the complex structure and molecular weight distribution of the RNA species in the Torula yeast RNA. The effect of RNA structure on the ultrafiltration behavior is discussed in detail in Chapter 4.

The actual sieving coefficient for the Torula yeast RNA through the Biomax 50 kD membrane is more than 8 times smaller than that through the Biomax 100 kD membrane due to the difference in membrane pore size; this is discussed in more detail subsequently. The solid curves in Figures 3-4 and 3-5 were generated using Equation (2-3) with the best fit values of S_a given above with k_m = 17 μm/s. The model is in very good agreement with the experimental data, providing further confirmation of the importance of concentration polarization on the observed sieving coefficient.

3.3.3 Hydrodynamic Analysis

In order to obtain additional insights into the sieving behavior, the results for the actual sieving coefficients were compared with predictions of available hydrodynamic models for membrane transport (Zeman and Wales 1981):

$$S_a = (1-\lambda)^2[2-(1-\lambda)^2]exp(-0.7146\lambda^2) \qquad (3\text{-}2)$$

where λ is the ratio of the solute radius (r_s) to the pore radius (r_p). Equation (3-2) is valid for the transport of non-interacting spheres in cylindrical pores under conditions when solute transport is dominated by convection, i.e., when S_a is independent of the filtrate flux (Zeman and Zydney 1996). Data for BSA transport through a 100 kDa membrane indicate that the assumption of constant S_a is valid for filtrate flux above ≈20 μm/s (Opong and Zydney 1991), which is the regime examined in this thesis. Calculations performed with more recent expressions for the actual sieving coefficient

were in excellent agreement with the results given by Equation (3-2). Several approaches were used to estimate the size of the RNA. The agarose gels shown in Figure 3-2 suggest that the RNA has between about 12 and 50 nucleotides. The length of a single RNA nucleotide is approximately 0.21 nm (Glass and Wertz 1980), which corresponds to a total length between 2.5 and 10.5 nm. However, this neglects the flexible structure and internal folding of the RNA. Hajdin et al. (Hajdin et al. 2010) used molecular dynamics to evaluate the radius of gyration of RNA-like structures up to 161 nucleotides in size, with the results best fit by the power-law expression:

$$\overline{R_g} = 0.38\, N^{\alpha} \tag{3-3}$$

where R_g is in nm, N is the number of nucleotides in the RNA, and $\alpha = 0.41$. Equation (3-3) would give R_g values between 1.1 and 1.9 nm, which is considerably smaller than the pore size of the membranes examined in this work. Werner (2011), obtained a correlation for the hydrodynamic radius of RNA molecules based on data from DLS, analytical ultracentrifugation, gel filtration, and fluorescence correlation spectroscopy:

$$D_H = 0.822 N^{0.42} \tag{3-4}$$

The values for the hydrodynamic radius (0.5 D_H), are 1.1 times larger than those of the radius of gyration, consistent with the elongated shape of the RNA molecule (Latulippe and Zydney 2010).

An independent estimate of the RNA size was obtained using dynamic light scattering, with typical results shown in Figure 3-6 for a 1 g/L solution of the Torula yeast RNA in Tris buffer. The DLS shows multiple peaks, with peak maxima at 0.56, 1.5, 7.0, and 72 nm. The overall mean size determined from the DLS was 3.0 nm (excluding the largest peak), this value is about a factor of two larger than the estimates obtained from the agarose gel, although they are well below the estimated contour length of the RNA. It is unclear why the DLS shows such distinct peaks. The peak at 72 nm would correspond to an RNA with more that 350,000 nucleotides (based on Equation 3-6), which is physically unrealistic for the Torula yeast RNA. This peak likely reflects some kind

of aggregate in the Torula yeast mixture; the strong signal from this peak is due to the very non-linear dependence of the light scattering amplitude on particle size.

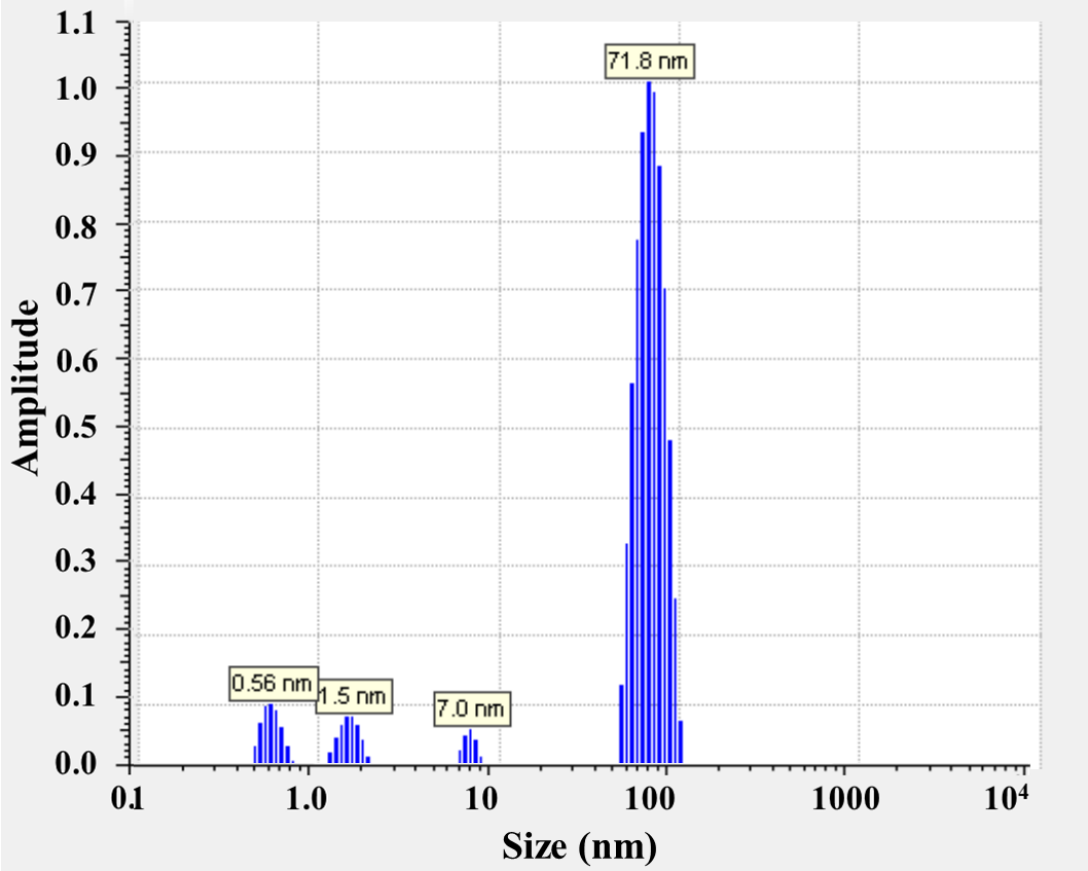

Figure **3-6.** Intensity distribution in Dynamic Light Scattering for 1 g/L solution of Torula Yeast RNA in 10 mM Tris buffer.

Figure 3-7 shows the calculated values of the actual sieving coefficient as a function of the pore radius for several different values of the RNA radius. The solid symbols are the experimental results for the Biomax membranes. The experimental data are in good agreement with the model calculations using r_s = 5 nm, which is somewhat larger than the estimated size of the Torula yeast RNA. This could reflect the increase in effective size associated with the diffuse electrical double

layer around the charged RNA, similar to previous reports for the effects of ionic strength on both DNA (Latulippe, Ager, and Zydney 2007) and protein (Pujar and Zydney) transport through porous membranes. More rigorous analysis of the sieving behavior would require consideration of the detailed size distribution for both the membrane pores and the RNA. The qualitative agreement between the data and model based on the transport of hard spherical solutes suggests that flow-induced RNA elongation has a negligible effect on RNA transport, which is in sharp contrast to previous results with plasmid DNA (Latulippe, Ager, and Zydney 2007). These differences are likely related to the very different structure and size of the RNA and DNA; plasmid DNA is a double-helix with a persistence length around 50 nm and a radius of gyration >100 nm.

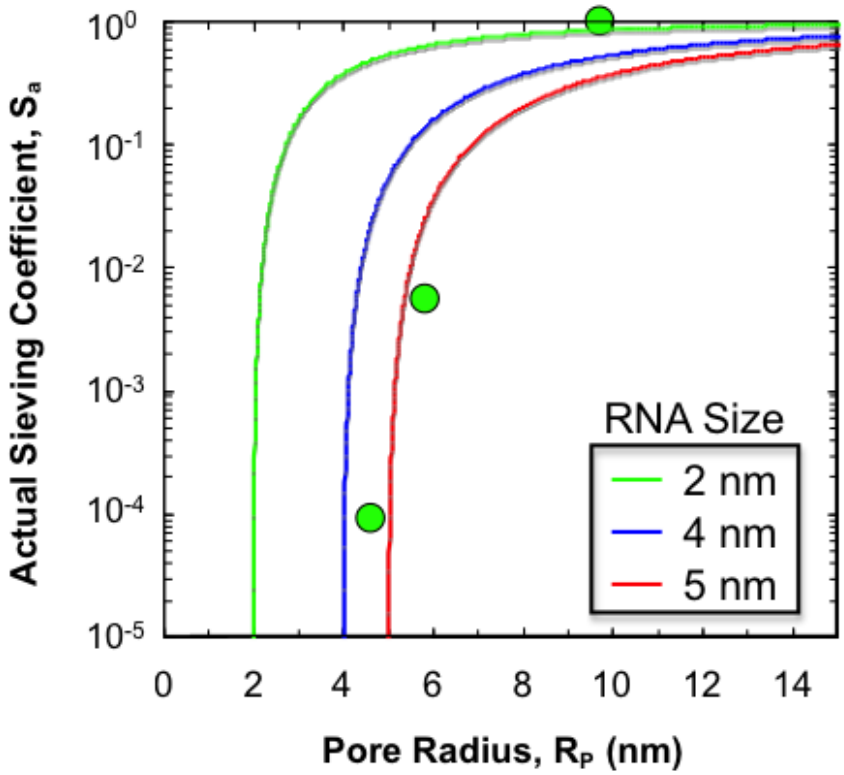

Figure **3-7.** Hindrance factor as a function of pore radius for several different values of the radius of the RNA. Solid curves are model calculations given by Equation (3-2).

3.3 Conclusions

The experimental data presented in this Chapter provide some of the first quantitative measurements of RNA transmission during ultrafiltration through different pore size and polymer membranes. RNA transmission through the Ultracel composite regenerated cellulose membranes was strongly affected by RNA adsorption, which caused a reduction in the RNA concentration in the permeate solution as RNA was "lost" within the porous membrane. RNA adsorption was minimal with the Biomax polyethersulfone membranes, which is likely due to electrostatic repulsive interactions between the negatively-charged RNA and the negatively-charged polyethersulfone membrane.

RNA transmission through the Biomax membranes was strongly influenced by concentration polarization affects associated with the accumulation of retained RNA at the upstream surface of the membrane. The experimental data were in good agreement with predictions of the classical concentration polarization model over a wide range of filtrate flux. The calculated values of the actual sieving coefficient were in reasonably good agreement with available hydrodynamic models for transport of spherical solutes through cylindrical pores, with the membrane pore size estimated from the measured hydraulic permeability. The best fit value of the RNA size was around 5 nm, which is smaller than the contour length of the RNA but larger than independent estimates of the radius by dynamic light scattering and from migration in the agarose gel. These factors are discussed in more detail in Chapter 4.

The results presented in this Chapter should be directly applicable to the development of membrane systems for the removal of RNA impurities from larger plasmid DNA in the preparation of DNA-based therapeutics; the Torula yeast RNA is likely to be a good model for the heterogeneous mixtures of RNA released upon cell lysis. The Biomax 50 kD membrane provided very good retention of the Torula yeast RNA at low filtrate flux, which might be attractive for the concentration and purification of small RNA therapeutics. The transmission of well defined RNA molecules through different ultrafiltration membranes is examined in Chapter 4.

Chapter 4

Impact of 3-dimensional structure on RNA ultrafiltration behavior

The work presented in this chapter is based on the published paper: Ivan Manzano, Grace Vezeau, Howard Salis, Andrew L. Zydney (2020), RNA size and 3-dimensional structure determine ultrafiltration behavior of small RNA molecules, *Separation and Purification Technology*. 237: 116372. https://doi.org/10.1016/j.seppur.2019.116372

4.1 Introduction

RNA plays a critical role in the coding, regulation, and expression of genetic information. Engineered RNAs also act as therapeutics by manipulating gene expression inside cells within the human body. For example, the discovery of RNA interference (RNAi) for gene silencing by Andrew Fire and Craig Mello (Fire et al. 1998) earned the 2006 Nobel Prize in Physiology or Medicine, reigniting interest in the development of RNA-based therapeutics for the treatment of a wide range of disease. RNA interference involves the cleavage of specific mRNA by enzymes (e.g., RNAse H) found in the RNA Induced Silencing Complex (RISC) (Gavrilov and Saltzman 2012; Wittrup and Lieberman 2015). RNA silencing inhibits translation of mRNA by attachment of a semi-complementary miRNA (micro RNA), leading to mRNA degradation by deadenylation, decapping, or exonuclease action (Huntzinger and Izaurralde 2011). In another example, RNA aptamers are short, structured RNAs that can be engineered to specifically bind human cell receptors, thereby manipulating cellular signaling pathways. RNA aptamers have been widely studied as antiviral agents (Gopinath 2007) as well as valuable analytical and diagnostic tools (Wolter and Mayer 2017). As a third example, CRISPR systems use engineered guide RNAs to

bind specific DNA sites on a cell's genome, thereby enabling targeted modification of DNA sequences or regulation of targeted genes (Josephs et al. 2015; Mout et al. 2017). As the development of RNA therapeutics reaches the clinic, their production and purification will become increasingly important.

RNA is composed of four monomer nucleotides: adenine, uracil, guanine, and cytosine. RNA is produced as a single-stranded polymer, but it can form complex structures, including duplexes, hairpins, cloverleafs, and G-quadruplexes (Hendrix, Brenner, and Holbrook 2005). The formation of structures is mediated mainly through nucleotide-nucleotide non-covalent interactions (e.g. hydrogen bonding and nucleotide stacking), called base pairing. Base pairing follows the canonical code (A:U and G:C), but the absence of the 3' hydroxyl in the ribose sugar also allows G:U base pairing. RNA structures often contain mismatched nucleotides that create bulges or unpaired nucleotides that create internal or terminal loops.

The successful commercialization of RNA therapeutics will require the development of appropriate manufacturing / purification processes suitable for the production of large quantities of high quality and high purity RNA with well-defined tertiary structures. Each of these RNA therapeutic molecules has specific sequence and structural requirements for the desired function; RNA purification processes must be robust and suitable for RNA with different lengths and structures. Ultrafiltration has the potential to play a major role in RNA processing, with the proper selection of membrane chemistry and pore size allowing for the removal of large molecular weight species (with the RNA collected in the permeate) or for RNA concentration / buffer exchange (with the RNA collected in the retentate). In addition, the preparation of riboprotein complexes (e.g. CRISPR-Cas9 and guide RNA) or RNA conjugated to exosomes or lipid nanoparticles (Shimanovich et al. 2011; Yu et al. 2010) will likely require the separation and removal of residual free RNA. This is examined in Chapter 5 of this thesis.

Several previous studies have demonstrated the potential of using tangential flow filtration (TFF) for RNA separations. Eon Duval et al. (2003) examined the removal of RNA from large plasmid DNA, with better resolution obtained using more dilute Tris buffers. The results in Chapter 3 showed that RNA transmission during ultrafiltration is a strong function of the filtrate flux due to concentration polarization effects, with nearly 100% transmission obtained at high flux even with membranes having nominal molecular weight cutoffs as small as 100 kDa. However, these studies were performed with crude RNA mixtures with a range of RNA size (number of nucleotides) and structures.

The objective of the work described in this chapter was to examine the ultrafiltration behavior of RNA with well-defined size and secondary structure over a range of filtrate flux and solution conditions. This included the effects of urea, widely used as a denaturant to disrupt RNA secondary structures, and NaCl, which shields inter- and intra-molecular electrostatic interactions. RNA composition and structure were also characterized by dynamic light scattering and gel electrophoresis to obtain further insights into the key properties governing RNA ultrafiltration.

4.2 Materials and methods

4.2.1 RNA

RNA molecules with four well-defined sequences were synthesized from their respective DNA template (IDT Technologies, San Jose, CA) as described in Chapter 2. Linear-20 and Linear-70 were designed to have minimal internal nucleotide pairing, while Hairpin-70 was designed to have a fully complementary 33-base pair hairpin closed by a tetraloop (consisting of the bases AAUA). Eba39c was developed by inserting the 86 nucleotide-long Eba aptamer domain from the *Erysipelotrichaceae bacterium* NiCo riboswitch within the interior of a 151 nucleotide sequence

containing additional structural elements (Furukawa et al. 2015). The specific sequences and physical properties of the RNA constructs are summarized in Table 2-1.

RNA was purified as described in Chapter 2 with the precipitated RNA resuspended in the appropriate buffer solution consisting of a base buffer of 10 mM Tris at pH 7.5 along with the addition of 100 mM NaCl and / or 2 M urea in some experiments.

4.2.2 RNA characterization

The effective RNA size in the presence / absence of added NaCl was examined by Dynamic Light Scattering (DLS) using a Zetasizer Nano ZS (Malvern Panalytical, Worcestershire, England). Freshly prepared samples at an RNA concentration of 200 μg/mL were loaded into disposable microcuvettes. System temperature was set at 25˚C with the scattering intensity evaluated at 173º scattering angle. The effective size was evaluated using refractive indices of 1.3302 for the Tris buffer alone and 1.3312 for Tris with 100 mM NaCl as determined using the Dispersants Manager in the Zetasizer Software 7.13.

The procedure used to prepare and run samples in urea–agarose gel electrophoresis was adapted from Hegedüs et al. (2009) with minor modifications. Gels of 1.5 % (*w*/*v*) agarose were prepared and run in 1× TAE buffer supplemented with 2 M urea, with or without 100 mM NaCl. RNA was stained by adding 1 μL/mL of GelStar™ Nucleic Acid stain (Lonza, Rockland, ME) to gels. The electrophoresis was run at 110 V in an electrophoretic tank at room temperature for 4 h in the absence of NaCl; the gels run in the presence of 100 mM NaCl were maintained at low voltage and at 4 ºC to prevent excessive heating.

4.2.3 Ultrafiltration

Ultrafiltration experiments were performed using an Amicon 8010 stirred cell (MilliporeSigma, Billerica, MA) with the stirring speed set at 730 rpm using a VWR 205 Autostirrer plate. Biomax® 50, 100 and 300 kDa nominal molecular weight cutoff polyethersulfone membranes were provided by MilliporeSigma. Data were obtained over a range of filtrate fluxes using an air-pressurized feed reservoir. Limited experiments were performed at constant filtrate flux using a Masterflex peristaltic pump on the permeate exit line. All experiments were performed at room temperature.

The RNA stock solution was diluted with 10 mM Tris buffer at pH 7.5 to obtain a concentration of 0.3 μg/mL (confirmed by the fluorescence assay described in Section 2.1.3), with the resulting feed solution added directly to the stirred cell. 500 μL samples were collected from both the permeate and bulk solutions after filtration of at least 2 mL to insure wash out of the hold-up volume (approximately 1 mL) in the filtration system. RNA concentrations in the permeate and bulk samples were determined by fluorescence intensity using 10X Ribogreen dye (Section 2.1.3).

4.3 Results and Analysis

4.3.1 RNA size / structure

Typical DLS data for the RNA are shown in Figure 4-1. In each case, a single peak was observed for each RNA construct, with the average size determined from the location of the peak maximum as summarized in Table 4-1. The RNA size in 10 mM Tris varies from D_{DLS} = 1.9 ± 0.8 nm for the Linear-20 RNA to D_{DLS} = 11.2 ± 0.5 nm for the Eba39c; the effective diameters in 10 mM Tris + 100 mM were slightly smaller than those obtained without any added NaCl. The measured diameter of the linear RNA constructs are similar to those calculated using the correlation presented by Werner (Werner 2011) based on data obtained from DLS, analytical ultracentrifugation, gel filtration, and fluorescence correlation spectroscopy:

$$D_H = 0.822 N^{0.42} \tag{3-4}$$

with D_H in nm and N the number of nucleotides. Equation (3-4) gives D_H = 2.9 nm for the Linear-20 and D_H = 4.9 nm for the Linear-70. The Hairpin-70 RNA has an effective diameter that is considerably smaller than that for the Linear-70 RNA (4.3 ± 1.4 nm versus 6.1 ± 1.5 nm in 10 mM Tris). However, the diameter of the Hairpin-70 RNA is more than twice that of the Linear-20 RNA.

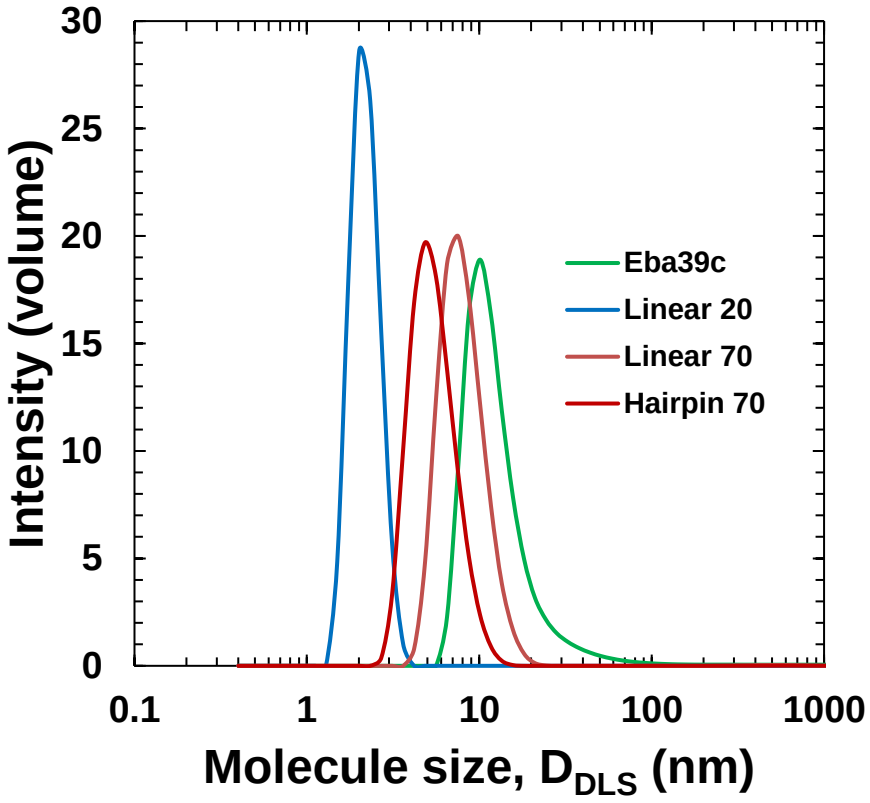

Figure **4-1**: Intensity distribution in dynamic light scattering for the different RNA sequences. Data obtained using sample volume of 70 µL with an RNA concentration of 0.20 µg/mL in 10 mM Tris at pH 7.5.

Table **4-1**: Average hydrodynamic diameter of RNA from dynamic light scattering and best fit values of the actual sieving coefficients and bulk mass transfer coefficients

		RNA Diameter, D_{DLS} (nm)				
RNA	MW (kDa)	10 mM Tris + 0 mM NaCl	10 mM Tris + 100 mM NaCl	Actual Sieving Coefficient, S_a	Mass Transfer Coefficient, k_m (μm/s)	r^2
Linear-20	7.16	1.9 ± 0.8	1.9 ± 0.4	0.0057	26	0.93
Linear-70	20.95	6.1 ± 1.5	5.9 ± 1.6	0.0016	32	0.90
Hairpin-70	21.57	4.3 ± 1.4	3.5 ± 0.7	0.0029	24	0.88
Eba39c	73.44	11 ± 1	10 ± 2	--	--	--

Additional insights into the structure of the RNA constructs were obtained by comparing the structure predictions using RNAfold, mFold (http://unafold.rna.albany.edu/?q=mfold), and NUPACK (http://www.nupack.org/). These programs use a dynamic programming approach to determine the minimum free energy and corresponding secondary structure of a nucleic acid given a set of structural energy parameters (Eddy 2004). The predicted structures of the 4 RNAs examined in this work were very similar, although there were some slight differences. In particular, mFold predicts that both the short and long single-stranded RNAs will contain a short hairpin. However, the folding free energy for these hairpin structures was slightly positive, 5.7 and 3.7 kcal/mol, respectively, for the Linear-20 and Linear-70. These states are therefore unlikely to be highly populated compared to the unstructured (linear) form, which by definition has a folding free energy of 0 kcal/mol. In addition, the different algorithms predicted slightly different structures for the Eba39c, although the overall degree of structure was conserved with approximately 50% base-pairing.

4.3.2 RNA ultrafiltration

4.3.2.a Filtrate flux behavior

Figure 4-2 shows the affect of filtrate flux (J) on RNA transmission through the Biomax® 100 kDa nominal molecular weight cutoff membrane for the four different RNA sequences. The results are plotted in terms of the observed sieving coefficient (S_o), defined as the ratio of the RNA concentration in the permeate to that in the bulk solution at each value of the filtrate flux. There was no evidence of any RNA degradation during the experiment, with agarose gels showing single bands for the RNA samples in both the permeate and retentate samples. The observed sieving coefficients for the different RNA samples increase with increasing filtrate flux due to concentration polarization effects, which have been discussed previously in the context of ultrafiltration of Torula yeast RNA, with no indication of RNA adsorption or fouling (Chapter 3).

The observed sieving coefficients for the Linear-20 RNA were much larger than those for the Linear-70 RNA as expected. The sieving coefficients for the Hairpin-70 RNA were very similar to those of the Linear-20 over the entire range of filtrate flux, despite the more than 3-fold difference in molecular weight. However, these values were highly consistent with the very similar size of these RNA as determined by dynamic light scattering (Table 4-1). The transmission of the Linear-70 RNA was well below that of the Hairpin-70, despite the very similar molecular weight for these RNA structures (within 3%), which is again consistent with the DLS data. For example, at a filtrate flux of 100 μm/s (corresponding to 360 L/m^2/h), the observed sieving coefficient of the Linear-70 is only $S_o = 0.04$ while that for the Hairpin-70 is greater than 0.25. The large Eba39c RNA is strongly retained over the entire range of filtrate flux, with $S_o \leq 0.04$ up to a filtrate flux of 150 μm/s. These results clearly demonstrate that the RNA size and structure both have a very strong effect on RNA transmission through the ultrafiltration membrane.

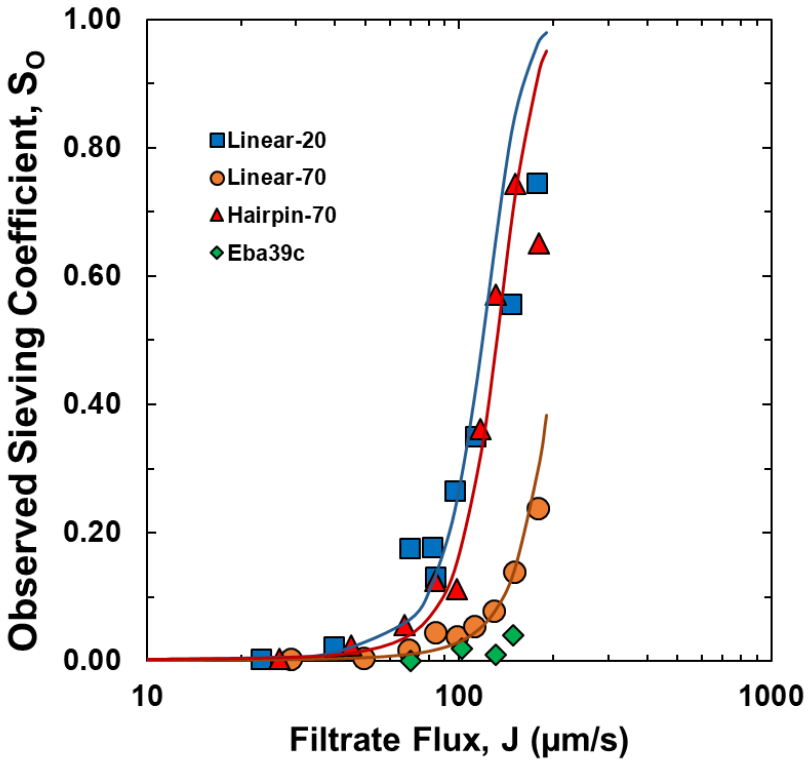

Figure **4-2**: Observed sieving coefficients for four different RNA sequences through 100 kDa Biomax® membranes as a function of filtrate flux. All samples were suspended in 10 mM Tris buffer at pH 7.5.

The solid curves in Figure 4-2 are model calculations accounting for the effects of concentration polarization (Equation 2-3) assuming constant values for both the actual sieving coefficient (S_a) and mass transfer coefficient (k_m):

$$S_O = \frac{S_a}{(1 - S_a)\exp\left(\frac{J}{k_m}\right) + S_a} \tag{2-3}$$

The actual sieving coefficient is equal to the ratio of the RNA concentration in the permeate to that in the solution immediately upstream of the membrane. The best fit values of S_a and k_m are shown in the final 2 columns of Table 4-1; it was not possible to evaluate these parameters for Eba39c due to the very low values of the observed sieving coefficients. The Linear-20 had the largest value of the actual sieving coefficient followed by the Hairpin-70 and Linear-70, in good agreement with the measured values of the RNA diameter given in Table 4-1. The very small values of S_a reflect the high degree of RNA retention seen at low values of the filtrate flux. The origin of the large value for the mass transfer coefficient for the Linear-70 RNA is unclear, although this may simply be due to the limited range of S_o data for this construct. The model curves are in good agreement with the experimental data for all three RNA constructs, with r^2 values around 0.9, providing further confirmation of the importance of concentration polarization in determining the RNA transmission.

4.3.2.b Pore size effects

Limited experiments were performed with membranes having different nominal molecular weight cutoffs to examine the effects of the membrane pore size on RNA retention. Results for the Hairpin-70 RNA at a filtrate flux of approximately 45 μm/s are shown in Figure 4-3 as a function of the membrane pore size evaluated from the measured values of the membrane hydraulic permeability (L_p as given by Equation 2-2) yielding pore radii of 4.6, 5.8, and 9.0 nm for the Biomax 50, 100 and 300 kDa membranes, respectively.

The observed sieving coefficients for the Hairpin-70 increased with increasing pore size as expected, with a nearly linear relationship on the semi-log plot. The Biomax 50 and 100 kDa membranes show high retention of the RNA ($S_o < 0.03$), even though the calculated pore radius is larger than the radius of the Hairpin-70 (3.1 ± 0.8 nm). In contrast, the Biomax 300 kDa membrane

shows very high transmission of the Hairpin-70 due to the combination of low intrinsic retention and the high degree of concentration polarization.

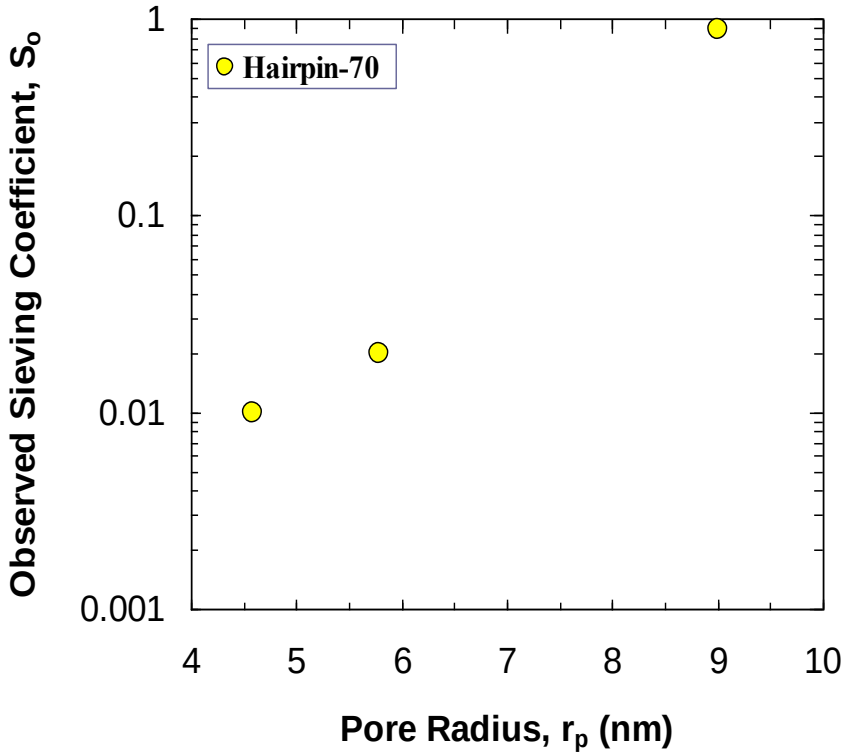

Figure **4-3**: Observed sieving coefficients for the Hairpin-70 RNA through a series of Biomax® membranes as a function of the calculated membrane pore radius. Data were obtained at a filtrate flux of approximately 45 µm/s using RNA in a 10 mM Tris buffer at pH 7.5.

4.3.3 Effect of NaCl and urea

Figure 4-4 shows the effects of NaCl and urea on the observed sieving coefficients for the Linear-70 and Hairpin-70 RNA at a flux of approximately 150 µm/s. The addition of 2 M urea had relatively little effect on the RNA transmission in the absence of added NaCl. The transmission of the Linear-70 RNA was very sensitive to the solution conditions, with the observed sieving coefficient increasing from $S_o = 0.24 \pm 0.01$ in the 10 mM Tris to $S_o > 0.8$ in the presence of 100

mM NaCl and 2 M urea. Similar effects were seen with the Hairpin-70, but with much higher transmission and a much weaker dependence on solution conditions. The net result is that the transmission of the Hairpin-70 is almost 3 times that of the Linear-70 in the 10 mM Tris, but the sieving coefficients of these RNA constructs differ by less than a factor of two in the presence of NaCl and by only 10% in the presence of 100 mM NaCl and 2 M urea.

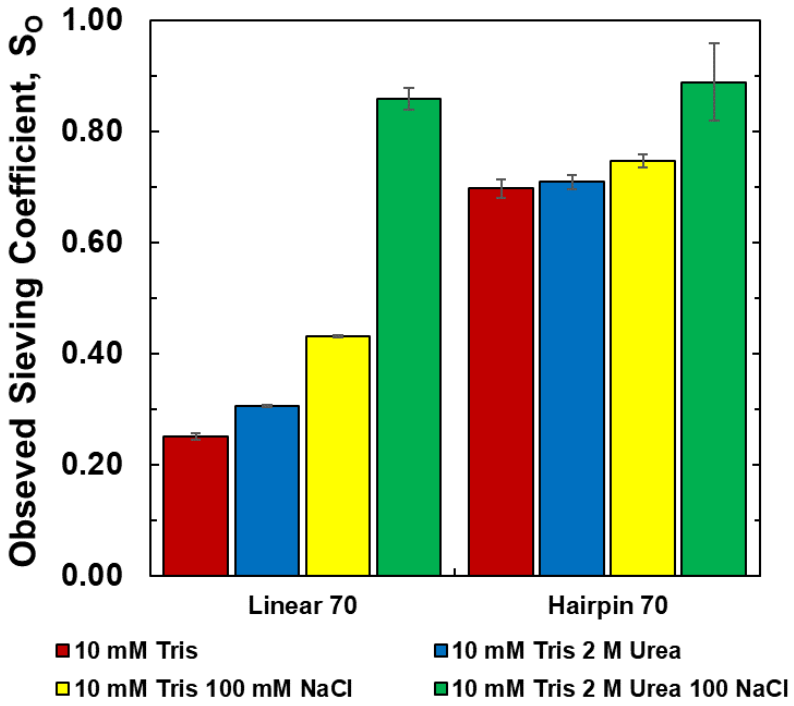

Figure **4-4**: Effect of urea and NaCl on the observed sieving coefficients for the Linear-70 and Hairpin-70 RNA samples through 100 kDa Biomax membranes at a filtrate flux of 150 µm/s. Error bars represent standard deviation from duplicate measurements.

The results presented in Figure 4-4 are in sharp contrast with the findings of Eon-Duval et al. (2003) in which much greater RNA removal was obtained at lower conductivity. However, the experiments performed by Eon-Duval et al. (2003) used clarified lysates containing DNA and

proteins that can form a gel layer on the membrane surface that hinders RNA transport, particularly in the presence of higher salt concentrations.

The increase in RNA transmission in the presence of 100 mM NaCl seen in Figure 4-4 is consistent with the reduction in effective size seen in the DLS data (Table 4-1), although the magnitude of the change in hydrodynamic radius (determined by DLS) is considerably smaller than the change in sieving coefficient. One possible explanation for this is that the added NaCl is also screening intermolecular electrostatic interactions between the negatively charged RNA and the negatively-charged Biomax membrane (Burns and Zydney 2000), a phenomenon that is well established for both protein (Pujar and Zydney 1994) and DNA (Latulippe and Zydney 2008) transport through porous membranes. The larger effect on the linear RNA is consistent with the greater surface area for electrostatic interactions. Alternatively, the DLS data may not provide an accurate indicator of the effective RNA size in the context of membrane ultrafiltration. The effective size in DLS is calculated from the measured value of the RNA diffusion coefficient, which is in turn determined by the hydrodynamic interactions between the RNA chain and water. In contrast, RNA transport during ultrafiltration is determined by the ability of the RNA to access (or partition into) the small membrane pores.

The increase in RNA transmission in the presence of 2 M urea is surprising. Urea is known to cause denaturation of RNA secondary structures (Priyakumar et al. 2009), but this would be expected to reduce transmission of the hairpin RNA due to the corresponding increase in size (i.e., as the hairpin becomes more linear). Note that typical denaturing procedures for gel electrophoresis use urea concentrations as high as 8 M (Summer, Grämer, and Dröge 2009); however, concentrations of 2 M have been shown to be sufficient to disrupt secondary structures in small RNAs (Miner and García 2017). The data in Figure 4-4 do show very similar transmission of the Hairpin-70 and Linear-70 RNA in the solution with 2 M urea and 100 mM NaCl, consistent with the disruption of secondary structure. It is possible that the interactions between urea and RNA lead

to a reduction in the effective RNA charge, which would enhance RNA transmission through the negatively-charged Biomax membrane. Note that Japrung et al. (2010) showed that the addition of urea increased the translocation of single-stranded DNA and RNA through the α-hemolysin pore due to the elimination of secondary structures, although in this case the RNA moves through the pore as an elongated chain. Molecular dynamics simulations of RNA in the presence of 2 M urea actually show a significant increase in radius of gyration and a reduction in melting temperature due to specific urea–RNA interactions (Miner and García 2017). Additional studies will be required to connect these changes in RNA structure to the ultrafiltration behavior.

4.3.4 Agarose Gel Electrophoresis

In order to obtain additional insights into the origin of the sieving behavior seen in Figures 4-2 to 4-4, the effective size of the different RNA constructs was also examined by agarose gel electrophoresis (AGE). Figure 4-5 is an agarose gel showing the migration of the four RNA sequences prepared and run in different buffers. The unlabeled lanes show RNA ladders running from 50 to 1000 base pairs. Gels for feed and permeate samples were identical under all conditions, indicating that the ultrafiltration caused no damage to the RNA. The band for the Hairpin-70 RNA appears at almost the same location as the band for the Linear-20 RNA in both panels 1 and 2, consistent with the very similar transmission of these RNA constructs during ultrafiltration (Figure 4-2). Note that the effective size of these RNA constructs, as determined by dynamic light scattering, differ by more than a factor of two (Table 4-1), suggesting that the migration in the agarose gel provides a better indicator of the transmission during ultrafiltration than the size determined by DLS.

The band for the Linear-70 RNA appears at a significantly larger size, with the Eba39c having the largest size. The bands for all 4 RNA constructs appear at the same location in the

presence / absence of 2 M urea (panels 1 and 2), consistent with the very small change in RNA transmission upon addition of urea seen in Figure 4-4. The bands for the gel run in the presence of 100 mM NaCl (panels 3 and 4) appear significantly closer together, this could be an indication that the addition of NaCl reduces the difference in effective size between the RNA constructs, qualitatively consistent with the changes in transmission of Linear-70 and Hairpin-70 RNA seen in Figure 4-4. However, is worth noting that the addition of NaCl to the gels adds a constraint to the voltage the gel can be run at, to prevent melting due to overheating. This reduction in voltage increases the time required to fully resolve the bands thereby increasing the blurriness of the bands.

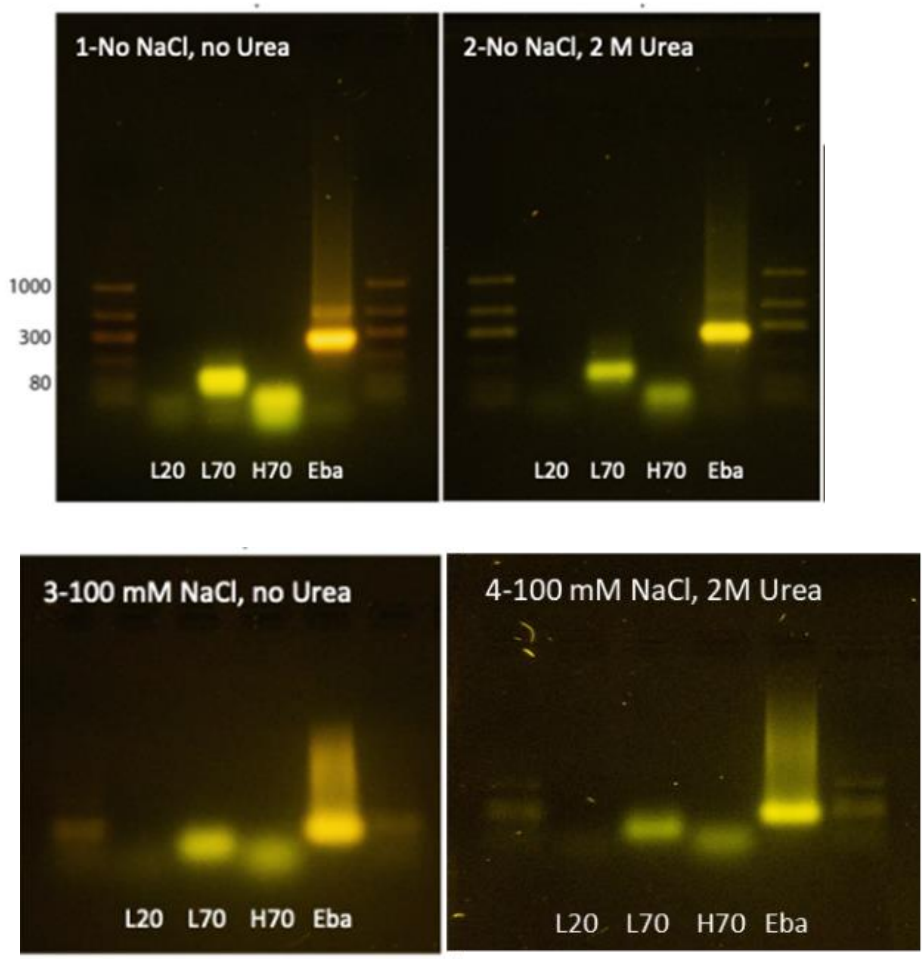

Figure **4-5**: Agarose gel electrophoresis for the Linear-20 (L20), Linear-70 (L70), Hairpin-70 (H70), and Eba39c RNA in 1 – No NaCl with no urea, 2 – No NaCl and 2 M urea, and 3 – 100 mM NaCl and no urea, 4-100 mM NaCl and 2 M urea.

4.4. Conclusions

The results presented in this chapter provide the first quantitative data on the transmission of RNA with different well-defined structures and length through commercially available ultrafiltration membranes. The transmission of the hairpin RNA is considerably larger than that of the linear RNA with equivalent number of nucleotides, consistent with the smaller effective size of

the hairpin RNA as determined by both dynamic light scattering and migration of the RNA in an agarose gel. The transmission of the Linear-20 and Hairpin-70 RNA were very similar, in good agreement with the agarose gels, suggesting that migration through the gel may provide a better indication of the ultrafiltration behavior than the RNA radius determined by DLS. RNA transmission also increases upon the addition of 100 mM NaCl, which appears to be due to a combination of changes in effective size and a reduction in electrostatic repulsion between the negatively-charged RNA and the negatively-charged membranes.

The addition of urea also had a large effect on RNA transmission for both the structured and linear RNA. The transmission of the Linear-70 RNA in the presence of 100 mM NaCl and 2 M urea was more than three times greater than that in Tris alone. Urea also caused a small increase in transmission of the Hairpin-70 RNA, even though the reduction in intramolecular interactions between bases would be disrupted in the presence of urea. Additional studies will be required to identify the underlying basis for these changes in RNA transmission and the potential for exploiting these phenomena for the purification of RNA-based therapeutics.

Chapter 5

Purification of Cas9-RNA ribonucleoprotein complexes using ultrafiltration

5.1 Introduction

Gene editing technologies like CRISPR-Cas9 have revolutionized the field of molecular biology, providing the ability to modify DNA at specific locations. Potential applications include the control of insect populations (Enright et al. 2003; Gokcezade, Sienski, and Duchek 2014), increasing crop yields (Voytas and Gao 2014; J. Li et al. 2016; Wang, Zhang, and Zhu 2019), and the development of novel therapeutics for the treatment of viral infections (Kennedy et al. 2014; Yin et al. 2017; Bella et al. 2018) and various genetic disorders (Park et al. 2015; H. L. Li et al. 2015). Despite being a widely used technique in the laboratory setting, large scale manufacturing of CRISPR-Cas9 can be quite challenging as CRISPR-Cas9 is a ribonucleoprotein complex (RNP), consisting of a Cas (CRISPR-associated endonuclease) protein coupled to a single strand guide RNA (complementary to the DNA sequence of interest), which must not only be purified but also delivered together to a specific area within the body.

5.1.1 CRISPR (Clustered Regularly Interspaced Short Palindromic Repeats) mechanism

The ribonucleoprotein complex (RNP) is formed by a protein, Cas (CRISPR-associated endonuclease), with an internal machinery for removing specific DNA sequences. The protein is coupled to a single strand nucleic acid, in most cases a small RNA molecule, that serves as a guide to bind to the specific target that for gene editing. This binding is highly specific and requires full complementarity between the guide's spacer and target sequence.

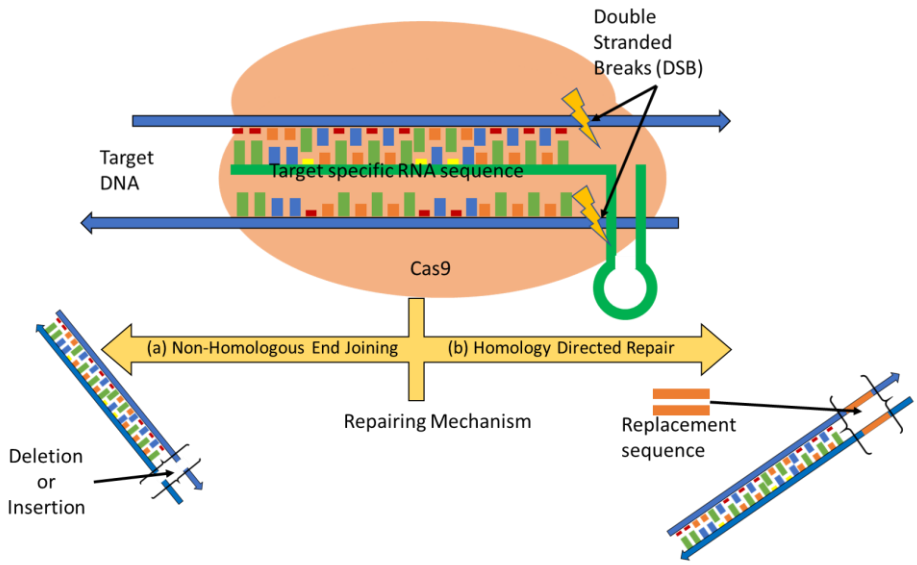

Figure **5-1**: CRISPR mechanism (a) Non-homologous join ending and (b) Homology directed repair.

The gene editing process starts once Cas9/guide RNA binds to the target DNA, and the Cas9 recognizes and binds to a short segment of the DNA adjacent to the target site (Fig. 5-1). This initiates unwinding of the helix allowing the RNA to bind to the target sequence of the DNA if the sequences are paired precisely. The Cas9 then cuts the DNA, forming a double stranded break, so that the cell's natural machinery can repair the cut sequence by non-homologous end joining (Fig 5-1.a). This joining adds a couple of nucleic bases and binds the strands together, causing the disruption of the original gene sequence. Larger segments can be deleted by using two different RNPs targeting a single gene sequence in two different sites simultaneously. This triggers the same repair process in the cell, joining the two strands but without the intermediate sequence.

Gene corrections are likely one of the most attractive features of the CRISP / Cas9 system. In this case, one administers a DNA template in addition to the Cas9 / guide RNA complex. This template has a defined sequence that matches exactly the sequence at the cut sites, allowing the cell to use it to repair the broken sequence in a process called Homology directed repair (Fig. 5-1.b).

This makes it possible to either insert a corrected gene for the replacement of a defective one or even insert completely new genetic information that can supplement the missing genetic material.

5.1.2 Other Cas proteins

A newly discovered set of CRISPR associated proteins, cas12 and Cas13, are now being studied as powerful diagnostic tools and alternative silencing technologies (Yan, Wang, and Zhang 2019). Cas13 that targets messenger RNA is now being evaluated for transcriptional gene silencing (Abudayyeh et al. 2017; Cox et al. 2017; Wessels et al. 2020). One of the advantages of this technology is the less complicated access to its gene targets compared to other genome editing that typically requires access to the nucleus of the cell.

More recently, Cas13 and Cas12 proteins have been used in combination with isothermal amplification for the detection of nucleic acids at the attomolar level and a single-base mismatch specificity. Gootenberg et al. (2017) developed a powerful diagnostics technique, named SHERLOCK for Specific High-Sensitivity Enzymatic Reporter UnLOCKing, that uses RNA targeted Cas13 enzymatic activity and fluorescent markers. SHERLOCK provides rapid nucleic acid detection and is capable of detecting different bacterial pathogens (e.g., *Klebsiella pneumoniae* carbapenemase, KPC or New Delhi metallo-β-lactamase 1, NDM-1) as well as differentiating between similar strains of Zika and Dengue viruses (Gootenberg et al. 2017). In contrast, Chen et al. (2018) studied the use of Cas12 as an alternative nucleic acid detection platform named DETECTR for DNA Endonuclease-Targeted CRISPR Trans Reporter. DETECTR uses a combination of isothermal amplification and Cas12a ssDNase activation for DNA detection at the attomole level; it can be used to detect human papillomavirus (HPV) in patient samples and to differentiate among two separate strains of the same virus (Chen et al. 2018).

5.1.3 Cas protein manufacturing strategies.

Although previous studies have shown that it is possible to target delivery of gene editing systems to specific cell types using viral vectors containing a single plasmid encoding both the Cas9 protein and the guide RNA, many patients have immunity against such vectors which would prevent the therapeutic from reaching the designated cells (Xu et al. 2019). In addition, if the plasmid does reach the cell, the ongoing expression of the Cas9 increases the risk of off-target cleavage of host DNA (R. Peng, Lin, and Li 2016). Thus, there are distinct advantages to providing the whole RNP complex directly to the cells of interest (Kim et al. 2014). In this case, the Cas9 and the guide RNA would be produced (and purified) separately before assembly into the RNP complex. Excess guide RNA can be used to ensure that all of the Cas9 protein is saturated, with any residual RNA removed from the RNP after formation of the complex.

There have yet to be any published studies of the separation of free RNA from the RNP complex. Although chromatographic separations are possible, the large RNP is likely to have low dynamic binding capacity and significant mass transfer limitations. Several recent studies have demonstrated that ultrafiltration can be used for the separation of glycoprotein complexes, formed by coupling a capsular bacterial polysaccharide to an immunogenic carrier protein (Emami et al. 2019), as well as pegylated proteins, formed by coupling a desired therapeutic protein to a polyethylene glycol chain (Molek and Zydney 2007). In both cases, the ultrafiltration membrane retained the large complex while allowing the process impurities (the unreacted polysaccharide, protein, and / or polyethylene glycol) to be removed in the permeate.

Almost all previous studies of RNA ultrafiltration have been focused on the behavior of relatively small RNA molecules. For example, in Chapter 4 we evaluated the transmission of linear and hairpin RNA (20 and 70 nucleotides in length respectively) through different ultrafiltration membranes. High transmission was achieved by operating at high filtrate flux to enhance

concentration polarization. However, the transmission of a 237 nucleotide RNA, with significant internal structural motifs, was less than 10%, suggesting that larger RNA, like the guide RNA used in CRISPR-Cas9 systems, may be difficult to clear through ultrafiltration membranes.

The objective of the work described in this chapter was to examine the potential of using ultrafiltration for the removal of excess RNA in the purification of functional RNP complexes. Initial filtration experiments were performed using purified Cas9 protein and a 40 kDa guide RNA to identify an appropriate membrane pore size as well as operating conditions that provided the required selectivity. A diafiltration process was then used for the separation of RNP from excess sgRNA, where the RNP was recovered in the retentate and the RNA was removed in the permeate. These results demonstrate that ultrafiltration could be an attractive technology for the purification of ribonucleoprotein complexes for use in gene editing technology.

5.2 Materials and methods

5.2.1 RNA and Cas9 preparation

A 40 kDa single guide RNA, comprised of a 100 nucleotide trcrRNA sequence and a 23 nucleotide target specific sequence, was synthesized from its respective DNA template (IDT Technologies, Coralville, IA), which was prepared from a gBlock fragment and amplified by PCR (*Section 2.1*). Figure 5-2a shows the expected minimum free energy structure (-42.10 kcal/mol) of the sgRNA determined using RNAfold (Lorenz et al. 2011).

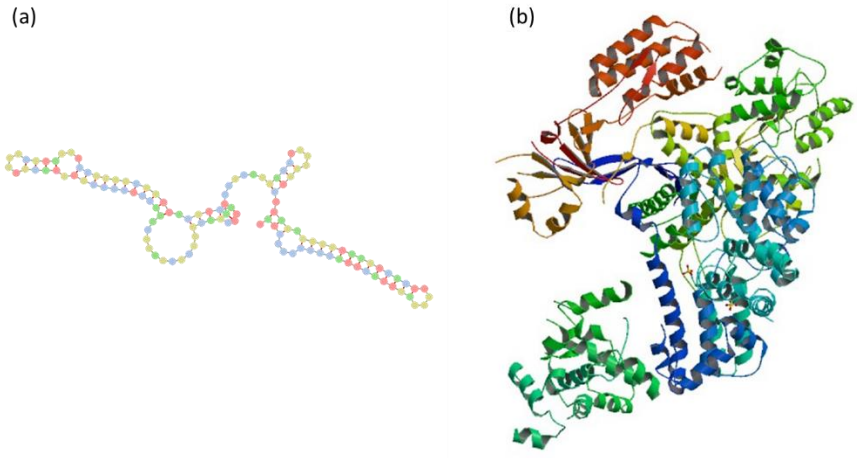

Figure **5-2**: Predicted structures of (a) sgRNA determined using RNAfold webserver http://rna.tbi.univie.ac.at/cgi-bin/RNAWebSuite/RNAfold.cgi and (b) *S. pyogenes* Cas9 protein https://www.rcsb.org/structure/4CMP (Jinek et al. 2014).

S. pyogenes Cas9 protein (Figure 5-2b) with a 6-His tag was produced in *E. coli* NiCo21 (DE3) cells transformed with pET-28a-Cas9-Cys plasmid (Addgene plasmid #53261; http://n2t.net/addgene:53261) (Ramakrishna et al. 2014). The Cas9 protein was purified using nickel affinity chromatography using an AKTA pure FPLC system using a 5 ml HisPur™ Ni-NTA (Thermo Fisher, Carlsbad, CA) column. The fractions containing the Cas9 were concentrated, dialyzed to remove imidazole, and buffer exchanged into 20 mM Tris + 300 mM NaCl buffer.

5.2.2 Ultrafiltration

Ultrafiltration experiments were performed using an Amicon 8010 stirred cell (MilliporeSigma, Billerica, MA), either unstirred or with the stirring speed set at 730 rpm using a VWR 205 Autostirrer. Biomax® 100 and 300 kDa nominal molecular weight cutoff polyethersulfone membranes were provided by MilliporeSigma. Data were obtained at constant

filtrate flux which was set using a peristaltic pump (Masterflex®, Vernon Hills, IL) placed on the permeate exit line, with fresh buffer supplied to maintain a constant volume in the stirred cell.

Initial experiments were performed with solutions of either sgRNA or Cas9 individually to simplify the analysis of feed and permeate samples. Stock solutions were diluted with 20 mM Tris buffer + 300 mM NaCl at pH 8.0 to the desired concentrations (7 µg/mL for the RNA and 15 µg/mL for the Cas9). The resulting solutions were loaded into the stirred cell, the pump was started, and 100 µL samples of the permeate were collected periodically for subsequent analysis. At the end of the experiment, the stirred cell was opened and a sample obtained to evaluate the RNA or Cas9 concentration in the retentate.

5.2.3 Diafiltration

Diafiltration is a simultaneous dilution / concentration process in which small impurities are removed (or washed) through a membrane while maintaining approximately the same concentration of a larger sized product. This study utilized diafiltration in dead-end mode to remove excess RNA from the RNP complex using a 300 kDa Biomax® ultrafiltration membrane in an Amicon 8010 stirred cell (MilliporeSigma, Billerica, MA) without stirring. The RNA was removed at a constant filtrate flux of 20 µm/s using a wash buffer containing 20 mM Tris + 300 mM NaCl at pH 8.0. Samples were collected periodically to determine the concentration of RNP and RNA in both the permeate and retentate using gel electrophoresis. Results are typically reported in terms of the number of diavolumes (N_D):

$$N_D = \frac{Cumulative\ filtrate\ volume}{Volume\ in\ stirred\ cell\ (retentate)} \tag{5-1}$$

Where the volume in the stirred cell is a constant.

5.2.4 Sample analysis

RNA concentrations were determined by fluorescence intensity using Ribogreen (cat# R11490) dye for concentrations between 0.02 – 0.5 µg/mL, as described in *Section 2.1.3*. An RNA Assay kit (cat# Q10213) was used for concentrations >0.5 µg/mL. Standards and samples (20 µL volume) were loaded to a 96-well black microplate and mixed with 200 µL of 1X Quant-it BR solution. Fluorescence intensity was evaluated using a Tecan microplate reader at 644/673 nm excitation/emission wavelengths.

The concentration of both Cas9 and the RNP complex were evaluated by a modified Bradford colorimetric assay (Zor and Selinger 1996; Ernst and Zor 2010). 100 µL samples and standards were loaded on 96-well clear microplates and incubated with 150 µL of Bradford reagent (Bio-Rad, Hercules, CA) for 15 min at 25 °C. Absorbance was measured at 590 and 450 nm using a Tecan microplate reader, with actual concentrations determined from appropriate calibration curves. Note that this method only determines the protein portion of the RNP.

Samples were also analyzed using gel electrophoresis, with pre-stained agarose gels for RNA visualization and SDS-PAGE for the Cas9 and RNP, respectively. Pre-stained agarose gels were formed using 1% agarose w/v and 0.5X SYBR gold dye in TBE buffer. Samples (33 µL) were incubated with 1 µL of 200X SYBR gold for at least 10 min (while being protected from light) before the addition of 7 µL of 6X loading dye. 25 µL of the resulting mixture were loaded into the wells of the gel. Gels were run for 60 min at 70 V with images obtained under UV light.

SDS-PAGE was conducted using Mini-PROTEAN® (BioRad, Hercules, CA) precast gels loaded with 20 µL of a digested protein sample. Digestion was performed by mixing 15 µL samples with an equal volume of BioRad Laemmli Sample buffer (Biorad, Hercules, CA) containing 355 mM of β-mercaptoethanol (Sigma Aldrich, St. Louis, MO), incubating at 95 °C for 5 min, and then loading into wells. Gels were run at 200 V for 30 min, fixed with 50% methanol v/v and 7% glacial

acetic acid v/v for 30 min, and incubated overnight in 60 mL of SYPRO Ruby stain (Thermo Scientific, Carlsbad, CA) on an orbital shaker. De-staining was performed using 10% methanol and 7% acetic acid solution for 1 h to reduce over exposure. Gels were rinsed with DI water and imaged under UV light.

5.2.5 Sample Characterization

The hydrodynamic radius of Cas9 was determined by Dynamic Light Scattering (DLS) using a Zetasizer Nano ZS (Malvern Panalytical, Worcestershire, England). The Cas9 was prepared in 20 mM Tris + 300 mM NaCl at pH 8.0 at a concentration of 3 mg/mL. 70 µL samples were loaded in a quartz cuvette, the system temperature was set at 25 °C, and the scattering intensity evaluated at 90° scattering angle. Fifteen 60 s measurements were obtained with three replicates, with the scattered intensity, size distribution, and hydrodynamic radius determined from the measured autocorrelation function using Zetasizer Software 7.13.

Multispectral Nanoparticle Track Analysis (NTA) was performed with a HORIBA ViewSizer® 3000 (HORIBA Instruments, Irvine, CA) to examine the extent of Cas9 aggregation. The instrument is equipped with three lasers (blue - 450 nm, green - 532 nm, and red - 635 nm); to simultaneously track and record the scattered light at different wavelengths. 10 videos with 300 frames per video were recorded per sample, with results obtained for both a fresh sample immediately after loading in the cell and then after stirring for 30 min using a magnetic stir bar.

5.3 Results and discussion

5.3.1 RNA ultrafiltration

Initial experimental studies were focused on evaluating the transmission of the guide RNA at different filtrate flux using Biomax® membranes that have previously demonstrated good performance for RNA separations as discussed in Chapter 3. Figure 5-3 shows results for both the Biomax 100 and 300 kDa membranes. The sieving coefficients through the Biomax 100 kDa membrane increase with increasing filtrate flux due to concentration polarization effects, in good agreement with the results in Chapters 3 and 4. As expected, the transmission is significantly greater for the Biomax 300 kDa membrane. For example, at a filtrate flux of 25 μm/s, the sgRNA sieving coefficient with the Biomax 100 is only 0.15 compared to more than 0.85 under identical conditions when using the Biomax 300 kDa membrane.

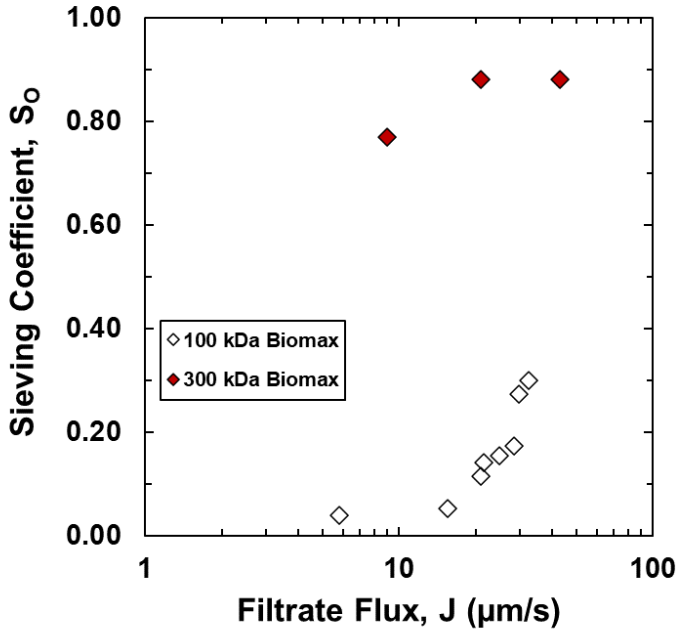

Figure **5-3**: Sieving coefficient as a function of filtrate flux for a 40 kDa guide RNA through 100 kDa and 300 kDa MWCO Biomax® membranes. sgRNA at a concentration of 0.5 μg/mL in a 20 mM Tris + 300 mM NaCl pH 8.0. Error bars were omitted when smaller than the size of the symbol.

All of the data in Figure 5-3 were taken "quickly", immediately after the washout of the hold-up volume in the stirred cell at a given value of the filtration flux. In order to explore the stability of the sgRNA filtration, an experiment was performed as a constant filtrate flux of 20 μm/s used the 40 kDa sgRNA at a concentration of 7.63 ± 0.16 μg/mL in a 20 mM Tris + 300 mM NaCl buffer at pH 8.0. Results for ultrafiltration through a Biomax® 300 kDa membrane are plotted in Figure 5-4 as a function of the volumetric throughput, defined as the cumulative filtrate volume divided by the membrane area during a 50 min experiment. The RNA concentration in the initial permeate sample (lower panel) was approximately 70% of that in the feed solution, although this initial data point may have had some dilution effect associated with buffer that was in the permeate line at the start of the experiment.. The filtration was performed with constant volume in the stirred

cell, which was maintained by continuous addition of buffer (without sgRNA) through the filtration. Thus, the permeate concentration decayed with time (or volumetric throughput) as the RNA is washed from the stirred cell.

The data in the lower panel of Figure 5-4 were used to calculate the RNA sieving coefficient, defined as the RNA concentration in the permeate divided by that in the stirred cell at the same point in the filtration. It was not possible to directly measure the RNA concentration in the stirred cell since the repeated opening / closing of the stirred cell would both disrupt the filtration and could potentially damage the membrane. Instead, the sgRNA concentration in the bulk solution within the stirred cell was evaluated from a simple mass balance:

$$C_B = C_{B,0} - \frac{q_P}{V}\int_0^t C_P\, dt \qquad (5\text{-}2)$$

where C_B is the concentration at time t and $C_{B,0}$ is the initial (feed) concentration. The first data point collected as the first drop from the permeate system is clearly diluted due to the remaining buffer from the hydraulic permeability and pump calibration tests, and thus was not used in the mass balance calculations. The permeate flow rate during the experiment was measured by timed collection as $q_p = 0.48 \pm 0.01$ mL/min, with no statistical variation over the course of the filtration. The integral in Equation (5-2) was evaluated numerically, with the calculated values of $S_o = C_P/C_B$ given in the upper panel of Figure 5-4. The observed sieving coefficient remained constant at a value of $S_o = 0.86 \pm 0.10$, indicating that there was no membrane fouling during the experiment. The calculated value of the bulk concentration at the end of the experiment ($C_B = 2.0 \pm 0.2$ µg/mL) was somewhat higher than that measured in a sample obtained directly from the stirred cell (1.57 ± 0.01 µg/mL), which could reflect some loss of RNA due to adsorption on / within the membrane.

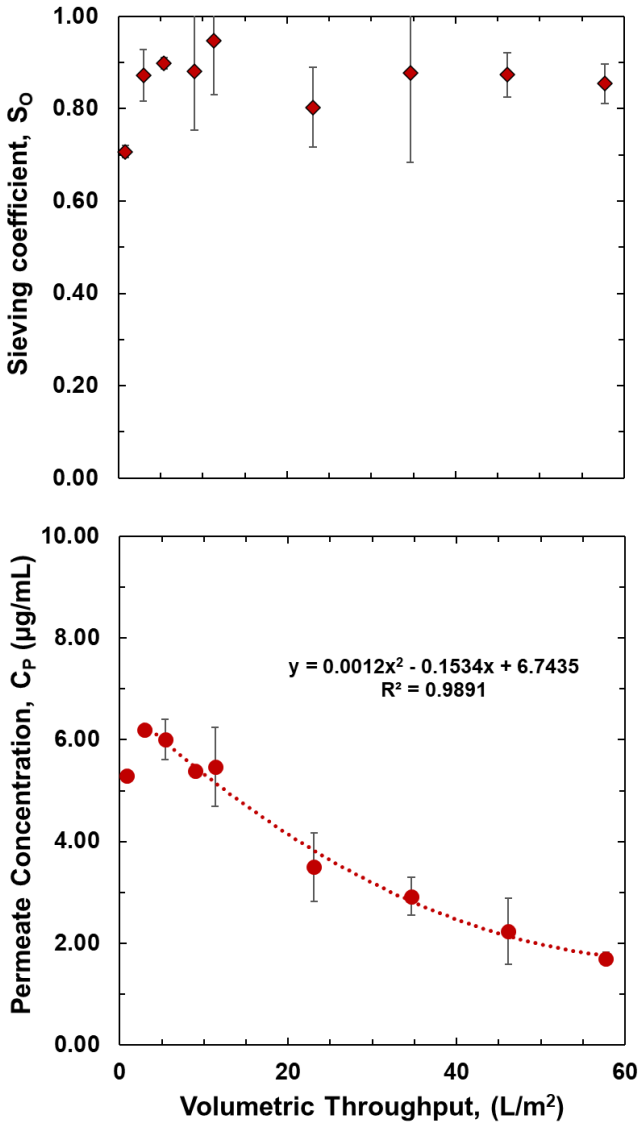

Figure **5-4**: Permeate concentration (lower panel) and calculated sieving coefficient (upper panel) during ultrafiltration of a 7.6 µg/mL sgRNA solution in a 20 mM Tris + 300 mM NaCl buffer through a 300 kDa Biomax® membrane at a constant filtrate flux of 20 µm/s. Error bars were omitted when smaller than the size of the symbol.

5.3.2 Cas9 ultrafiltration

Before examining the ultrafiltration behavior of the ribonucleoprotein complex, we decided to study the transmission properties of the *S. pyogenes* Cas9 protein; this eliminates any

complexities associated with the assays and / or intermolecular interactions between the RNP and any free RNA present in the system. Experimental data for the transmission of Cas9 through both the Biomax® 100 and 300 kDa membranes are shown in Figure 3 as a function of filtrate flux. The data were obtained by monotonically increasing the flux, beginning at the lowest value, with the system allowed to equilibrate at each filtrate flux. The sieving coefficients for the 100 kDa membrane were less than 0.04 at all filtrate flux, consistent with the very high retention of the 164 kDa protein. Somewhat higher transmission was obtained with the 300 kDa membrane, with the sieving coefficient increasing with increasing filtrate flux to a value of $S_o = 0.19$ at a flux of 46 μm/s.

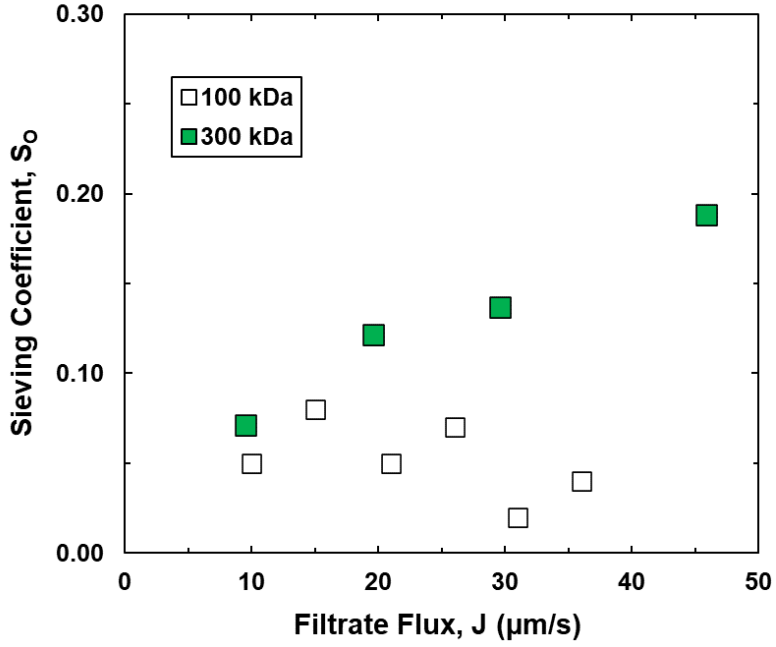

Figure **5-5**: Sieving coefficient as a function of filtrate flux for Cas9 protein through 100 kDa and 300 kDa MWCO Biomax® membranes. Samples were filtered using 20 mM Tris + 300 mM NaCl pH 8.0. Error bars were omitted when smaller than the size of the symbol.

The relatively high retention of the Cas9 protein by the 300 kDa membrane is somewhat surprising. Dynamic light scattering (DLS) results confirmed that the Cas9 was present as a monomer with mean diameter of 11 nm (Figure 5-6). This value of the diameter is consistent with previous studies showing that monoclonal antibodies with MW of approximately 150 kDa have an effective size of 10-12 nm as determined by DLS (Nobbmann et al. 2007).

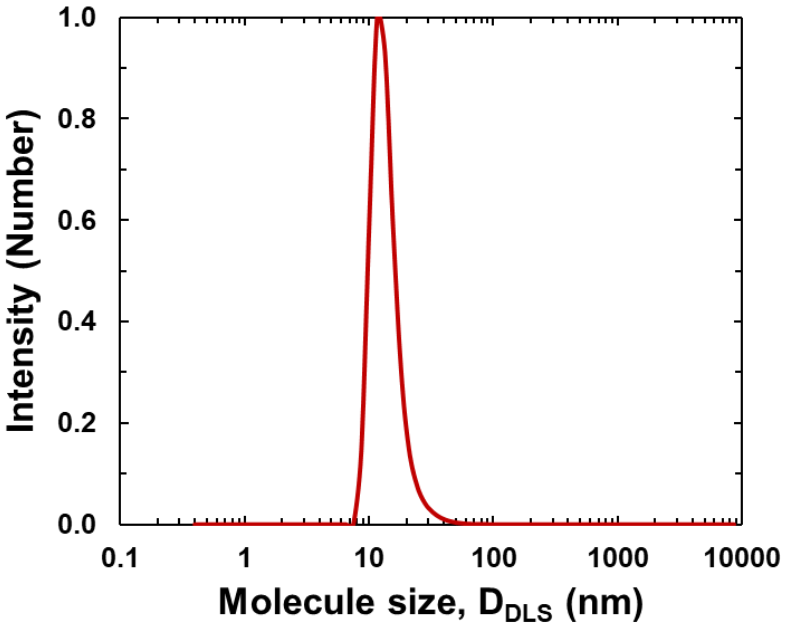

Figure **5-6**: Intensity distribution for a 3 mg/mL solution of Cas9 in 20 mM Tris + 300 mM NaCl at pH 8.0 determined by dynamic light scattering.

Subsequent filtration experiments with Cas9 showed very high retention by the 300 kDa membrane, with permeate concentrations below the detection limit of the Bradford assay (corresponding to $S_o < 0.01$). This high retention was apparently due to protein fouling either within and / or on the external surface of the membrane. Fouling inside the pores would clearly lead to a reduction in the effective pore size, while an external fouling layer would provide an additional resistance to Cas9 transport in series with that of the membrane.

The high degree of protein fouling observed during Cas9 ultrafiltration was apparently related to protein aggregation in the stirred cell. Previous studies have reported significant Cas9 aggregation at pH 8 (near the protein isoelectric point). The presence of aggregates was examined by nanoparticle tracking analysis, with a typical image of the scattered light from the protein sample

shown in Figure 5-7. The upper panel shows very little scattered light, consistent with a very low degree of aggregation. However, the sample obtained after stirring for 30 min (lower panel) shows a number of very large aggregates ranging to as much as 1000 nm in size, with the peak maxima at approximately 40 nm. The high polydispersity of these samples made it impossible to accurately determine the mean size of the aggregates.

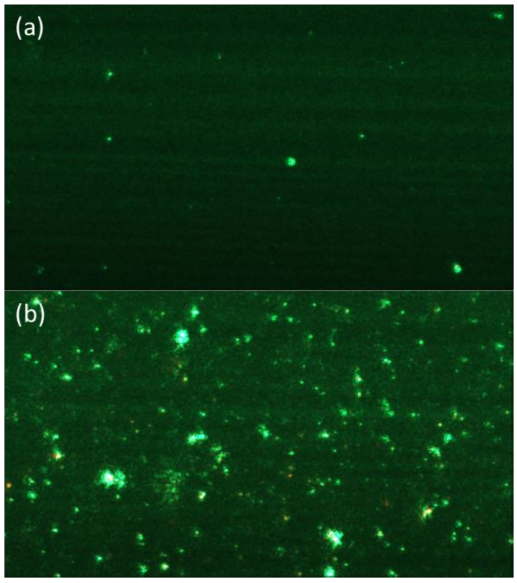

Figure **5-7**: Light scattering images from the Horiba Viewsizer 3000 NTA for a 3 mg/mL Cas9 solution in 20 mM Tris + 300 mM NaCl at pH 8.0. Images were obtained (a) before and (b) after stirring.

5.3.3 Unstirred filtration

As discussed above, stirring of the Cas9 solution causes significant protein aggregation, which is the likely cause of the low transmission seen in some experiments. We thus conducted a series of Cas9 filtration experiments with no stirring (magnet removed from stirred cell apparatus). Typical data are shown in Figure 5-8 for ultrafiltration of a feed solution with a Cas9 concentration of 15 µg/mL in 20 mM Tris buffer at pH 8.0 + 300 mM NaCl through a 300 kDa Biomax® membrane. Filtrate flux was maintained constant at 20 µm/s throughout the experiment. In this

case, the calculated values of the sieving coefficient (determined from the measured permeate concentrations with the bulk concentration evaluated by numerical integration of the mass balance) remained relatively constant at S_o = 0.05 throughout the 60 L/m^2 filtration (corresponding to an operation time of 1.5 h and 550 mg of Cas9 per m^2 of membrane area).

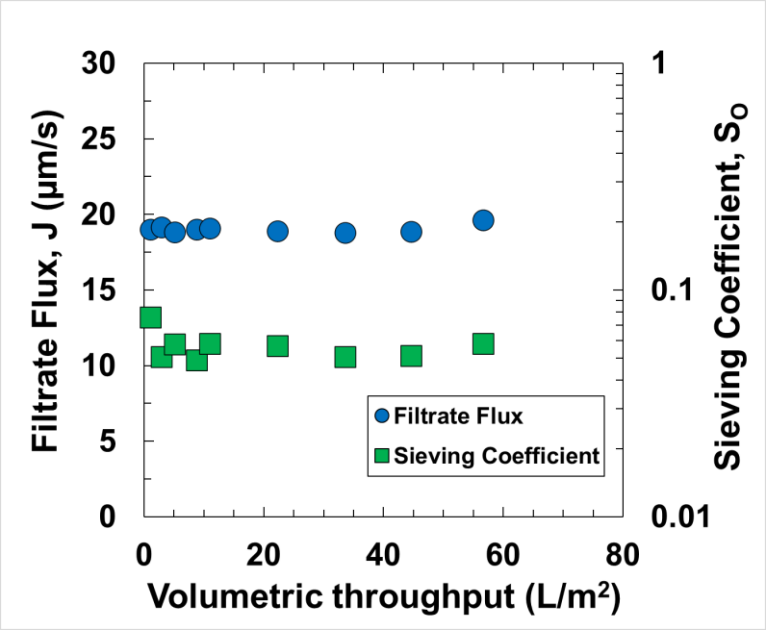

Figure **5-8**: Filtration profile for 15 µg/mL Cas9 through a 300 kDa Biomax® membrane. Constant filtrate flux of 20 µm/s and 20 mM Tris pH 8.0 + 300 mM NaCl buffer. Error bars were omitted when smaller than the size of the symbol.

The low observed sieving coefficient for Cas9 (S_O = 0.05) in comparison with the relatively high transmission of the sgRNA (*Section 5.3.1*) suggests that it would be possible to use ultrafiltration for the removal of the unreacted sgRNA from an assembled Cas9-sgRNA ribonucleoprotein complex, with selectivity values of more than 10. This is discussed in detail in the next section of this chapter.

5.3.4 RNP purification

The ribonucleoprotein complex was formed by incubating a mixture of Cas9 (15 µg/mL) and the sgRNA (7 µg/mL) for 30 min at room temperature. This corresponds to a 1:2 molar ratio; thus, the final solution should contain at least 3.5 µg/mL of free (excess) RNA. The resulting solution was loaded into a stirred cell and filtered through a Biomax 300 kDa membrane at a filtrate flux of 20 µm/s based on the results obtained in the earlier sections of this chapter. Fresh Tris buffer was added to the stirred cell to maintain a constant solution volume throughout the experiment.

The concentration of sgRNA and RNP in permeate samples obtained during the diafiltration were determined by agarose gel electrophoresis and SDS-PAGE, respectively, with results shown in the top and bottom panels of Figure 5-10. The different lanes are labeled with the number of diavolumes, equal to the ratio of the cumulative filtrate volume divided by the constant (feed) volume in the stirred cell. There was no evidence of RNP in any of the permeate samples (with the possible exception of a faint spot in the first permeate sample in the lane at 0.03 diavolumes in the upper panel). In addition, the intensity of the RNP band in the retentate sample obtained directly from the stirred cell at the end of the experiment was similar to that for the initial feed solution (first lane). The band for the free sgRNA in the first permeate sample was nearly as bright as that in the feed, with the subsequent samples becoming less intense over the course of the diafiltration. The sgRNA was undetectable in the bands for 0.92 diavolumes and higher, nor was there any evidence of sgRNA in the retentate sample obtained at the end of the experiment. The gels clearly demonstrate that the diafiltration process is able to effectively remove excess sgRNA from the RNP, with high recovery of the RNP in the final retentate solution.

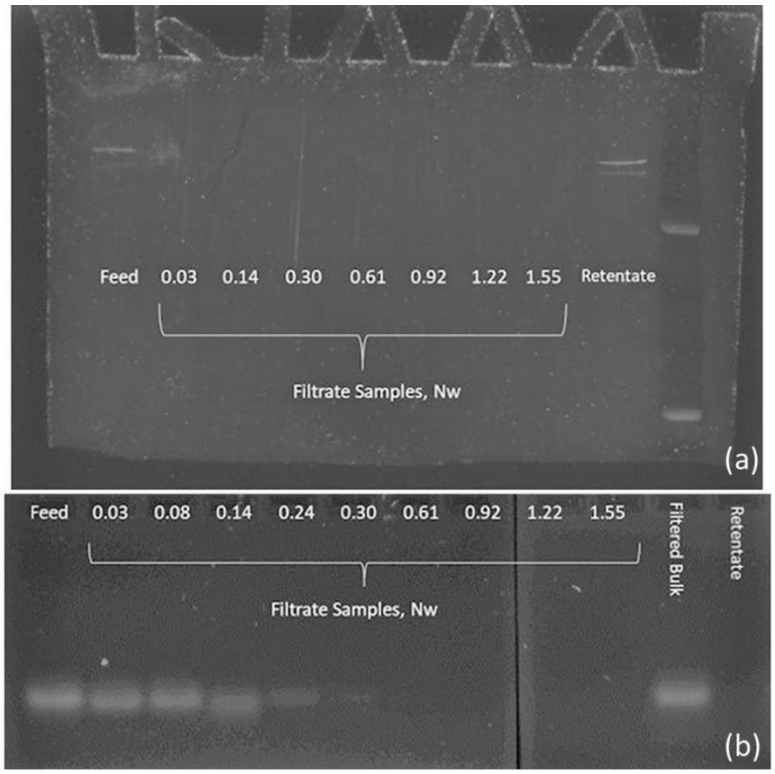

Figure **5-9**: Gel electrophoresis images for Ribonucleoprotein complex through a 300 kDa Biomax® membrane. Experiments performed at constant filtrate flux of 20 µm/s and 20 mM Tris pH 8.0 + 300 mM NaCl buffer. (a) SDS-PAGE for protein and (b) AGE for RNA visualization.

Although the gel electrophoresis provides qualitative evidence for the successful membrane separation process, it is difficult to quantify the yield and purification from the brightness of the bands in the gels. Thus, a separate experiment was performed using a mixture of RNA and RNP with a very large excess of sgRNA. Data for the normalized concentrations of both the RNP and free RNA are shown in Figure 5-10, with the RNP concentration determined directly from the Bradford assay based on the protein content. The RNP concentration decreases very slowly during the diafiltration, with the final normalized concentration of 0.92 ± 0.02 after 1.5 diavolumes. This would correspond to a sieving coefficient of $S_o = 0.06 \pm 0.02$, consistent with the

results in Figure 5-8. It was not possible to quantify the sgRNA since the highly sensitive fluorescent dye did not discern between free and associated sgRNA. The quantitative data for sgRNA (red) was obtained from an independent filtration experiment using a pure sgRNA solution.

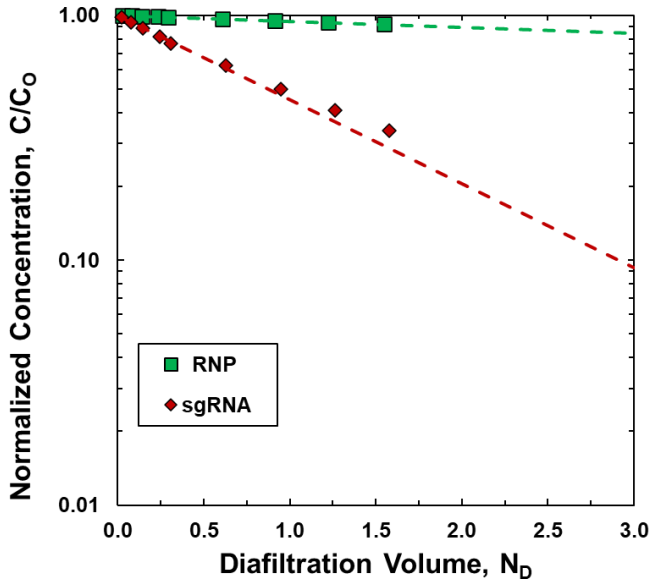

Figure **5-10**: Ribonucleoprotein (RNP) complex purity and diafiltration profile for sgRNA and RNP through a 300 kDa Biomax® membrane. Constant filtrate flux of 20 µm/s and 20 mM Tris pH 8.0 + 300 mM NaCl buffer.

The dashed lines in Figure 5-10 are model calculations determined by solution of the mass balance assuming constant sieving coefficient:

$$\frac{C_B}{C_{B,0}} = \exp\left(-N_D S_O\right) \tag{5-3}$$

The lines in Figure 5-10 were developed using S_o = 0.05 for the RNP and S_o = 0.86 for the sgRNA as determined by linear regression fits to the data on a semi-log plot. The 1.5 diavolume process removed nearly 70% of the sgRNA initially present in the system; Equation (5-3) predicts that this could be increased to more than 90% removal after 3 diavolumes and more than 98% after 5

diavolumes. Such a process would still provide more than 80% yield of RNP based on Equation (5-3) using the best fit value of the sieving coefficient for the RNP.

5.4 Conclusions

The results presented in this chapter provide the first demonstration that ultrafiltration can be used for the purification of the type of ribonucleoprotein complex of interest in gene-editing based on CRISPR technologies. Data obtained with the purified guide RNA showed sieving coefficients greater than 0.85 for extended filtration through the Biomax 300 kDa membrane at a filtrate flux around 20 μm/s. Corresponding data for both the pure Cas9 protein and for the RNP showed high retention ($S_o < 0.1$) under the same conditions. Experiments performed with a mixture of the RNP with excess sgRNA showed excellent removal of the free RNA (as determined by an agarose gel) with high recovery of the RNP (as determined by SDS PAGE). Limited quantitative data indicate that the diafiltration provided more than 70% removal of the sgRNA after only 1.5 diavolumes; this could be increased to more than 90% sgRNA removal using a 3 diavolume process. RNP yield was greater than 90%, clearly demonstrating the potential of using ultrafiltration as an attractive option for the purification of Cas ribonucleoprotein complexes.

The high degree of membrane fouling seen in some experiments with the Cas9 protein alone was surprising. This fouling was directly linked to the formation of large protein aggregates, which were easily seen in light scattering analysis after exposing the Cas9 to shear. This fouling could be eliminated by performing the ultrafiltration in an unstirred system. There was also no evidence of any fouling when using the RNP, suggesting that attachment of the guide RNA may provide some stabilization of the Cas9 protein. Note that previous studies have shown that coupling of guide RNA into the Cas9 protein causes structural changes in the RNP complex that protect it

from proteolysis (Jiang et al. 2015). Additional experiments will be required to fully identify the conditions associated with Cas9 aggregation, both for isolated Cas9 and for the RNP complex, including the effects of pumping and shear in the type of tangential flow filtration (TFF) systems used for large scale bioprocessing (either TFF cassettes or hollow fiber modules).

Chapter 6

Polyamines as additives for plasmid DNA membrane based separations

The majority of the work presented in this chapter is published in Li, Y., Manzano, I. and Zydney, A.L. (2019), Effects of polyamines on the ultrafiltration of plasmid DNA. *Biotechnology Progress*. 35: e2765. https://doi.org/10.1002/btpr.2765

6.1. Introduction

In addition to RNA, there has been considerable interest in the development of DNA-based therapeutics for both gene therapy and as vaccines (Han et al. 2009). DNA is much more stable than RNA, providing the potential for long-term treatment of genetic disorders. For example, there have been a number of attempts to develop gene therapies for treatment of hemophilia, with the DNA sequence for the required blood clotting factors transcribed into an appropriate vector that is then delivered to patients (Lusher et al. 2004; Park et al. 2015). DNA-based vaccines can potentially generate a longer term (and stronger) immunologic response since the DNA can produce the specific antigenic compound over an extended period of time, potentially eliminating the need for multiple injections (booster shots)(Ferraro et al. 2011a).

It is well established that the structure of plasmid DNA is a strong function of solution ionic conditions due to changes in intramolecular electrostatic interactions between the charged phosphate groups along the DNA backbone. Multivalent cations like spermine and spermidine play a critical role in compacting and controlling the structure of supercoiled DNA in living cells.

Polyamines are organic compounds having two or more amino groups ($-NH_2$). Spermidine (which contains 3 amine groups) and spermine (which contains 4 amine groups) are two naturally

occurring polyamines (Figure 6-1), both of which are synthesized in living cells via highly regulated pathways and are critical in controlling a variety of cellular activities (Kusano et al. 2008). In particular, the presence of physiological levels of polyamines (approximately millimolar) has been shown to inhibit topoisomerase catalyzed relaxation of negative supercoils in DNA (Peng and Jackson 2000). Several studies suggest that DNA supercoiling, and in turn its biological activity, are controlled by systematic regulation of the concentrations of these polyamines (Sato et al. 2005).

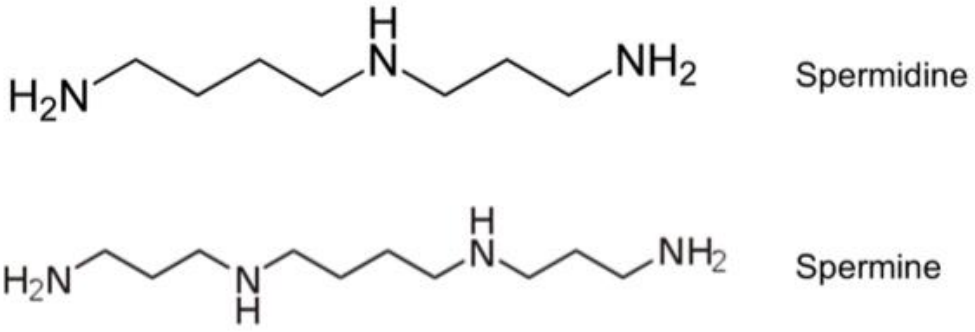

Figure **6-1**: Chemical structure of spermidine and spermine. The basic amino (NH_2) groups become protonated at physiological pH to become positively charged.

Polyamines can directly interact with DNA molecules in two ways. First, the positively charged amine groups can interact electrostatically with the negatively charged phosphates along the DNA backbone, similar to the interactions that occur with both mono- and di-valent cations (C. Ma and Bloomfield 1994). Cation binding is generally found to stabilize the right handed, B-form, double helix structure (Tabor 1962) and protect the DNA from damage due to radiation or oxidation (Ha et al. 1998). Second, polyamines can bind in the major and minor grooves of DNA, forming hydrogen bonds with bases from the opposing strands of the DNA double helix as revealed by recent crystal structures and infrared spectra of polyamine-DNA complexes (Jain, Zon, and Sundaralingam 1989; Tari and Secco 1995; Ouameur and Tajmir-Riahi 2004). This reduces denaturation of DNA and favors formation of writhes instead of unwinding of DNA. Shao et al.

(2012) used single molecule experiments to demonstrate that the presence of spermine or spermidine produced more compact plectonemes in DNA in the presence of high concentrations of monovalent salts. Theoretical models confirmed that binding of polyamines reduces the radius and increases the density of DNA supercoils.

Sato et al. (2005) studied the conformational transition of a 12.5 kbp supercoiled plasmid induced by spermine using fluorescence microscopy. The hydrodynamic radius of the plasmid decreased from more than 250 nm to less than 150 nm as the spermine concentration was increased from 0 to 10 μM; these concentrations are far too low to cause any significant increase in electrostatic shielding due to the increase in solution ionic strength. Murphy et al. (2003) showed that the equilibrium adsorption capacity of a Q-Sepharose anion-exchange resin for a 5.9 kbp supercoiled plasmid DNA at 600 mM NaCl was enhanced by up to 40% in the presence of 2.5 mM spermine. This was primarily due to compaction of the plasmid by spermine, which allowed the large plasmid to access the surface of small pores within the adsorbents.

Multivalent salts can also induce DNA condensation by neutralizing the high negative charge of the DNA, thereby reducing inter-helix electrostatic repulsion. Wilson and Bloomfield (1979) used the counter-ion condensation theory developed by Manning (1978) to calculate that DNA condensation occurs when approximately 90% of the DNA charge is neutralized. Inter-molecular bridging between DNA helices also helps promote condensation at low ionic strength (Bancroft et al. 1994). DNA condensation primarily occurs via intramolecular interactions at low DNA concentrations (below 5 μg/mL), with the resulting condensates having a compact spherical or toroidal shape as observed by both electron and atomic force microscopy (Chattoraj, Gosule, and Schellman 1978; Lin et al. 1998). The hydrodynamic radius of DNA condensates resulting from collapse of λ-phage DNA by spermine is 41±5 nm as determined by dynamic light scattering (Vijayanathan et al. 2001).

Although polyamines are known to have a significant effect on DNA structure, there is currently no information on the possible impact of these multivalent cations on the ultrafiltration of plasmid DNA. Previous studies by Laulippe and Zydney (Latulippe and Zydney 2008) have shown that DNA transmission increases with increasing concentrations of monovalent and divalent salts due to shielding of electrostatic interactions, but the polyamines have much more complex interactions with DNA. The objective of the work described in this chapter was to evaluate the effects of spermine and spermidine on the transmission of supercoiled, linear, and open-circular plasmid DNA during ultrafiltration and to explore the opportunity for enhancing the purification of specific plasmid isoforms by proper addition of these polyamines. Data were obtained using Biomax 300 kDa polyethersulfone membranes with different concentrations of the polyamines, both with and without other monovalent salts. The results clearly demonstrate that the addition of these polyamines dramatically reduces the transmission of different DNA isoforms, providing a large increase in selectivity for the separation of DNA from a model protein.

6.2 Materials and methods

6.2.1 Sample preparation

Ultrafiltration experiments were performed with gWIZ-GFP (5.7 kilobase pairs = kbp) and pMDY (9.8 kbp) plasmids in the supercoiled, open circular, and linear isoforms. These plasmids have been widely used as model DNA in previous studies of plasmid ultrafiltration (Latulippe and Zydney 2008, 2009, 2010). Plasmid gWIZ-GFP contains a reporter gene for green fluorescent protein (GFP), while pMDY contains a 6,840 bp insert of the mouse dystrophin cDNA. Both plasmids are constructed from the pBluescript® II KS+ plasmid vector and are typical of the

plasmid size used in gene therapy applications. DNA stock solutions were obtained as the supercoiled isoform from Aldevron (Fargo, ND) in Tris-EDTA (TE) buffer. Linear and open circular isoforms were prepared by enzymatic digestion of the supercoiled plasmid by appropriate restriction enzymes (see *Section 2.2.1* for details).

Plasmid DNA solutions were prepared in TE buffer with NaCl concentrations ranging from 1 to 100 mM. Spermine (MW= 202.34, ≥97%) and spermidine (MW=145.25, ≥97%) were obtained from SigmaAldrich (St. Louis, MO) and stored at -20°C prior to use. Stock solutions of TE buffer containing 10 mM spermine or spermidine with / without added NaCl were prepared and then slowly added to the DNA solution to obtain the desired final polyamine concentration. The DNA and polyamines were allowed to interact on a bench top orbital shaker for at least 1 h before use in the ultrafiltration experiment.

Limited ultrafiltration experiments were performed in the presence of bovine serum albumin (BSA) with molecular weight of approximately 66 kDa. BSA was purchased from Sigma Aldrich (St. Louis, MO) as a powder and then dissolved in 10 mM Tris- 1mM EDTA buffer + 10 mM NaCl. The solution was slowly agitated and then filtered through a 0.22 μm syringe filter to eliminate any protein aggregates. Supercoiled DNA and spermine were added to this solution immediately prior to the ultrafiltration experiment. BSA concentrations were determined from the absorbance at 280 nm as measured using a Tecan Infinite 200 Pro multimode microplate reader (Switzerland) based on appropriate calibration curves.

6.2.2 Ultrafiltration

Ultrafiltration experiments were performed in a stirred cell with Biomax 300 kDa polyethersulfone ultrafiltration membranes provided by MilliporeSigma (Bedford, MA). The stirred cell was filled with the DNA solution, and the stirrer was set to 600 rpm. Data were obtained

at constant pressure with the DNA concentration in the permeate and feed evaluated by fluorescence intensity using the Quant-iT PicoGreen dye (Invitrogen, Carlsbad, CA). Separate calibration curves were conducted at each polyamine concentration to account for the effects of the polyamine on the fluorescence intensity. Limited experiments were performed at constant filtrate flux by connecting a peristaltic pump to the filtrate outlet.

The use of spermidine concentrations above 50 μM caused significant interference with the PicoGreen assay; thus, samples were instead analyzed by Agarose Gel Electrophoresis. 1% agarose in TAE buffer gel was stained with GelStar® DNA dye for nucleic acid visualization. Samples were run for 90 min at 70 V, and images were obtained using the FluorChem FC2® imaging system from Cell Biosciences (Santa Clara, CA).

6.3 Results and Discussions

6.3.1 Supercoiled isoform

Figure 6-2 shows data for transmission of a solution containing 0.3 μg/mL of the supercoiled 9.8 kbp plasmid during filtration through the Biomax 300 kDa membrane. The DNA was dissolved in TE buffer containing 10 mM NaCl with different concentrations of spermine. DNA transmission was largely unaffected by the spermine for concentrations ranging from 0 to 10 μM. For example, the DNA sieving coefficients at a filtrate flux of 75 μm/s were $S_o \approx 0.84$ in both the 0 and 2 μM spermine solutions, while the sieving coefficient for DNA in the 10 μM spermine was $S_o = 0.74$. The increase in DNA transmission with increasing filtrate flux is due to flow-induced elongation in the converging flow field approaching the membrane pores (Figure 6-3, upper panel) as discussed elsewhere (Latulippe and Zydney 2009). In contrast to the data at low spermine concentrations, DNA transmission at spermine concentrations of 15 and 30 μM was

negligible over the entire range of filtrate flux, suggesting the presence of a threshold spermine concentration above which the plasmid is unable to elongate and pass through the pores of the membrane (Figure 6-3, bottom panel). Vijayanathan et al. (2001) also observed a critical spermine concentration of approximately 10 µM for DNA condensation in a 10 mM sodium cacodylate buffer. DNA condensates have been shown to have a toroidal shape with large hydrodynamic radius, e.g., 41 nm for a 48.5 kbp plasmid (Vijayanathan et al. 2001; Gosule and Schellman 1976), which could explain the high retention observed in these experiments.

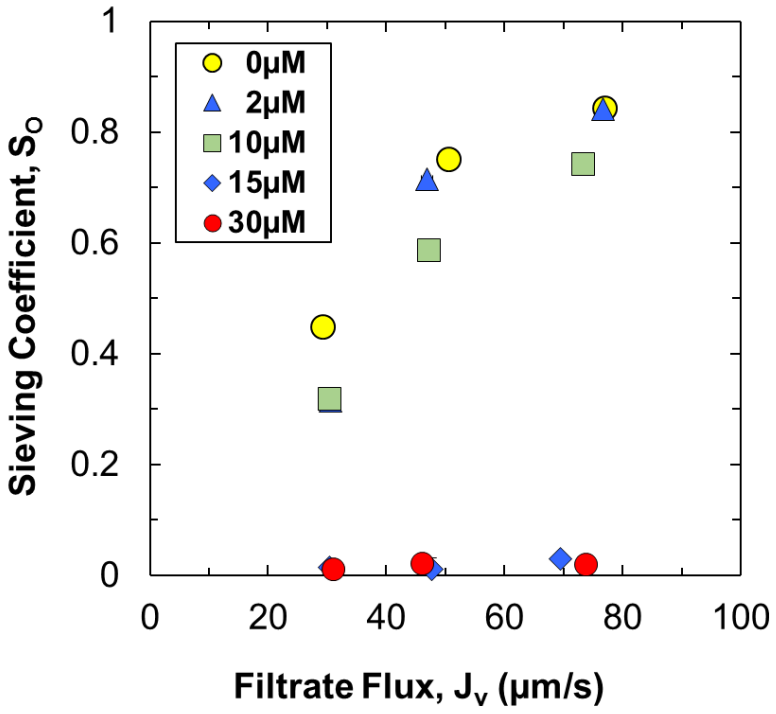

Figure **6-2**: Observed sieving coefficients for the supercoiled 9.8 kbp plasmid through a 300 kDa Biomax membrane as a function of filtrate flux for experiments performed with 0, 2, 10, 15, and 30 µM spermine in TE buffer containing 10 mM NaCl. The standard deviations, calculated from repeated measurements, were smaller than the size of the symbols and are thus omitted.

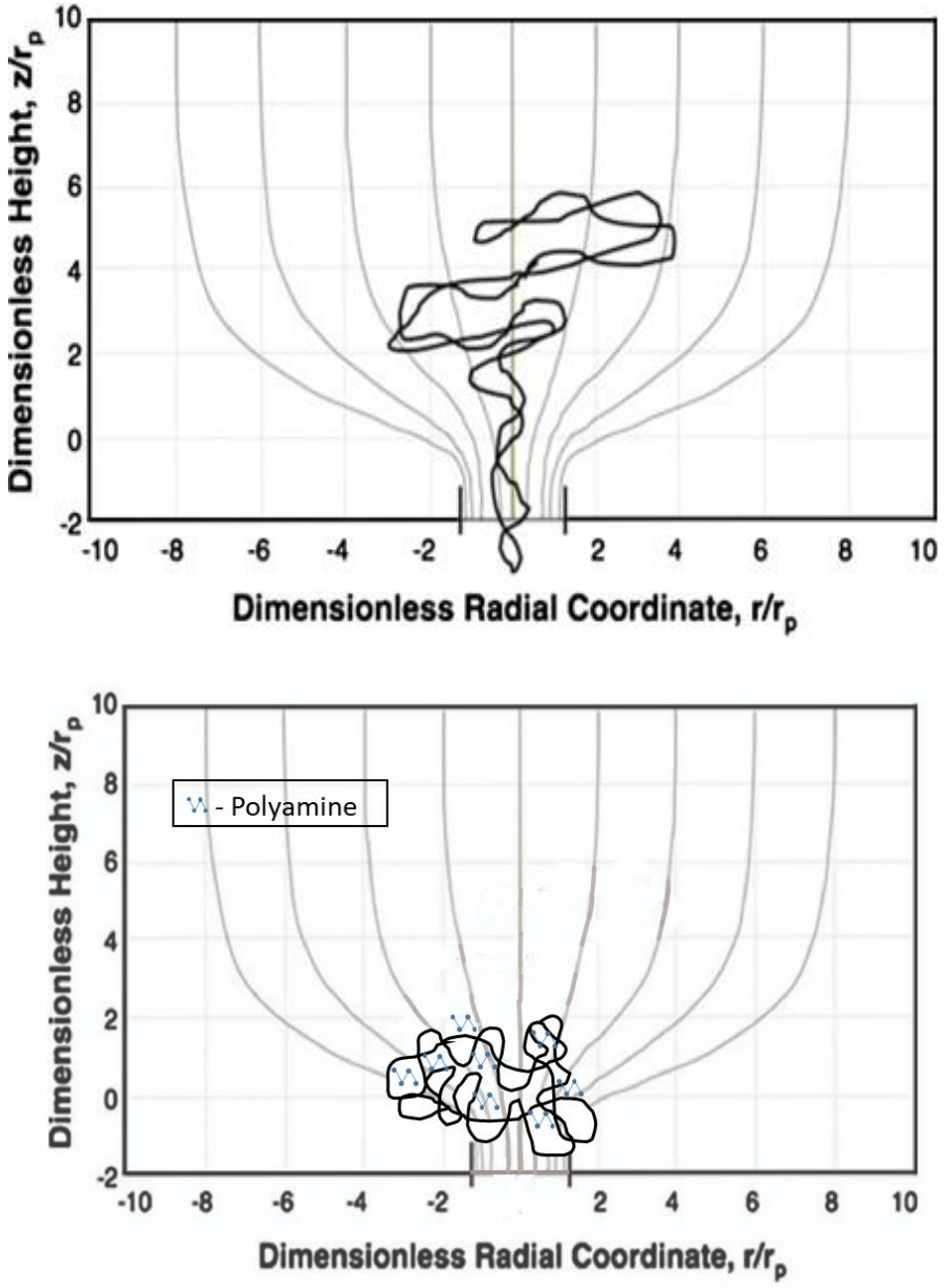

Figure **6-3**: Schematic of the flow induced elongation for plasmid DNA (upper panel) and effect of plasmid DNA compaction by polyamines (bottom panel).

Latulippe and Zydney (2008) showed that the addition of monovalent or divalent cations (Na^+ or Mg^{2+}) caused an increase in DNA transmission during ultrafiltration due to an increase in electrostatic shielding. This is exactly opposite to the effect of spermine seen in Figure 6-2,

suggesting that spermine alters DNA transmission by some type of direct binding to the DNA. A series of experiments were thus performed by varying the DNA concentration at a fixed value of the filtrate flux (50 µm/s) using a spermine concentration of 15 µM (Figure 6-4). DNA transmission increased with increasing DNA concentration, with the sieving coefficient at the highest DNA concentration (10 µg/mL) in the presence of 15 µM spermine (S_o = 0.74) nearly identical to the value obtained in the absence of any spermine (S_o = 0.71). Thus, at sufficiently high DNA concentrations, there is too little spermine to effectively compact the DNA.

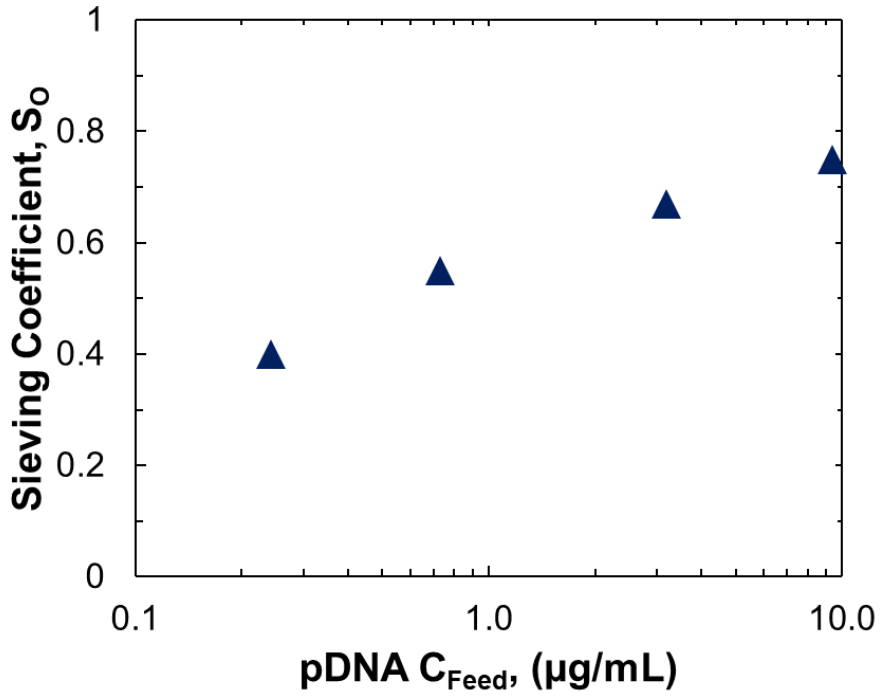

Figure **6-4:** Observed sieving coefficients for the supercoiled 9.8 kbp plasmid through a 300 kDa Biomax membrane as a function of DNA feed concentration for experiments performed with 15 µM spermine in TE buffer containing 10 mM NaCl. The standard deviations, calculated from repeated measurements, were smaller than the size of the symbols and are thus omitted.

Experimental results from a series of 5 independent experiments performed over a range of concentrations for both the pMDY (9.8 kbp) plasmid DNA and the spermine are shown in Figure 6-5 along with more limited data for the gWIZ-GFP (5.7 kbp) plasmid from a single experiment.

A fresh 300 kD membrane was used for each experiment, with hydraulic permeability values all within ±10%. The sieving coefficients obtained at a filtrate flux of 50 μm/s, are plotted as a function of the molar ratio of the spermine to DNA concentrations, where the molar concentrations were determined directly from the mass concentrations based on the molecular weights ($MW_{spermine}$ = 202 g/mol, $MW_{DNA} = N_{bp}$*660 g/mol where N_{bp} is the number of base pairs). The DNA sieving coefficient is nearly constant at a value of $S_o \approx 0.75$ for molar ratios below 10, with the DNA transmission decreasing with increasing values of the spermine:DNA ratio. There is considerable scatter in the data, particularly at large values of the spermine:DNA ratio, but in general the results for both plasmids collapse to a single curve when plotted in this manner, consistent with the presence of a direct binding interaction between the spermine and DNA that is independent of the DNA length. Note that the scatter in the data may well reflect the distribution of DNA-spermine complexes in the solution, with nearly complete retention of those plasmids that have sufficient numbers of bound spermine.

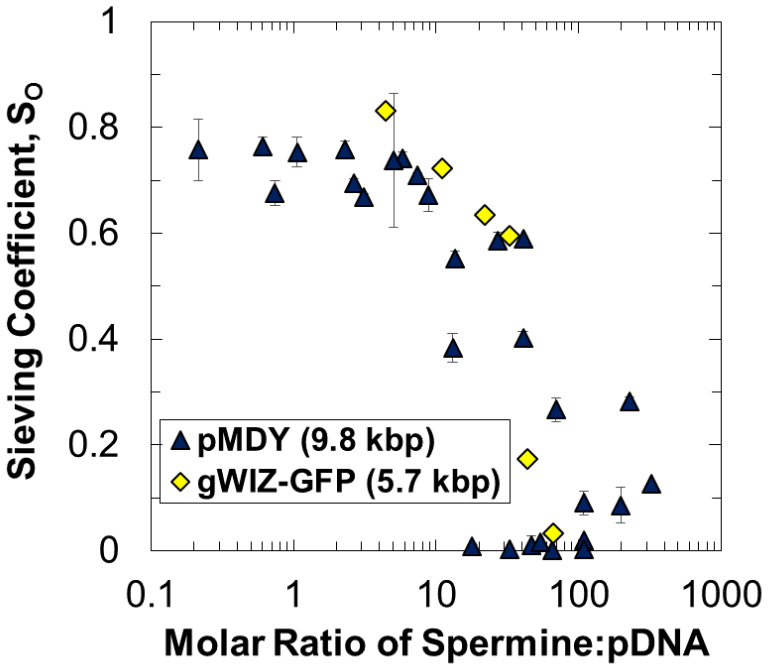

Figure **6-5**: Observed sieving coefficients for the supercoiled 5.7 and 9.8 kbp plasmids through a 300 kDa Biomax membrane at a filtrate flux of 50 µm/s. Data were obtained for DNA concentrations between 0.15 and 15 µM (0.1 to 10 µg/mL) and spermine concentrations between 0 and 30 µM. Results are plotted as a function of the ratio of the molar concentration of spermine to DNA. Error bars reflect the standard deviation calculated from repeat measurements of the DNA concentrations and are omitted when the size of the symbol is larger than the error range.

6.3.2 Salt effects on spermine binding

Since spermine directly alters the inter- and intra-molecular electrostatic interactions between the negatively-charged phosphate groups in DNA, a series of sieving experiments were performed using the supercoiled 9.8 kbp plasmid in TE buffer with different spermine and NaCl concentrations. Results are shown in Figure 6-6 for data obtained in the presence of 1, 10, and 100 mM NaCl. Increasing the concentration of the monovalent salt significantly increased the plasmid transmission, consistent with results obtained by Latulippe and Zydney (2008) and Li et al. (2016) The DNA transmission decreased with increasing spermine concentrations, becoming negligible at very high spermine concentrations. Note that the ionic strength (I) contributed by the 1, 10 and 100 µM spermine solutions, calculated as:

$$I = \frac{1}{2}\left(\sum_i c_i z_i^2\right) \tag{6-1}$$

where c_i and z_i are the concentration and valence of each ionic species, are approximately 8, 80 and 800 µM, compared to the 11.6 mM contributed by the TE buffer itself and the 1, 10, or 100 mM from the NaCl.

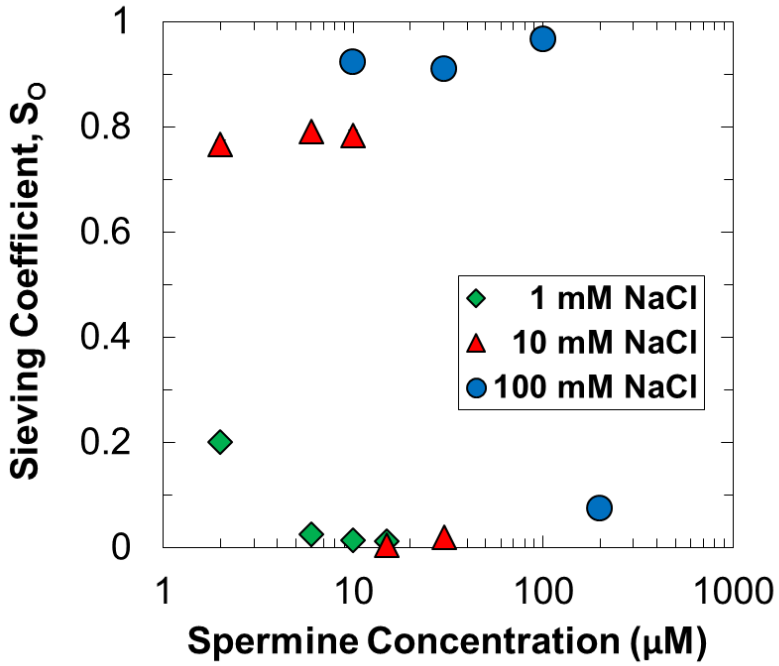

Figure **6-6:** Effect of spermine concentration on the observed sieving coefficients for the supercoiled 9.8 kbp plasmid through 300 kDa Biomax membranes at a filtrate flux of 50 µm/s. Data obtained in TE buffer containing 1, 10, and 100 mM NaCl. Error bars are not shown since they are all smaller than the size of the symbol.

The critical spermine concentration, defined as the spermine concentration at which the DNA sieving coefficient drops to nearly zero, was around 6 µM in the TE buffer with 1 mM NaCl but this increased to 15 µM for the buffer with 10 mM NaCl and to more than 200 µM for the 100 mM NaCl. This behavior is consistent with results obtained by Hoopes and McClure (1981) for DNA precipitation, in which the addition of 100 mM salt increased the concentration of spermine needed for DNA precipitation by more than 10-fold.

6.3.3 Effects of spermidine

Figure 6-7 shows the effects of spermidine, with three amine groups, on the transmission of the 5.7 kbp supercoiled plasmid at a constant filtrate flux of 30 μm/s (set using a peristaltic pump on the permeate line). Also shown for comparison are results obtained with the 9.8 kbp plasmid in the presence of spermine. The transmission of the two plasmids in the absence of any polyamines are nearly identical, consistent with results reported elsewhere showing that DNA transmission is nearly independent of the DNA length (Latulippe and Zydney 2009). The addition of spermidine initially causes a slight increase in DNA transmission, with the sieving coefficient then remaining constant at a value around $S_o = 0.68$ up to spermidine concentrations of at least 50 μM. This behavior is in sharp contrast to the results with spermine where the DNA transmission becomes negligible ($S_o < 0.01$) for spermine concentrations above 15 μM. Note that the 9.8 kbp plasmid would actually be expected to require a higher concentration of spermine than the 5.7 kbp plasmid to achieve the same change in sieving coefficient based on the data in Figure 6-4 showing that the molar ratio of spermine to DNA is the critical factor determining the DNA transmission.

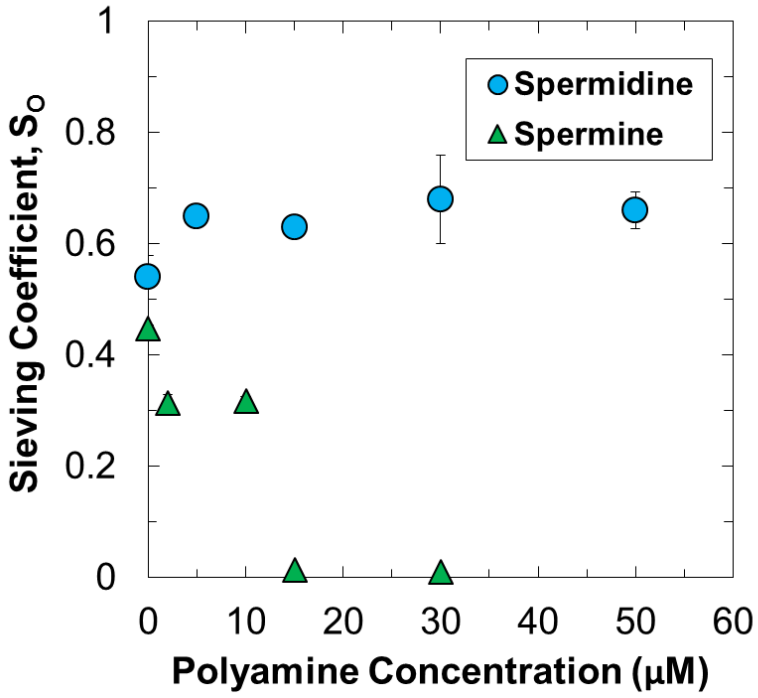

Figure **6-7:** Observed sieving coefficients for the 5.7 kpb plasmid (with spermidine) and the 9.8 kbp plasmid (with spermine) through a 300 kDa Biomax membrane at a constant filtrate flux of 30 μm/s. Experiments were performed using TE buffer containing 10 mM NaCl. Error bars reflect the standard deviation calculated from repeat measurements of the DNA concentration and are omitted when the size of the symbol is larger than the error range.

It was not possible to obtain data at higher spermidine concentrations using the PicoGreen assay. Thus, DNA samples from the feed, permeate, and retentate were analyzed by agarose gel electrophoresis as shown in Figure 6-8. The lower band is the 5.7 kbp plasmid (as determined from a DNA ladder). The plasmid appears at the same location in the gel for the samples from the feed (F), permeate (P), and retentate (R), confirming that the ultrafiltration caused no degradation of the plasmid. The upper band is likely a dimer or possibly some of the open-circular isoform; this band is completely retained under all conditions. The permeate band was easily visible at spermidine concentrations of 30 and 100 μM but was almost completely absent in the experiment performed

with 300 µM spermidine. This behavior is in good agreement with results from Thomas et al. (1991) showing that 280 µM spermidine was required for compaction of B-DNA.

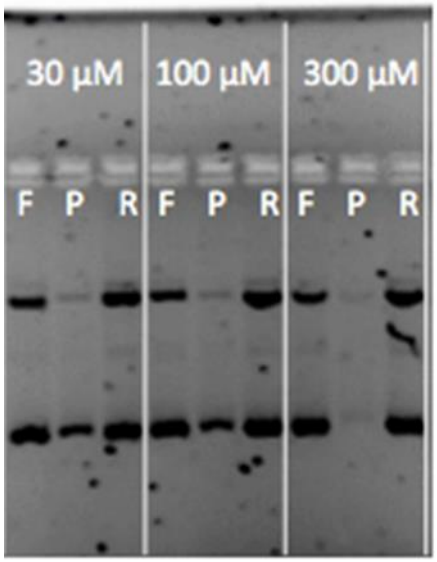

Figure **6-8**: Agarose gel for the 5.7 kpb plasmid in the feed, permeate, and final retentate for ultrafiltration experiments at spermine concentrations of 30, 100, and 300 µM. Lower band is the plasmid of interest.

6.3.4 Isoform separation

Ultrafiltration experiments were also performed with the linear and open-circular versions of the 9.8 kbp plasmid using the same Biomax 300 kDa membranes. Figure 6-9 shows the effect of spermine on the sieving coefficients for the different plasmid isoforms in TE buffer containing 10 mM NaCl at a constant filtrate flux of 50 µm/s. The greatest transmission was obtained with the linear isoform which has the greatest elongational flexibility followed by the supercoiled isoform; the open-circular isoform was highly retained by the membrane due to the difficulty in fully stretching the open ring (Latulippe and Zydney 2011). The transmission of the linear and

supercoiled plasmids both dropped to nearly zero when the spermine concentration was above 15 µM. The transmission of the open-circular isoform was very low over the entire range of spermine concentrations.

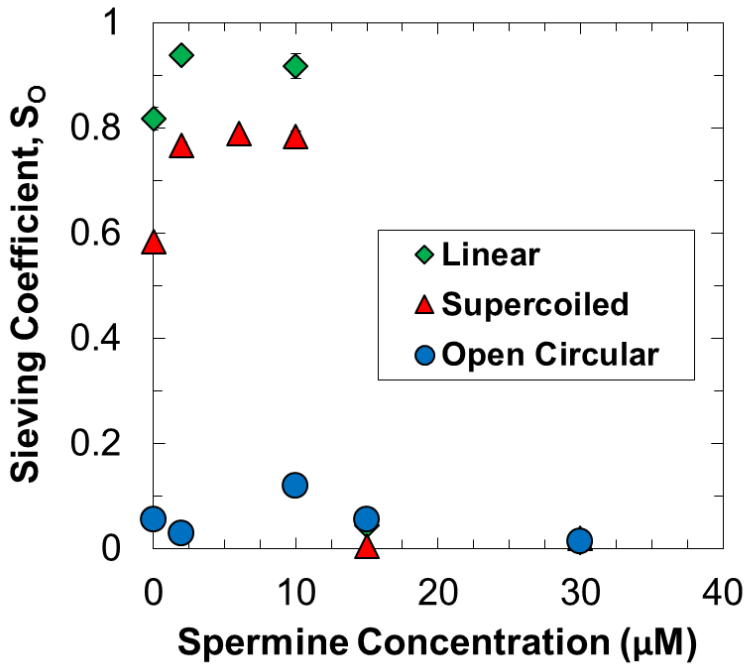

Figure **6-9**: Observed sieving coefficients for the different isoforms of the 9.8 kbp plasmid through a 300 kDa Biomax membrane as a function of spermine concentration. All initial DNA concentrations of 0.3 µg/mL using TE buffer containing 10 mM NaCl. Error bars since they are smaller than the size of the symbol.

Figure 6-10 shows the selectivity (ψ) between the supercoiled and open-circular isoforms at a filtrate flux of 50 µm/s, where the selectivity is defined as the ratio of the sieving coefficient of the supercoiled isoform to that of the open-circular isoform. The selectivity is the critical factor governing the design of membrane processes for the separation of partially retained species (Van Reis and Saksena 1997). The selectivity was maximum in the 10 mM NaCl solution in the presence of 2 µM spermine with $\psi = 19$, although this is only slightly larger than the selectivity in the absence

of any spermine ($\psi \approx 14$). The selectivity decreased significantly at high spermine concentrations due to the large reduction in transmission of the supercoiled plasmid under these conditions.

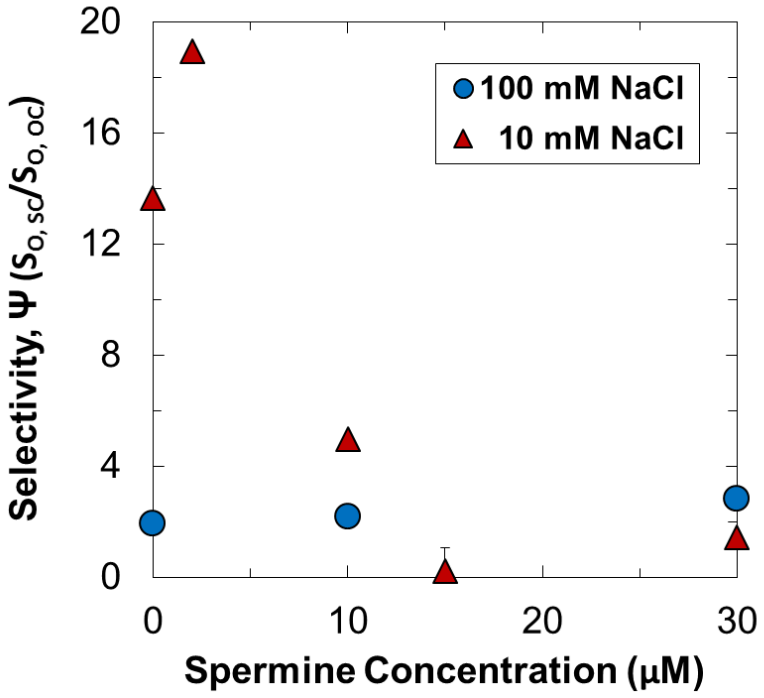

Figure **6-10:** Selectivity for separation of the supercoiled and open-circular 9.8 kbp plasmids through a 300 kDa Biomax membrane as a function of spermine concentration for experiments performed at filtrate flux of 50 μm/s in TE buffer containing 10 and 100 mM NaCl. Error bars reflect the standard deviation calculated from repeat measurements and are omitted when they are smaller than the size of the symbol.

6.3.5 DNA-Protein separation

In addition to the separation of DNA isoforms, ultrafiltration can also potentially be used to remove host cell proteins in the purification of plasmid DNA products or for the removal of DNA in the preparation of recombinant protein products. Ultrafiltration experiments were thus performed using a mixture of plasmid DNA and bovine serum albumin (BSA) as a model impurity

/ recombinant product. Results are summarized in Figure 6-11 for data obtained using a mixture with 0.5 µg/mL of supercoiled gWIZ-GFP plasmid and 1.7 mg/mL of BSA at a filtrate flux of 80 µm/s either with or without 30 µM spermine. The BSA and plasmid have very similar sieving coefficients in the absence of spermine (S_o = 0.89 and 0.85, respectively); thus, it would be impossible to separate these two species by ultrafiltration under these conditions. However, the transmission of the plasmid decreases to less than 0.01 upon addition of 30 µM spermine, in good agreement with the data in Figure 6-2 for the plasmid alone. The net result is that the Biomax 300 kDa membrane provides more than 100-fold selectivity between the plasmid and the BSA under these conditions, which would provide for a high resolution purification of either the plasmid (in the retentate) or the protein (in the permeate) using an appropriately designed membrane process.

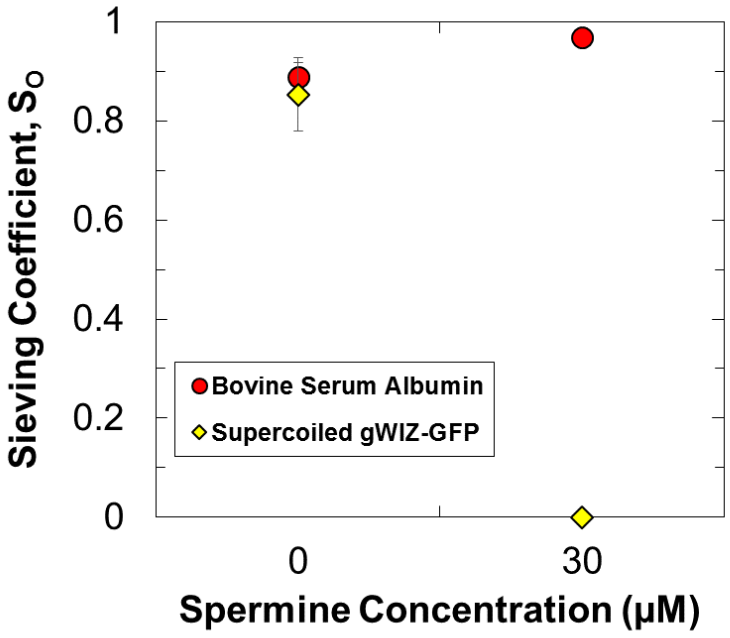

Figure **6-11**: Observed sieving coefficients for the supercoiled gWIZ-GFP plasmid (5.7 kbp) and BSA during ultrafiltration of a mixture through a Biomax membrane 300 kDa with 0 and 30 µM spermine. Data were obtained at filtrate flux of 80 µm/s in TE buffer containing 10 mM NaCl. Error bars reflect the standard deviation calculated from repeat measurements of the DNA / BSA concentrations.

6.4. Conclusions

The results presented in this chapter provide the first data for the effects of spermine and spermidine, small polyvalent amines, on the transmission of the supercoiled, linear, and open-circular plasmid isoforms through ultrafiltration membranes. Adding low concentrations of spermine (<10 μM) had minimal effect on plasmid transmission. However, higher spermine concentrations caused a dramatic reduction in DNA transmission, which is likely associated with the condensation of the DNA into a structure that can no longer be elongated by the flow field into the membrane pores. DNA condensation appeared to happen at a threshold spermine concentration, above which the plasmids became almost completely retained by the membrane. Much higher concentrations of the trivalent spermidine were required to induce similar compaction effects, in good agreement with literature data.

Transmission data for different size plasmids over a wide range of DNA and spermine concentrations collapse to a single curve when plotted as a function of the molar concentration ratio, consistent with the assumption that the change in transmission is due to polyamine binding (Matulis, Rouzina, and Bloomfield 2000). The addition of spermine led to a very large increase in selectivity for the separation of DNA from a model protein, which could potentially facilitate the purification of a plasmid DNA product or the removal of residual DNA from a recombinant protein. However, spermine had relatively little effect on the selectivity between the supercoiled and open-circular isoforms at low concentrations and caused a large reduction in selectivity at high concentrations. These results clearly demonstrate that polyamines like spermine and spermidine can be used to control DNA transmission during ultrafiltration, potentially enhancing the purification (or removal) of DNA during membrane separation processes.

Chapter 7

Effect of membrane orientation on DNA isoform separation in TFF

7.1 Introduction

As discussed in Chapter 6, membrane processes are particularly attractive for the purification of DNA since they eliminate the diffusional mass transfer limitations in chromatographic processes and they employ mild operating conditions without the need of harsh chemicals as those used in extraction or precipitation. However, previous studies have shown that membrane fouling can often limit the performance of the filtration process (Carroll 2001; Borujeni and Zydney 2014). A number of strategies have been developed to reduce the extent of fouling, including the use of stirring / or high shear rates, adjusting the ionic strength to reduce interactions between the feed components and the membrane, and operating at low filtrate flux to reduce the accumulation of retained solutes at the membrane surface, among others. Other groups have examined the use of membrane surface modification, backflushing, and ultrasound / vibrations, particularly in the context of wastewater treatment (Saqib and Aljundi 2016; Kochkodan and Hilal 2015; Yalcinkaya et al. 2020) and the purification of biologics (Hadidi and Zydney 2014; H. Ma et al. 2001; Ahmad et al. 2012).

The work presented in Chapter 6 and the extensive studies by Latulippe and Zydney (2009, 2010) have demonstrated the DNA transport through small pore size ultrafiltration membranes occurs by elongation in the converging flow field that occurs as the flow approaches the individual pores in the membrane surface. The extent of elongation is a function of both the filtration velocity and the membrane pore size. Li, Borujeni and Zydney, (2015) showed that it was also possible to control the extent of elongation by first passing the plasmid through a larger pore size pre-filter. This “preconditioning” not only made it easier for the DNA to pass through the membrane pores at

a given filtrate flux, it also significantly reduced the extent of membrane fouling by minimizing the probability of the DNA becoming trapped at the entrance to the pore. Since most ultrafiltration membranes have an asymmetric structure, with a tight selective skin layer on top of a more microporous support, it was possible to accomplish this preconditioning by simply using these membranes in the reverse orientation, i.e., with the selective skin oriented away from the feed as shown schematically in Figure 7-1.

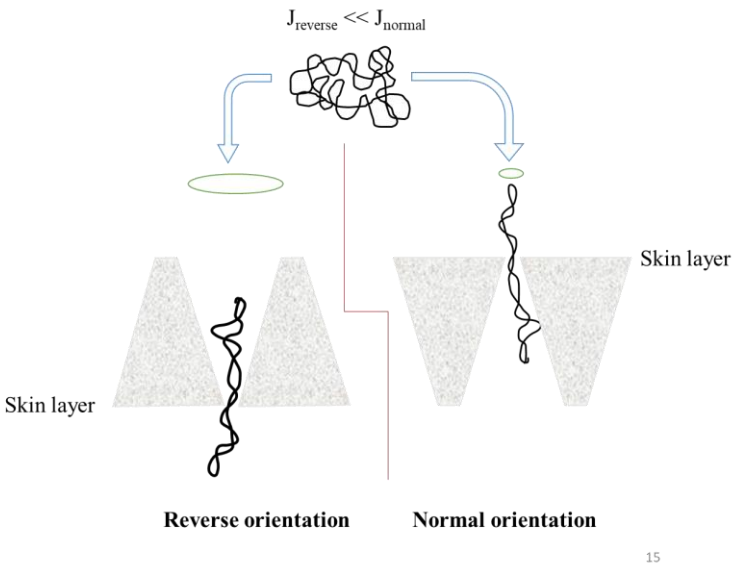

Figure **7-1**: Plasmid DNA elongation during ultrafiltration in normal and reverse orientation.

However, all of the preconditioning experiments conducted by Li et al. (2015) were performed using small flat sheet membrane discs, while large scale membrane processes are typically performed using tangential flow filtration devices. The objective of the work described in this chapter was to evaluate the potential of using commercially available hollow fiber TFF modules with the flow in the reverse orientation (from open region to the selective layer) for the separation of the different plasmid DNA isoforms.

7.2 Materials and methods

Ultrafiltration experiments were performed with a 5.7 kbp gWIZ-GFP plasmid DNA in the supercoiled and linear isoforms. The plasmid feed solutions were prepared at 0.3 μg/mL concentration in 10 mM Tris buffer with 1 mM EDTA at pH 7.5 with 150 mM NaCl. The linear isoform was obtained by enzymatic digestion of the supercoiled gWIZ-GFP. DNA concentrations were determined by fluorescence assay using the Quant-it PicoGreen® dye (see *Section 2.2*). Since PicoGreen® cannot distinguish between the different isoforms of the double stranded DNA; thus, experiments were performed independently with purified solutions of the individual isoforms.

Data were obtained in MidiKros modules containing modified polyethersulfone (mPES) hollow fiber membranes with a filtration area of 20 cm^2 (Repligen, Rancho Dominguez, CA, catalog number C02-E050-05-S). The membrane permeability was evaluated using TE buffer (without any added DNA) by measuring the filtrate flux over a range of transmembrane pressure (TMP):

$$TMP = \frac{P_i + P_o}{2} - P_f \tag{7-1}$$

where P_i, P_o and P_f are the inlet, outlet, and permeate pressures, all measured by pressure gauges connected immediately before or after the module entrance / exit ports.

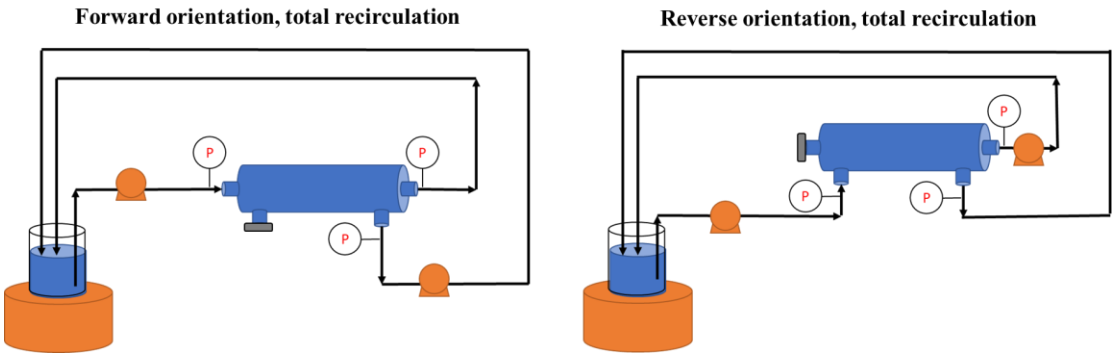

Figure **7-2**: Total recirculation operation of the hollow fiber membrane module in both the forward (left) and reverse (right) orientations.

Approximately 50 mL of a 0.3 µg/mL solution of DNA was added to a solution reservoir and fed to the hollow fiber module at a constant rate of 50 ml/min. The system was operated in a total recycle mode to reduce the volume of pDNA required for the experiment (Figure 7-2). The feed was either directed in through the fiber lumens (forward flow orientation) or in through the shell region (reverse flow orientation). In both cases, a second peristaltic pump was used to maintain a constant filtrate flux.

Initial screening experiments were performed over a range of filtrate fluxes, with the pDNA recirculated through the system for at least 3 min before collecting a permeate sample to insure steady state operation. Subsequent experiments were performed over extended operation times (up to 60 min) at a constant filtrate flux, with permeate samples collected periodically over the course of the experiment. The filtrate flux was then increased by manually adjusting the setting on the permeate pump without stopping / disrupting the operation of the filter.

7.3 Results and discussion

Figure 7-3 shows data for the sieving coefficient for the linear and supercoiled gWIZ-GFP plasmid over a range of filtrate flux in both the forward flow (red symbols, FW) and reverse flow (green symbols, RW) orientations. The transmission of both isoforms increases with increasing filtrate flux, consistent with previous studies of the ultrafiltration of pDNA (Latulippe, Ager, and Zydney 2007). The sieving coefficients were slightly higher for the linear plasmid compared to those for the supercoiled plasmid. For example, when operating in the forward orientation at a filtrate flux value of 45 μm/s, the sieving coefficient for the linear isoform is $S_o = 0.1$, whereas there was essentially no supercoiled plasmid detected in a permeate sample obtained under the same conditions. The sieving coefficients with the reverse orientation are markedly larger for both isoforms with sieving coefficients >0.80 at the same 45 μm/s filtrate flux. Data obtained at a filtrate flux of 20 μm/s with the reverse flow gave $S_o = 0.9$ and 0.6 for the linear and supercoiled isoforms, respectively, while $S_o < 0.02$ for both isoforms in the forward flow orientation at the same filtrate flux.

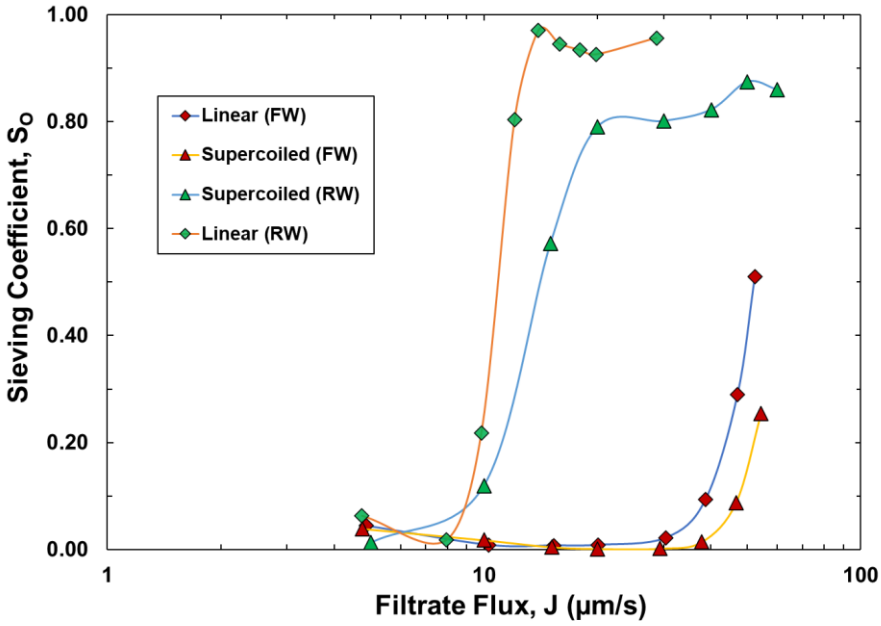

Figure **7-3**: Sieving coefficients of linear and supercoiled isoforms through a 50 kDa PES MidiKros® hollow fiber membranes in forward and reverse flow orientations.

The effect of membrane orientation on DNA transmission seen in Figure 7-3 is in good agreement with earlier studies using small flat sheet membrane discs (Y. Li, Borujeni, and Zydney 2015). Thus, the presence of the tangential flow seemed to have little effect on the ultrafiltration behavior of the plasmid DNA.

Based on the results in Figure 7-3, it seemed that it might be possible to obtain significant separation between the linear and supercoiled isoforms by operating the hollow fiber module in the reverse flow orientation at a filtrate flux of approximately 11 µm/s (equal to 40 L/m^2/h) with results shown in Figure 7-4 for two separate experiments, one using the linear isoform and then one using the supercoiled gWIZ-GFP plasmid. The results for the linear isoform are surprising, with the sieving coefficient increasing with increasing volumetric throughput. The low values of the transmission seen at the start of this experiment could be due to dilution effects associated with the

buffer initially present in the fiber lumens, or it could be due to the loss of some DNA that is captured in some of the pores of the membrane; there was no evidence of any fouling based on the stable transmembrane pressure throughout the filtration. The experiment was stopped after processing 26 L/m^2 of permeate. The entire system was then flushed with TE buffer containing 150 mM NaCl before filling the feed reservoir with a solution of the supercoiled gWIZ-GFP at a concentration of 0.3 µg/mL. The observed sieving coefficient of the supercoiled plasmid at the start of the experiment was slightly greater than 0.4, which is much higher than anticipated based on the data in Figure 7-3. It is possible that this initial spike in DNA transmission is due to the release of previously trapped linear DNA that might have remained in the system. The sieving coefficient of the supercoiled plasmid decreased during the initial stage of the filtration, attaining a nearly steady value of $S_o = 0.1$. This would correspond to a selectivity of nearly 5-fold, where the selectivity is defined as the ratio of the sieving coefficient of the more permeable species (in this case the linear isoform) to that of the more highly retained component (in this case the supercoiled isoform).

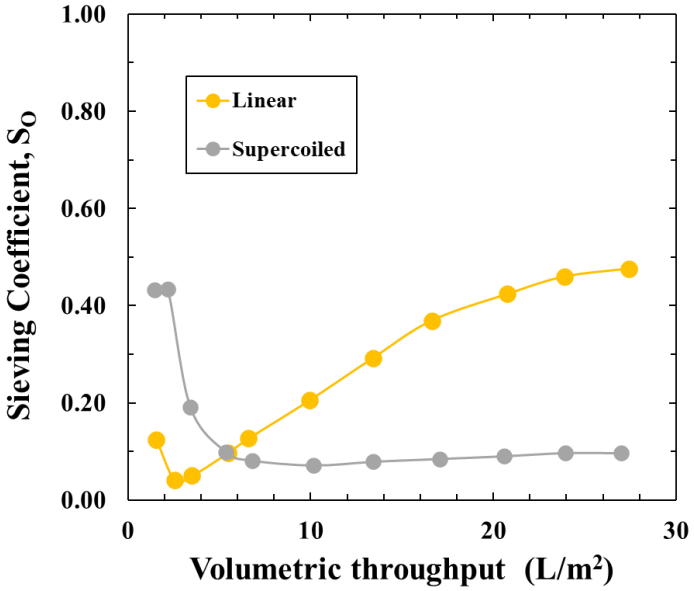

Figure **7-4**: Sieving coefficient of the linear and supercoiled isoforms through a 50 kDa mPES MidiKros hollow fiber module in reverse orientation at a constant filtrate flux of 11 µm/s.

Since the microporous support structure of the hollow fiber membranes have micron-sized pores, the DNA should have little difficulty entering these large pores even when operating at low filtrate flux. Thus, the high retention of the supercoiled plasmid would indicate that a significant amount of the plasmid is *trapped* in the microporous support, most likely near the interface between the large macropores and the very small (<10 nm) pores in the selective skin layer. In order to determine if it was possible to recover this trapped plasmid, an experiment was performed using a 0.3 µg/mL solution of the supercoiled pDNA solution in TE buffer + 150 mM NaCl. The plasmid was initially filtered through the module at a relatively low filtrate flux (10 µm/s) for 30 min. The filtrate flux was then rapidly increased to a value of 25 µm/s by manual adjustment of the permeate pump, with the filtration continued for an additional 30 min without any disruption to the feed flow, with results summarized in Figure 7-5.

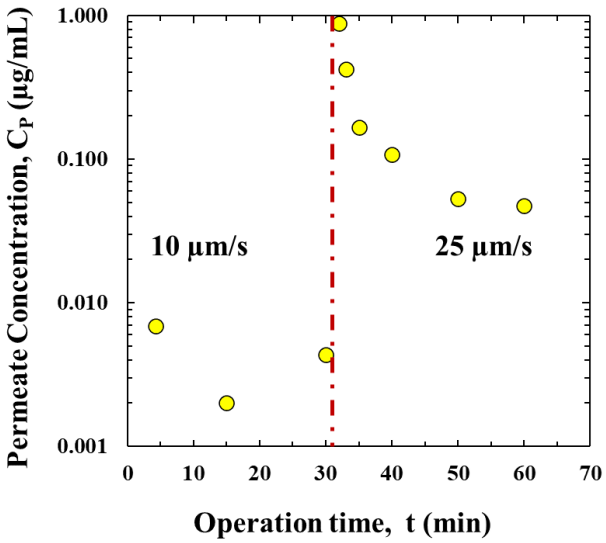

Figure 7-5: Effect of filtrate flux effect on the measured permeate concentration for filtration of the supercoiled gWIZ-GFP pDNA through a 50 kDa mPES MidiKros® hollow fiber in reverse orientation.

The permeate concentrations for all samples collected during the initial 30 min filtration were all <0.01 µg/mL, corresponding to a sieving coefficient of S_o < 0.03, which is somewhat smaller than the data in Figures 7-3 and 7-4. The increase in filtrate flux caused an immediate increase in DNA transmission, with the initial permeate sample having a concentration that is approximately three times that in the feed. This very high permeate concentration clearly demonstrates that there is significant recovery of the plasmid DNA that had initially been trapped (and thus accumulated) within the porous matrix of the hollow fiber membrane during operation at low filtrate flux. The large increase in transmission upon increasing the filtrate flux is due to the increased elongation of the supercoiled plasmid at high filtration velocity as seen in Figure 7-3. The permeate concentration then decreased with time as the trapped DNA was washed through the

membrane, with the sieving coefficient approaching a value of approximately 0.2 at long times. This steady-state transmission is considerably smaller than the sieving coefficients seen in Figure 7-3; the reason for this discrepancy is unclear.

7.4 Conclusions

The data presented in this chapter provide the first demonstration that it is possible to at least partially recover previously trapped DNA from within the macropores of a hollow fiber membrane when used in the reverse flow orientation (selective skin oriented away from the feed). This is a critical result if these hollow fiber membranes are to be used for purification of the desired supercoiled isoform from a feed stream containing a mixture of the linear and supercoiled DNA. This would be accomplished using a two-phase diafiltration process. In the first phase, the feed would be circulated through the hollow fiber module at low filtrate flux, allowing the linear isoform to be gradually washed through the membrane while retaining the supercoiled isoform in a diafiltration process; a sufficient number of diavolumes would be used to reduce the concentration of the linear plasmid to below a desired target value. At this point, the filtrate flux would be increased so that the supercoiled plasmid that had previously been "trapped" within the microporous support could be recovered in the permeate. High degrees of recovery of the supercoiled plasmid could then be obtained by continuing the diafiltration for an appropriate number of diavolumes, with the supercoiled plasmid washed through the membrane during the second phase of the diafiltration. The final purified product would have relatively little linear DNA since the linear isoform would have been largely removed in the first phase of the diafiltration. Additional studies would clearly be needed to quantify the effectiveness of this two-phase diafiltration process for purification of supercoiled plasmids.

Chapter 8

Conclusions and recommendations for future work

8.1 Conclusions

There is growing interest in using both RNA and DNA as therapeutic molecules, which will place significant pressures on the development and scale-up of appropriate separation processes for the purification and isolation of these nucleic acids. One attractive potential method for RNA / DNA purification is ultrafiltration using semipermeable membranes. However, there are still considerable uncertainties regarding the key factors governing the ultrafiltration behavior of these nucleic acid therapeutics. The experimental studies presented in this thesis provide some of the first quantitative studies of RNA ultrafiltration, providing a framework for the analysis and design of membrane filtration systems for RNA purification, while also extending our understanding of DNA ultrafiltration.

The results presented in Chapter 3 with Torula yeast RNA demonstrated that RNA transmission increases with increasing filtrate flux, with the observed dependence of the flux being in good agreement with predictions of the classical stagnant film model for concentration polarization. Surprisingly, much greater fouling was observed during RNA filtration through cellulose membranes, which is likely due to interactions between the ribose sugars in the RNA and the glucose monomers in the cellulose. Relatively little fouling was seen with polyethersulfone (PES) membranes due to electrostatic repulsion between the negatively-charged RNA and the negatively-charged PES. These results clearly demonstrate that it should be possible to use ultrafiltration to remove residual RNA in the permeate while recovering a large biotherapeutic (either a recombinant protein product or potentially a large plasmid DNA) in the retentate.

The experiments in Chapter 4 examined the ultrafiltration of four different RNA molecules with well-defined structural motifs; these are the first data ever presented examining the effect of different RNA structures on the ultrafiltration behavior. The transmission of the hairpin RNA is considerably larger than that of the linear RNA with equivalent number of nucleotides, consistent with the smaller effective size of the hairpin RNA as determined by both dynamic light scattering and migration of the RNA in an agarose gel. The transmission of the Linear-20 and Hairpin-70 RNA were very similar, in good agreement with the agarose gels, suggesting that migration through the gel may provide a better indication of the ultrafiltration behavior than the RNA radius determined by DLS. RNA transmission also increases upon the addition of 100 mM NaCl, which appears to be due to a combination of changes in effective size and a reduction in electrostatic repulsion between the negatively-charged RNA and the negatively-charged membranes.

The addition of urea also had a large effect on RNA transmission for both the structured and linear RNA. The transmission of the Linear-70 RNA in the presence of 100 mM NaCl and 2 M urea was more than three times greater than that in Tris alone. Urea also caused a small increase in transmission of the Hairpin-70 RNA, even though the reduction in intramolecular interactions between bases would be expected to cause an increase in RNA size in the presence of urea. These results provide new insights into the ultrafiltration behavior of well-defined and structured RNA of interest in the development of RNA vaccines, gene editing technologies based on CRISP-Cas9, and other RNA-based therapeutics..

In Chapter 5 we presented ultrafiltration as a potentially attractive separation process for the purification of a functional ribonucleoprotein complex from free (unbound) RNA. Similar to the behavior presented in Chapter 4, RNA transmission increased upon addition of NaCl, providing an attractive opportunity for the separation of the aforementioned molecules. Data obtained with the purified guide RNA showed sieving coefficients greater than 0.85 for extended filtration through the Biomax 300 kDa membrane at a filtrate flux around 20 μm/s. Corresponding data for

both the pure Cas9 protein and for the RNP showed high retention (S_o < 0.1) under the same conditions.

Experiments performed with a mixture of the RNP with excess sgRNA showed excellent removal of the free RNA (as determined by an agarose gel) with high recovery of the RNP (as determined by SDS PAGE). Limited quantitative data indicate that the diafiltration provided more than 70% removal of the sgRNA after only 1.5 diavolumes; this could be increased to more than 90% sgRNA removal using a 3 diavolume process. RNP yield was greater than 90%, clearly demonstrating the potential of using ultrafiltration as an attractive option for the purification of Cas ribonucleoprotein complexes.

The high degree of membrane fouling seen in some experiments with the Cas9 protein alone was surprising. This fouling was directly linked to the formation of large protein aggregates, which were easily seen in light scattering analysis after exposing the Cas9 to shear. This fouling could be eliminated by performing the ultrafiltration in an unstirred system. There was also no evidence of any fouling when using the RNP, suggesting that attachment of the guide RNA may provide some stabilization of the Cas9 protein. Note that previous studies have shown that coupling of guide RNA into the Cas9 protein causes structural changes in the RNP complex that protects it from proteolysis. Additional experiments will be required to fully identify the conditions associated with Cas9 aggregation, both for isolated Cas9 and for the RNP complex, including the effects of pumping and shear in the type of tangential flow filtration (TFF) systems used for large scale bioprocessing (either TFF cassettes or hollow fiber modules).

The results presented in Chapter 6 provide the first data for the effects of spermine and spermidine on the transmission of the supercoiled, linear, and open-circular plasmid isoforms through ultrafiltration membranes. Adding low concentrations of spermine (<10 μM) had minimal effect on plasmid transmission. However, higher spermine concentrations caused a dramatic reduction in DNA transmission, which is likely associated with the condensation of the DNA into

a structure that can no longer be elongated by the flow field into the membrane pores. DNA condensation appeared to happen at a threshold spermine concentration, above which the plasmids became almost completely retained by the membrane. Much higher concentrations of the trivalent spermidine were required to induce similar compaction effects.

Transmission data for different size plasmids over a wide range of DNA and spermine concentrations collapse to a single curve when plotted as a function of the molar concentration ratio, consistent with the assumption that the change in transmission is due to polyamine binding. The addition of spermine led to a very large increase in selectivity for the separation of DNA from a model protein, which could potentially facilitate the purification of a plasmid DNA product or the removal of residual DNA from a recombinant protein. However, spermine had relatively little effect on the selectivity between the supercoiled and open-circular isoforms at low concentrations and caused a large reduction in selectivity at high concentrations.

The data presented in Chapter 7 provide the first demonstration that it is possible to at least partially recover previously trapped DNA from within the macropores of a hollow fiber membrane when used in the reverse flow orientation (selective skin oriented away from the feed). This is a critical result if these hollow fiber membranes are to be used for purification of the desired supercoiled isoform from a feed stream containing a mixture of the linear and supercoiled DNA. This could be accomplished using a two-phase diafiltration process. In the first phase, the feed would be circulated through the hollow fiber module at low filtrate flux, allowing the linear isoform to be gradually washed through the membrane while retaining the supercoiled isoform in a diafiltration process. At this point, the filtrate flux would be increased so that the supercoiled plasmid that had previously been “trapped” within the microporous support could be recovered in the permeate. Additional studies would clearly be needed to quantify the effectiveness of this two-phase diafiltration process for purification of supercoiled plasmids.

Overall, the results from this dissertation provide new insights into the potential opportunities for using membrane ultrafiltration in the preparation of high quality / high purity nucleic acids for therapeutic applications. In addition, these results provide an initial framework for the development and design of large-scale processes for purification of both RNA and DNA therapeutics.

8.2 Future work

Although the experimental studies presented in this thesis provide significant insights into the ultrafiltration behavior of RNA / DNA, there are a number of areas that would benefit from additional study. In particular, the high degree of RNA fouling of the cellulosic membranes was unexpected; these hydrophilic membranes tend to show very low degrees of fouling when used in protein ultrafiltration. Additional experimental studies performed over a range of solution conditions using RNA with well-defined structural motifs would provide important fundamental information on the factors controlling RNA fouling during ultrafiltration.

The large changes in RNA transmission in the presence of NaCl and urea were not surprising given the know effects of salt and denaturing agents on the structure of RNA. However, the increase in transmission of the hairpin RNA upon addition of urea / NaCl is surprising given that these agents would be expected to reduce the intramolecular interactions and thus increase the effective size of the hairpin RNA. Additional studies will be needed to more fully explore the origin of these changes in transmission and their connection to the underlying structure and intramolecular interactions that determine the effective size and structure of the RNA.

One of the significant bottlenecks in the application of nucleic acids as therapeutics is the efficient delivery of these molecules to specific cells within the body. Different approaches have been used to overcome this obstacle, including encapsulation of the nucleic acid cargo into

liposomes or nanoparticles. This would likely require the separation of the loaded nanoparticles from free RNA, similar to the separation between the ribonucleoprotein complex and free RNA that was examined in Chapter 5. It would be very interesting to examine the potential of using ultrafiltration membranes for the purification of these functional therapeutic vehicles.

The development of CRISPR-based gene editing technologies using Cas9 and Cas13 proteins for DNA and mRNA targeting, respectively, as well as the use of Cas12 proteins as a diagnostic tool in viral outbreaks has created a need to produce large volumes of these proteins. Improvement in upstream processes for the production of the Cas proteins will lead to increased titers that will likely cause new challenges in downstream processing. Membrane filtration could potentially play an increasingly important role in the purification of these biomolecules, but only if one can effectively address issues related to membrane fouling. We strongly recommend that future efforts be focused on the filtration behavior of these Cas proteins at high concentration, including the effects of shear and solution conditions on protein aggregation and fouling. In addition, experiments could be performed by spiking a small amount of fluorescently-labelled Cas protein into the feed solution so that it would be possible to identify the location and extent of fouling and adsorption and its dependence on the underlying properties and structure of the Cas proteins.

The data obtained with spermine clearly demonstrated that it was possible to dramatically reduce the transmission of plasmid DNA using only micromolar levels of this polyamine. It is necessary to perform additional experiments with mixtures of genomic DNA and small therapeutic proteins, both with and without spermine, to determine whether this approach can be used to enhance the removal of genomic DNA in the purification of recombinant protein products and to confirm that the high selectivity can be maintained over long processing times. Similar studies could be performed using mixtures of DNA and RNA to examine whether it would be possible to use spermine to increase the selectivity between these double-stranded and single-stranded nucleic acids. In this case, it would also be necessary to demonstrate that it is also possible to eliminate the

polyamine from the solution after the desired separation is conducted. Preliminary data suggested that sodium chloride can be used to reduce the binding of polyamines to DNA potentially disrupting the spermine-DNA complex so that the spermine can be removed by a second diafiltration process. This might well require the use of a smaller MWCO membrane to obtain sufficiently high yield of the nucleic acid in this type of membrane separation process.

References

Abudayyeh, Omar O., Jonathan S. Gootenberg, Patrick Essletzbichler, Shuo Han, Julia Joung, Joseph J. Belanto, Vanessa Verdine, et al. 2017. "RNA Targeting with CRISPR-Cas13." *Nature* 550 (7675): 280–84. https://doi.org/10.1038/nature24049.

Ahmad, A. L., N. F. Che Lah, S. Ismail, and B. S. Ooi. 2012. "Membrane Antifouling Methods and Alternatives: Ultrasound Approach." *Separation and Purification Reviews* 41(4): 318-346 https://doi.org/10.1080/15422119.2011.617804.

Alberts, Bruce, Alexander Johnson, Julian Lewis, Martin Raff, Keith Roberts, and Peter Walter. 2002. "Molecular Biology of the Cell." In *Molecular Biology of the Cell*, 4th editio. New York: Garland Science.

Anders, Carolin, and Martin Jinek. 2014. "In Vitro Enzymology of Cas9." In *Methods in Enzymology*, 546:1–20. Academic Press Inc. https://doi.org/10.1016/B978-0-12-801185-0.00001-5.

Andersson, Kent, and Rolf Hjorth. 1985. "Isolation of Bacterial Plasmids by Density Gradient Centrifugation in Cesium Trifluoroacetate (CsTFA) without the Use of Ethidium Bromide." *Plasmid* 13 (1): 78–80. https://doi.org/10.1016/0147-619X(85)90059-9.

Arraiano, Cecília M., José M. Andrade, Susana Domingues, Inês B. Guinote, Michal Malecki, Rute G. Matos, Ricardo N. Moreira, et al. 2010. "The Critical Role of RNA Processing and Degradation in the Control of Gene Expression." *FEMS Microbiology Reviews* 34(5): 883-923 https://doi.org/10.1111/j.1574-6976.2010.00242.x.

Ashley-Koch, A., Q. Yang, and R. S. Olney. 2000. "Sickle Hemoglobin (Hb S) Allele and Sickle Cell Disease: A HuGE Review." *American Journal of Epidemiology* 151 (9): 839–45. https://doi.org/10.1093/oxfordjournals.aje.a010288.

Bancroft, Daniel, Loren Dean Williams, Alexander Rich, and Martin Egli. 1994. "The Low-Temperature Crystal Structure of the Pure-Spermine Form of Z-DNA Reveals Binding of a Spermine Molecule in the Minor Groove." *Biochemistry* 33 (5): 1073–86. https://doi.org/10.1021/bi00171a005.

Bella, Ramona, Rafal Kaminski, Pietro Mancuso, Won Bin Young, Chen Chen, Rahsan Sariyer, Tracy Fischer, et al. 2018. "Removal of HIV DNA by CRISPR from Patient Blood Engrafts in Humanized Mice." *Molecular Therapy - Nucleic Acids* 12 (September): 275–82. https://doi.org/10.1016/j.omtn.2018.05.021.

Binabaji, Elaheh, Junfen Ma, Suma Rao, and Andrew L Zydney. 2016. "Ultrafiltration of Highly Concentrated Antibody Solutions: Experiments and Modeling for the Effects of Module and Buffer Conditions." *Biotechnology Progress* 32 (3): 692–701. https://doi.org/10.1002/btpr.2252.

Booth, Catherine, Baba Inusa, and Stephen K. Obaro. 2010. "Infection in Sickle Cell Disease: A Review." *International Journal of Infectious Diseases*. 14(1): e2-e12 https://doi.org/10.1016/j.ijid.2009.03.010.

Borujeni, Ehsan Espah. 2015. "Purification of Plasmid DNA Using Membrane-Based Processes." PhD Thesis. The Pennsylvania State University.

Borujeni, Ehsan Espah, Ying Li, and Andrew L. Zydney. 2015. "Application of Periodic Backpulsing to Reduce Membrane Fouling during Ultrafiltration of Plasmid DNA." *Journal of Membrane Science* 473 (January): 102–8. https://doi.org/10.1016/j.memsci.2014.08.059.

Borujeni, Ehsan Espah, and Andrew L. Zydney. 2014. "Membrane Fouling during Ultrafiltration of Plasmid DNA through Semipermeable Membranes." *Journal of Membrane Science* 450 (0): 189–96. https://doi.org/http://dx.doi.org/10.1016/j.memsci.2013.08.032.

Borujeni, Ehsan Espah, and Andrew L Zydney. 2012. "Separation of Plasmid DNA Isoforms Using Centrifugal Ultrafiltration." *BioTechniques* 53 (1): 49–56.

Burns, Douglas B., and Andrew L. Zydney. 2000. “Buffer Effects on the Zeta Potential of Ultrafiltration Membranes.” *Journal of Membrane Science* 172 (1–2): 39–48. https://doi.org/10.1016/S0376-7388(00)00315-X.

Carroll, T. 2001. “The Effect of Cake and Fibre Properties on Flux Declines in Hollow-Fibre Microfiltration Membranes.” *Journal of Membrane Science* 189 (2): 167–78. https://doi.org/http://dx.doi.org/10.1016/S0376-7388(01)00412-4.

Castano, Juan;, Claire; Scanlan, Mark; Wagner, Jeffrey; Shumway, and Ruta Waghmare. 2014. “Downstream Purification and Formulation of Fab Antibody Fragments.” *BioPharm International* 27 (1): 3–5. http://www.biopharminternational.com/biopharm/Formulation/Challenges-and-Strategies-for-the-Downstream-Purif/ArticleStandard/Article/detail/832391.

Chattoraj, Dhruba K., Leonard C. Gosule, and John A. Schellman. 1978. “DNA Condensation with Polyamines: II. Electron Microscopic Studies.” *Journal of Molecular Biology* 121 (3): 327–37. https://doi.org/10.1016/0022-2836(78)90367-4.

Chen, Janice S., Enbo Ma, Lucas B. Harrington, Maria Da Costa, Xinran Tian, Joel M. Palefsky, and Jennifer A. Doudna. 2018. “CRISPR-Cas12a Target Binding Unleashes Indiscriminate Single-Stranded DNase Activity.” *Science* 360 (6387): 436–39. https://doi.org/10.1126/science.aar6245.

Childs-Disney, Jessica L., and Matthew D. Disney. 2015. “Small Molecule Targeting of a MicroRNA Associated with Hepatocellular Carcinoma.” *ACS Chemical Biology* 11 (2): 375-380 https://doi.org/10.1021/acschembio.5b00615

Chomczynski, Piotr, and Nicoletta Sacchi. 1987. “Single-Step Method of RNA Isolation by Acid Guanidinium Thiocyanate-Phenol-Chloroform Extraction.” *Analytical Biochemistry*. 162 (1): 156-159 https://doi.org/10.1016/0003-2697(87)90021-2.

Chomczynski, Piotr, and Nicoletta Sacchi. 2006. “The Single-Step Method of RNA Isolation by

Acid Guanidinium Thiocyanate-Phenol-Chloroform Extraction: Twenty-Something Years On." *Nature Protocols*.1: 581-585 https://doi.org/10.1038/nprot.2006.83.

Cox, David B.T., Jonathan S. Gootenberg, Omar O. Abudayyeh, Brian Franklin, Max J. Kellner, Julia Joung, and Feng Zhang. 2017. "RNA Editing with CRISPR-Cas13." *Science* 358 (6366): 1019–27. https://doi.org/10.1126/science.aaq0180.

Easton, Laura E., Yoko Shibata, and Peter J. Lukavsky. 2010. "Rapid, Nondenaturing RNA Purification Using Weak Anion-Exchange Fast Performance Liquid Chromatography." *RNA* 16 (3): 647–53. https://doi.org/10.1261/rna.1862210.

Eddy, Sean R. 2004. "How Do RNA Folding Algorithms Work?" *Nature Biotechnology*.22: 1457-1458. https://doi.org/10.1038/nbt1104-1457.

Emami, Parinaz, Seyed Pouria Motevalian, Erin Pepin, and Andrew L. Zydney. 2019. "Purification of a Conjugated Polysaccharide Vaccine Using Tangential Flow Diafiltration." *Biotechnology and Bioengineering* 116 (3): 591–97. https://doi.org/10.1002/bit.26867.

Emery, Alan E.H. 2002. "The Muscular Dystrophies." In *Lancet*, 359:687–95. Elsevier Limited. https://doi.org/10.1016/S0140-6736(02)07815-7.

Enright, A J, B John, U Gaul, T Tuschl, C Sander, and D S Marks. 2003. "MicroRNA Targets in Drosophila." *Genome Biology*. 5 R1 https://doi.org/10.1186/gb-2003-5-1-r1

Eon-Duval, Alex, Robert H MacDuff, Carol A Fisher, Mark J Harris, and Chris Brook. 2003. "Removal of RNA Impurities by Tangential Flow Filtration in an RNase-Free Plasmid DNA Purification Process." *Analytical Biochemistry* 316 (1): 66–73. https://doi.org/10.1016/S0003-2697(03)00050-2.

Ernst, Orna, and Tsaffrir Zor. 2010. "Linearization of the Bradford Protein Assay." *Journal of Visualized Experiments : JoVE*, no. 38 (April): 1918. https://doi.org/10.3791/1918.

Ferraro, Bernadette, Matthew P Morrow, Natalie A Hutnick, Thomas H Shin, Colleen E Lucke, and David B Weiner. 2011a. "Clinical Applications of DNA Vaccines: Current Progress."

Clinical Infectious Diseases 53 (3): 296–302. https://doi.org/10.1093/cid/cir334.

Ferraro, Bernadette, Matthew P Morrow, Natalie A Hutnick, Thomas H Shin, Colleen E Lucke, and David B Weine. 2011b. "Clinical Applications of DNA Vaccines: Current Progress." *Clinical Infectious Diseases : An Official Publication of the Infectious Diseases Society of America* 53 (3): 296–302. https://doi.org/10.1093/cid/cir334.

Fire, Andrew, SiQun Xu, Mary K. Montgomery, Steven A. Kostas, Samuel E. Driver, and Craig C. Mello. 1998. "Potent and Specific Genetic Interference by Double-Stranded RNA in Caenorhabditis Elegans." *Nature* 391 (6669): 806–11. https://doi.org/10.1038/35888.

Furukawa, Kazuhiro, Arati Ramesh, Zhiyuan Zhou, Zasha Weinberg, Tenaya Vallery, Wade C. Winkler, and Ronald R. Breaker. 2015. "Bacterial Riboswitches Cooperatively Bind Ni2+ or Co2+ Ions and Control Expression of Heavy Metal Transporters." *Molecular Cell* 57 (6): 1088–98. https://doi.org/10.1016/J.MOLCEL.2015.02.009.

Gao, Yinghong, Jie Qin, Zhiwei Wang, and Stein W. Østerhus. 2019. "Backpulsing Technology Applied in MF and UF Processes for Membrane Fouling Mitigation: A Review." *Journal of Membrane Science*. 587 (1): 117136 https://doi.org/10.1016/j.memsci.2019.05.060.

Gavrilov, Kseniya, and W Mark Saltzman. 2012. "Therapeutic SiRNA: Principles, Challenges, and Strategies." *The Yale Journal of Biology and Medicine* 85 (2): 187–200. http://www.pubmedcentral.nih.gov/articlerender.fcgi?artid=PMC3375670.

Geall, Andrew J., Christian W. Mandl, and Jeffrey B. Ulmer. 2013. "RNA: The New Revolution in Nucleic Acid Vaccines." *Seminars in Immunology*. 25 (2): 152-159 https://doi.org/10.1016/j.smim.2013.05.001.

Ginn, Samantha L., Ian E. Alexander, Michael L. Edelstein, Mohammad R. Abedi, and Jo Wixon. 2013. "Gene Therapy Clinical Trials Worldwide to 2012 - an Update." *The Journal of Gene Medicine* 15 (2): 65–77. https://doi.org/10.1002/jgm.2698.

Glass, J, and G W Wertz. 1980. "Different Base per Unit Length Ratios Exist in Single-Stranded

RNA and Single-Stranded DNA." *Nucleic Acids Research* 8 (23): 5739–51. http://www.ncbi.nlm.nih.gov/pubmed/6162153.

Gokcezade, Joseph, Grzegorz Sienski, and Peter Duchek. 2014. "Efficient CRISPR/Cas9 Plasmids for Rapid and Versatile Genome Editing in Drosophila." *G3: Genes, Genomes, Genetics* 4 (11): 2279–82. https://doi.org/10.1534/g3.114.014126.

Gootenberg, Jonathan S., Omar O. Abudayyeh, Jeong Wook Lee, Patrick Essletzbichler, Aaron J. Dy, Julia Joung, Vanessa Verdine, et al. 2017. "Nucleic Acid Detection with CRISPR-Cas13a/C2c2." *Science* 356 (6336): 438–42. https://doi.org/10.1126/science.aam9321.

Gopinath, S C B. 2007. "Antiviral Aptamers." *Archives of Virology* 152 (12): 2137–57. https://doi.org/10.1007/s00705-007-1014-1.

Gosule, Leonard C, and John A Schellman. 1976. "Compact Form of DNA Induced by Spermidine." *Nature* 259 (5541): 333–35. https://doi.org/10.1038/259333a0.

Grohmann, Katja, Markus Schuelke, Alexander Diers, Katrin Hoffmann, Barbara Lucke, Coleen Adams, Enrico Bertini, et al. 2001. "Mutations in the Gene Encoding Immunoglobulin μ-Binding Protein 2 Cause Spinal Muscular Atrophy with Respiratory Distress Type 1." *Nature Genetics* 29 (1): 75–77. https://doi.org/10.1038/ng703.

Ha, H C, N S Sirisoma, P Kuppusamy, J L Zweier, P M Woster, and R A Casero. 1998. "The Natural Polyamine Spermine Functions Directly as a Free Radical Scavenger." *Proceedings of the National Academy of Sciences of the United States of America* 95 (19): 11140–45. https://doi.org/10.1073/PNAS.95.19.11140.

Hadidi, Mahsa, John J. Buckley, and Andrew L. Zydney. 2015. "Ultrafiltration Behavior of Bacterial Polysaccharides Used in Vaccines." *Journal of Membrane Science* 490: 294–300. https://doi.org/10.1016/j.memsci.2015.04.047.

Hadidi, Mahsa, and Andrew L. Zydney. 2014. "Fouling Behavior of Zwitterionic Membranes: Impact of Electrostatic and Hydrophobic Interactions." *Journal of Membrane Science* 452

(February): 97–103. https://doi.org/10.1016/j.memsci.2013.09.062.

Hajdin, Christine E, Feng Ding, Nikolay V Dokholyan, and Kevin M Weeks. 2010. “On the Significance of an RNA Tertiary Structure Prediction.” *RNA (New York, N.Y.)* 16 (7): 1340–49. https://doi.org/10.1261/rna.1837410.

Han, Ying, Shan Liu, Jenny Ho, Michael K. Danquah, and Gareth M. Forde. 2009. “Using DNA as a Drug-Bioprocessing and Delivery Strategies.” *Chemical Engineering Research and Design*. 87 (3): 343-348 https://doi.org/10.1016/j.cherd.2008.09.010.

Hegedüs, Éva, Endre Kókai, Alexander Kotlyar, Viktor Dombrádi, and Gábor Szabó. 2009. “Separation of 1-23-Kb Complementary DNA Strands by Urea-Agarose Gel Electrophoresis.” *Nucleic Acids Research* 37 (17): e112. https://doi.org/10.1093/nar/gkp539.

Hendrix, Donna K., Steven E. Brenner, and Stephen R. Holbrook. 2005. “RNA Structural Motifs: Building Blocks of a Modular Biomolecule.” *Quarterly Reviews of Biophysics*. 38 (3): 221-243 https://doi.org/10.1017/S0033583506004215.

Hoopes, Barbara C, and William R. Mcclure. 1981. “Studies on the Selectivity of DNA Precipitation by Spermine” 9 (20): 5493-5504. https://doi.org/10.1093/nar/9.20.5493.

Hoyer, Leon W. 1994. “Hemophilia A.” *New England Journal of Medicine* 330 (1): 38–47. https://doi.org/10.1056/NEJM199401063300108.

Huntzinger, Eric, and Elisa Izaurralde. 2011. “Gene Silencing by MicroRNAs: Contributions of Translational Repression and MRNA Decay.” *Nature Reviews Genetics* 12 (2): 99–110. https://doi.org/10.1038/nrg2936.

Jain, S., G. Zon, and M. Sundaralingam. 1989. “Base Only Binding of Spermine in the Deep Groove of the A-DNA Octamer d(GTGTACAC).” *Biochemistry* 28: 2360–64. https://doi.org/10.2210/PDB1DNS/PDB.

Japrung, Deanpen, Marsiyana Henricus, Qiuhong Li, Giovanni Maglia, and Hagan Bayley. 2010. “Urea Facilitates the Translocation of Single-Stranded DNA and RNA through the Alpha-

Hemolysin Nanopore." *Biophysical Journal* 98 (9): 1856–63. https://doi.org/10.1016/j.bpj.2009.12.4333.

Jiang, Fuguo, Kaihong Zhou, Linlin Ma, Saskia Gressel, and Jennifer A. Doudna. 2015. "A Cas9-Guide RNA Complex Preorganized for Target DNA Recognition." *Science* 348 (6242): 1477–81. https://doi.org/10.1126/science.aab1452.

Jinek, M., F. Jiang, D. W. Taylor, S. H. Sternberg, E. Kaya, E. Ma, C. Anders, et al. 2014. "Structures of Cas9 Endonucleases Reveal RNA-Mediated Conformational Activation." *Science* 343 (6176): 1247997–1247997. https://doi.org/10.1126/science.1247997.

Josephs, Eric A., D. Dewran Kocak, Christopher J. Fitzgibbon, Joshua McMenemy, Charles A. Gersbach, and Piotr E. Marszalek. 2015. "Structure and Specificity of the RNA-Guided Endonuclease Cas9 during DNA Interrogation, Target Binding and Cleavage." *Nucleic Acids Research* 43 (18): 8924–41. https://doi.org/10.1093/nar/gkv892.

Kelley, Brian. 2009. "Industrialization of MAb Production Technology: The Bioprocessing Industry at a Crossroads." *MAbs* 1 (5): 443–52. http://www.ncbi.nlm.nih.gov/pubmed/20065641.

Kennedy, E. M., A. V. R. Kornepati, M. Goldstein, H. P. Bogerd, B. C. Poling, A. W. Whisnant, M. B. Kastan, and B. R. Cullen. 2014. "Inactivation of the Human Papillomavirus E6 or E7 Gene in Cervical Carcinoma Cells by Using a Bacterial CRISPR/Cas RNA-Guided Endonuclease." *Journal of Virology* 88 (20): 11965–72. https://doi.org/10.1128/jvi.01879-14.

Kim, Sojung, Daesik Kim, Seung Woo Cho, Jungeun Kim, and Jin Soo Kim. 2014. "Highly Efficient RNA-Guided Genome Editing in Human Cells via Delivery of Purified Cas9 Ribonucleoproteins." *Genome Research* 24 (6): 1012–19. https://doi.org/10.1101/gr.171322.113.

Kitos, Paul A., and Harold Amos. 1973. "Adsorption of Polyadenylate and Other Polynucleotides to Unmodified Cellulose." *Biochemistry* 12 (25): 5086–91.

https://doi.org/10.1021/bi00749a010.

Kochkodan, Victor, and Nidal Hilal. 2015. “A Comprehensive Review on Surface Modified Polymer Membranes for Biofouling Mitigation.” *Desalination*. 356: 187-207. https://doi.org/10.1016/j.desal.2014.09.015.

Kole, Ryszard, Adrian R Krainer, and Sidney Altman. 2012. “RNA Therapeutics: Beyond RNA Interference and Antisense Oligonucleotides.” *Nature Reviews. Drug Discovery* 11 (2): 125–40. https://doi.org/10.1038/nrd3625.

Kong, Yi W, David Ferland-McCollough, Thomas J Jackson, Martin Bushell, B Zhang, X Pan, GP Cobb, et al. 2012. “MicroRNAs in Cancer Management.” *The Lancet. Oncology* 13 (6): e249-58. https://doi.org/10.1016/S1470-2045(12)70073-6.

Kusano, T., T. Berberich, C. Tateda, and Y. Takahashi. 2008. “Polyamines: Essential Factors for Growth and Survival.” *Planta* 228 (3): 367–81. https://doi.org/10.1007/s00425-008-0772-7.

Lam, Jenny K W, Michael Y T Chow, Yu Zhang, and Susan W S Leung. 2015. “SiRNA Versus MiRNA as Therapeutics for Gene Silencing.” *Molecular Therapy. Nucleic Acids* 4 (9): e252. https://doi.org/10.1038/mtna.2015.23.

Latulippe, David R. 2010. “Purification of Plasmid DNA Therapeutics: New Opportunities for Membrane Processes.” The Pennsylvania State University.

Latulippe, David R., Kimberly Ager, and Andrew L. Zydney. 2007. “Flux-Dependent Transmission of Supercoiled Plasmid DNA through Ultrafiltration Membranes.” *Journal of Membrane Science* 294 (1–2): 169–77. https://doi.org/10.1016/j.memsci.2007.02.033.

Latulippe, David R., and A.L. Zydney. 2009. “Elongational Flow Model for Transmission of Supercoiled Plasmid DNA during Membrane Ultrafiltration.” *Journal of Membrane Science* 329 (1–2): 201–8. https://doi.org/10.1016/j.memsci.2008.12.045.

Latulippe, David R., and Andrew L. Zydney. 2008. “Salt-Induced Changes in Plasmid DNA Transmission through Ultrafiltration Membranes.” *Biotechnology and Bioengineering* 99 (2):

390–98. https://doi.org/10.1002/bit.21575.

Latulippe, David R., and Andrew L. Zydney. 2010. “Radius of Gyration of Plasmid DNA Isoforms from Static Light Scattering.” *Biotechnology and Bioengineering* 107 (1): 134–42. https://doi.org/10.1002/bit.22787.

Latulippe, David R., and Andrew L. Zydney. 2011. “Separation of Plasmid DNA Isoforms by Highly Converging Flow through Small Membrane Pores.” *Journal of Colloid and Interface Science* 357 (2): 548–53. https://doi.org/10.1016/j.jcis.2011.02.029.

Ledgerwood, Julie E, Theodore C Pierson, Sarah A Hubka, Niraj Desai, Steve Rucker, Ingelise J Gordon, Mary E Enama, et al. 2011. “A West Nile Virus DNA Vaccine Utilizing a Modified Promoter Induces Neutralizing Antibody in Younger and Older Healthy Adults in a Phase I Clinical Trial.” *The Journal of Infectious Diseases* 203 (10): 1396–1404. https://doi.org/10.1093/infdis/jir054.

Li, Hongmei Lisa, Naoko Fujimoto, Noriko Sasakawa, Saya Shirai, Tokiko Ohkame, Tetsushi Sakuma, Michihiro Tanaka, et al. 2015. “Precise Correction of the Dystrophin Gene in Duchenne Muscular Dystrophy Patient Induced Pluripotent Stem Cells by TALEN and CRISPR-Cas9.” *Stem Cell Reports* 4 (1): 143–54. https://doi.org/10.1016/j.stemcr.2014.10.013.

Li, Jun, Xiangbing Meng, Yuan Zong, Kunling Chen, Huawei Zhang, Jinxing Liu, Jiayang Li, and Caixia Gao. 2016. “Gene Replacements and Insertions in Rice by Intron Targeting Using CRISPR-Cas9.” *Nature Plants* 2 (10): 1–6. https://doi.org/10.1038/nplants.2016.139.

Li, Ying. 2017. “Purification of Plasmid DNA Using Ultrafiltration Membranes.” The Pennsylvania State University.

Li, Ying, Ehsan Espah Borujeni, and Andrew L. Zydney. 2015. “Use of Preconditioning to Control Membrane Fouling and Enhance Performance during Ultrafiltration of Plasmid DNA.” *Journal of Membrane Science* 479 (April): 117–22.

https://doi.org/10.1016/j.memsci.2015.01.029.

Li, Ying, David Currie, and Andrew L. Zydney. 2016. “Enhanced Purification of Plasmid DNA Isoforms by Exploiting Ionic Strength Effects during Ultrafiltration.” *Biotechnology and Bioengineering* 113 (4): 783–89. https://doi.org/10.1002/bit.25836.

Lin, Zhang, Chen Wang, Xizeng Feng, Maozi Liu, Jianwei Li, and Chunli Bai. 1998. “The Observation of the Local Ordering Characteristics of Spermidine-Condensed DNA: Atomic Force Microscopy and Polarizing Microscopy Studies.” *Nucleic Acids Research* 26 (13): 3228–34. https://doi.org/10.1093/nar/26.13.3228.

Liu, M. A. 2003. “DNA Vaccines: A Review.” *Journal of Internal Medicine* 253 (4): 402–10. https://doi.org/10.1046/j.1365-2796.2003.01140.x.

Lopes, Alessandra, Gaëlle Vandermeulen, and Véronique Préat. 2019. “Cancer DNA Vaccines: Current Preclinical and Clinical Developments and Future Perspectives.” *Journal of Experimental and Clinical Cancer Research*. 38: e146. https://doi.org/10.1186/s13046-019-1154-7.

Lorenz, Ronny, Stephan H Bernhart, Christian zu Siederdissen, Hakim Tafer, Christoph Flamm, Peter F Stadler, and Ivo L Hofacker. 2011. “ViennaRNA Package 2.0.” *Algorithms for Molecular Biology* 6 (1): 26. https://doi.org/10.1186/1748-7188-6-26.

Lunn, Mitchell R., and Ching H. Wang. 2008. “Spinal Muscular Atrophy.” *The Lancet*.371 (9630): 2120-2133. https://doi.org/10.1016/S0140-6736(08)60921-6.

Lusher, J, C Abildgaard, S Arkin, P M Mannucci, R Zimmermann, L Schwartz, and D Hurst. 2004. “Human Recombinant DNA-Derived Antihemophilic Factor in the Treatment of Previously Untreated Patients with Hemophilia A: Final Report on a Hallmark Clinical Investigation.” *Journal of Thrombosis and Haemostasis : JTH* 2 (4): 574–83. https://doi.org/10.1111/j.1538-7933.2004.00646.x.

Ma, C., and Victor A. Bloomfield. 1994. “Condensation of Supercoiled DNA Induced by MnCl2.”

Biophysical Journal 67 (4): 1678–81. https://doi.org/10.1016/S0006-3495(94)80641-1.

Ma, Huimin, Luis F Hakim, Christopher N Bowman, and Robert H Davis. 2001. "Factors Affecting Membrane Fouling Reduction by Surface Modification and Backpulsing." *Journal of Membrane Science* 189 (2): 255–70. https://doi.org/http://dx.doi.org/10.1016/S0376-7388(01)00422-7.

Mack, George S. 2007. "MicroRNA Gets down to Business." *Nature Biotechnology* 25 (6): 631–38. https://doi.org/10.1038/nbt0607-631.

Manning, G S. 1978. "The Molecular Theory of Polyelectrolyte Solutions with Applications to the Electrostatic Properties of Polynucleotides." *Quarterly Reviews of Biophysics* 11 (2): 179–246. https://doi.org/10.1017/S0033583500002031.

Manzano, Ivan, Patricia Guerrero-German, Rosa Maria Montesinos-Cisneros, and Armando Tejeda-Mansir. 2015. "Plasmid DNA Pre-Purification by Tangential Flow Filtration." *Biotechnology & Biotechnological Equipment*, February, 1–6. https://doi.org/10.1080/13102818.2015.1014421.

Manzano, Ivan, and Andrew L. Zydney. 2017. "Quantitative Study of RNA Transmission through Ultrafiltration Membranes." *Journal of Membrane Science* 544 (September): 272–77. https://doi.org/10.1016/j.memsci.2017.09.042.

Martins, Rita, Cláudio J. Maia, João António Queiroz, and Fani Sousa. 2012. "A New Strategy for RNA Isolation from Eukaryotic Cells Using Arginine Affinity Chromatography." *Journal of Separation Science* 35 (22): 3217–26. https://doi.org/10.1002/jssc.201200338.

Martins, Rita, João António Queiroz, and F. Sousa. 2010. "A New Affinity Approach to Isolate Escherichia Coli 6S RNA with Histidine-Chromatography." *Journal of Molecular Recognition* 23 (6): 519–24. https://doi.org/10.1002/jmr.1078.

Martins, Rita, João António Queiroz, and Fani Sousa. 2012. "Histidine Affinity Chromatography-Based Methodology for the Simultaneous Isolation of Escherichia Coli Small and Ribosomal

RNA." *Biomedical Chromatography* 26 (7): 781–88. https://doi.org/10.1002/bmc.1729.

Mastrianni, James A. 2010. "The Genetics of Prion Diseases." *Genetics in Medicine*. 12: 187-195. https://doi.org/10.1097/GIM.0b013e3181cd7374.

Matulis, Daumantas, Ioulia Rouzina, and Victor A. Bloomfield. 2000. "Thermodynamics of DNA Binding and Condensation: Isothermal Titration Calorimetry and Electrostatic Mechanism." *Journal of Molecular Biology* 296 (4): 1053–63. https://doi.org/10.1006/JMBI.1999.3470.

Mercuri, Eugenio, Richard S. Finkel, Francesco Muntoni, Brunhilde Wirth, Jacqueline Montes, Marion Main, Elena Mazzone, et al. 2018. "Diagnosis and Management of Spinal Muscular Atrophy: Part 1: Recommendations for Diagnosis, Rehabilitation, Orthopedic and Nutritional Care." *Neuromuscular Disorders* 28 (2): 103–15. https://doi.org/10.1016/j.nmd.2017.11.005.

Merten, O. W. 2002. "Virus Contaminations of Cell Cultures - A Biotechnological View." In *Cytotechnology*, 39:91–116. Springer. https://doi.org/10.1023/A:1022969101804.

Miner, Jacob C., and Angel E. García. 2017. "Equilibrium Denaturation and Preferential Interactions of an RNA Tetraloop with Urea". *The Journal of Physical Chemistry*. 121 (15): 3734–46. https://doi.org/10.1021/acs.jpcb.6b10767.

Molek, J.R., and A.L. Zydney. 2007. "Separation of PEGylated α-Lactalbumin from Unreacted Precursors and Byproducts Using Ultrafiltration." *Biotechnology Progress* 23 (6): 1417–24. https://doi.org/10.1021/bp070243w.

Mout, Rubul, Moumita Ray, Yi-Wei Wei Lee, Federica Scaletti, and Vincent M. Rotello. 2017. *In Vivo Delivery of CRISPR/Cas9 for Therapeutic Gene Editing: Progress and Challenges*. *Bioconjugate Chemistry*. 28(4): 880-884. https://doi.org/10.1021/acs.bioconjchem.7b00057.

Muralidhara, Bilikallahalli K., Rinku Baid, Steve M. Bishop, Min Huang, Wei Wang, and Sandeep Nema. 2016. "Critical Considerations for Developing Nucleic Acid Macromolecule Based Drug Products." *Drug Discovery Today* 21 (3): 430–44. https://doi.org/10.1016/j.drudis.2015.11.012.

Murphy, Jason C, George E Fox, and Richard C Willson. 2003. “Enhancement of Anion-Exchange Chromatography of DNA Using Compaction Agents.” *Journal of Chromatography. A* 984 (2): 215–21. https://doi.org/10.1016/S0021-9673(02)01814-9.

Nobbmann, Ulf, Malcolm Connah, Brendan Fish, Paul Varley, Chris Gee, Sandrine Mulot, Juntao Chen, et al. 2007. “Dynamic Light Scattering as a Relative Tool for Assessing the Molecular Integrity and Stability of Monoclonal Antibodies.” *Biotechnology and Genetic Engineering Reviews* 24 (1): 117–28. https://doi.org/10.1080/02648725.2007.10648095.

Noll, Bernhard, Stephan Seiffert, Frank Hertel, Harald Debelak, Philipp Hadwiger, Hans-Peter Vornlocher, and Ingo Roehl. 2011. “Purification of Small Interfering RNA Using Nondenaturing Anion-Exchange Chromatography.” *Nucleic Acid Therapeutics* 21 (6): 383–93. https://doi.org/10.1089/nat.2011.0317.

Nunes, José C., António M. Morão, Catherine Nunes, Maria Teresa Pessoa de Amorim, Isabel C. Escobar, and João António Queiroz. 2012. “Plasmid DNA Recovery from Fermentation Broths by a Combined Process of Micro- and Ultrafiltration: Modeling and Application.” *Journal of Membrane Science* 415–416 (0): 24–35. https://doi.org/10.1016/j.memsci.2012.04.055.

Nunes, José C., Maria Teresa Pessoa de Amorim, Isabel C. Escobar, João António Queiroz, and António M. Morão. 2014. “Plasmid DNA/RNA Separation by Ultrafiltration: Modeling and Application Study.” *Journal of Membrane Science* 463 (August): 1–10. https://doi.org/10.1016/j.memsci.2014.03.036.

Opong, W. Senyo, and Andrew L. Zydney. 1991. “Diffusive and Convective Protein Transport through Asymmetric Membranes.” *AIChE Journal* 37 (10): 1497–1510. https://doi.org/10.1002/aic.690371007.

Ouameur, Amin Ahmed, and Heidar-Ali Tajmir-Riahi. 2004. “Structural Analysis of DNA Interactions with Biogenic Polyamines and Cobalt(III)Hexamine Studied by Fourier

Transform Infrared and Capillary Electrophoresis." *The Journal of Biological Chemistry* 279 (40): 42041–54. https://doi.org/10.1074/jbc.M406053200.

Park, Chul Yong, Duk Hyoung Kim, Jeong Sang Son, Jin Jea Sung, Jaehun Lee, Sangsu Bae, Jong Hoon Kim, Dong Wook Kim, and Jin Soo Kim. 2015. "Functional Correction of Large Factor VIII Gene Chromosomal Inversions in Hemophilia A Patient-Derived IPSCs Using CRISPR-Cas9." *Cell Stem Cell* 17 (2): 213–20. https://doi.org/10.1016/j.stem.2015.07.001.

Peng, H F, and V Jackson. 2000. "In Vitro Studies on the Maintenance of Transcription-Induced Stress by Histones and Polyamines." *The Journal of Biological Chemistry* 275 (1): 657–68. https://doi.org/10.1074/JBC.275.1.657.

Peng, Rongxue, Guigao Lin, and Jinming Li. 2016. "Potential Pitfalls of CRISPR/Cas9-Mediated Genome Editing." *FEBS Journal*. 283 (7): 1218-1231. https://doi.org/10.1111/febs.13586.

Priyakumar, U. Deva, Changbong Hyeon, D. Thirumalai, and Alexander D. MacKerell. 2009. "Urea Destabilizes RNA by Forming Stacking Interactions and Multiple Hydrogen Bonds with Nucleic Acid Bases." *Journal of the American Chemical Society* 131 (49): 17759–61. https://doi.org/10.1021/ja905795v.

Pujar, Narahari S., and Andrew L. Zydney. 1994. "Electrostatic and Electrokinetic Interactions during Protein Transport through Narrow Pore Membranes." *Industrial & Engineering Chemistry Research* 33 (10): 2473–82. https://doi.org/10.1021/ie00034a032.

Ramakrishna, Suresh, Abu Bonsrah Kwaku Dad, Jagadish Beloor, Ramu Gopalappa, Sang Kyung Lee, and Hyongbum Kim. 2014. "Gene Disruption by Cell-Penetrating Peptide-Mediated Delivery of Cas9 Protein and Guide RNA." *Genome Research* 24 (6): 1020–27. https://doi.org/10.1101/gr.171264.113.

Rees, David C., Thomas N. Williams, and Mark T. Gladwin. 2010. "Sickle-Cell Disease." In *The Lancet*, 376:2018–31. Elsevier. https://doi.org/10.1016/S0140-6736(10)61029-X.

Reis, Robert Van, and Skand Saksena. 1997. "Optimization Diagram for Membrane Separations."

Journal of Membrane Science 129 (1): 19–29. https://doi.org/10.1016/S0376-7388(96)00319-5.

Reis, Robert van, and Andrew Zydney. 2001. “Membrane Separations in Biotechnology.” *Current Opinion in Biotechnology* 12 (2): 208–11. https://doi.org/10.1016/S0958-1669(00)00201-9.

Rohani, Mahsa M., and Andrew L. Zydney. 2009. “Effect of Surface Charge Distribution on Protein Transport through Semipermeable Ultrafiltration Membranes.” *Journal of Membrane Science* 337 (1–2): 324–31. https://doi.org/10.1016/j.memsci.2009.04.007.

Saqib, J., and Isam H. Aljundi. 2016. “Membrane Fouling and Modification Using Surface Treatment and Layer-by-Layer Assembly of Polyelectrolytes: State-of-the-Art Review.” *Journal of Water Process Engineering*. 11: 68-87. https://doi.org/10.1016/j.jwpe.2016.03.009.

Sato, Yuko T., Tsutomu Hamada, Koji Kubo, Ayako Yamada, Tsunao Kishida, Osam Mazda, and Kenichi Yoshikawa. 2005. “Folding Transition into a Loosely Collapsed State in Plasmid DNA as Revealed by Single-Molecule Observation.” *FEBS Letters* 579 (14): 3095–99. https://doi.org/10.1016/j.febslet.2005.04.072.

Schutz, G., M. Beato, and P. Feigelson. 1972. “Isolation of Eukaryotic Messenger RNA on Cellulose and Its Translation in Vitro.” *Biochemical and Biophysical Research Communications* 49 (3): 680–89. https://doi.org/10.1016/0006-291X(72)90465-2.

Shanagar, Jamil. 2005. “Purification of a Synthetic Oligonucleotide by Anion Exchange Chromatography: Method Optimisation and Scale-Up.” *Journal of Biochemical and Biophysical Methods* 64 (3): 216–25. https://doi.org/10.1016/j.jbbm.2005.08.004.

Shao, Qing, Sachin Goyal, Laura Finzi, and David Dunlap. 2012. “Physiological Levels of Salt and Polyamines Favor Writhe and Limit Twist in DNA.” *Macromolecules* 45 (7): 3188–96. https://doi.org/10.1021/ma300211t.

Shimanovich, Ulyana, Vadim Volkov, Dror Eliaz, Adva Aizer, Shulamit Michaeli, and Aharon

Gedanken. 2011. “Stabilizing RNA by the Sonochemical Formation of RNA Nanospheres.” *Small* 7 (8): 1068–74. https://doi.org/10.1002/smll.201002238.

Shukla, Abhinav A., Brian Hubbard, Tim Tressel, Sam Guhan, and Duncan Low. 2007. “Downstream Processing of Monoclonal Antibodies—Application of Platform Approaches.” *Journal of Chromatography B* 848 (1): 28–39. https://doi.org/10.1016/j.jchromb.2006.09.026.

Sohocki, Melanie M., Isabelle Perrault, Bart P. Leroy, Annette M. Payne, Sharola Dharmaraj, Shomi S. Bhattacharya, Josseline Kaplan, et al. 2000. “Prevalence of AIPL1 Mutations in Inherited Retinal Degenerative Disease.” *Molecular Genetics and Metabolism* 70 (2): 142–50. https://doi.org/10.1006/mgme.2000.3001.

Srisawat, Chatchawan, and David R. Engelke. 2002. “RNA Affinity Tags for Purification of RNAs and Ribonucleoprotein Complexes.” *Methods* 26 (2): 156–61. https://doi.org/10.1016/S1046-2023(02)00018-X.

Stellwagen, Earle, and Nancy C. Stellwagen. 2002. “Determining the Electrophoretic Mobility and Translational Diffusion Coefficients of DNA Molecules in Free Solution.” *ELECTROPHORESIS* 23 (16): 2794–2803. https://doi.org/10.1002/1522-2683(200208)23:16<2794::AID-ELPS2794>3.0.CO;2-Y.

Stevens, Debra, Melanie K. Claborn, Brooke L. Gildon, Tiffany L. Kessler, and Cheri Walker. 2020. “Onasemnogene Abeparvovec-Xioi: Gene Therapy for Spinal Muscular Atrophy.” *Annals of Pharmacotherapy*, 00(0): 1-9. https://doi.org/10.1177/1060028020914274.

Straub, Volker, and Kevin P. Campbell. 1997. “Muscular Dystrophies and the Dystrophin-Glycoprotein Complex.” *Current Opinion in Neurology* 10 (2): 168–75. https://doi.org/10.1097/00019052-199704000-00016.

Summer, Heike, René Grämer, and Peter Dröge. 2009. “Denaturing Urea Polyacrylamide Gel Electrophoresis (Urea PAGE).” *Journal of Visualized Experiments : JoVE*, no. 32 (October):

1485. https://doi.org/10.3791/1485.

Tabor, Herbert. 1962. “The Protective Effect of Spermine and Other Polyamines Against Heat Denaturation of Deoxyribonucleic Acid.” *Biochemistry* 1 (3): 496–501. https://doi.org/10.1021/bi00909a021.

Tang, Choon Kit, and Geoffrey A. Pietersz. 2009. “Intracellular Detection and Immune Signaling Pathways of DNA Vaccines.” *Expert Review of Vaccines*. 8(9): 1161-1170. https://doi.org/10.1586/erv.09.79.

Tari, Leslie W, and Anthony S Secco. 1995. “Base-Pair Opening and Spermine Binding-B-DNA Features Displayed in the Crystal Structure of a Gal Operon Fragment: Implications for Protein-DNA Recognition.” *Nucleic Acids Research* 23 (11): 2065–73. https://doi.org/10.1093/nar/23.11.2065.

Thomas, T J, Uma B Gunnia, and Thresia Thomas. 1991. “Polyamine-Induced B-DNA to Z-DNA Conformational Transition of a Plasmid DNA with (dG-dC)n Insert*.” *The Journal of biological chemistry*. 266 (10): 6137–41.

Ulmer, Jeffrey B, and Andrew J Geall. 2016. “Recent Innovations in MRNA Vaccines.” *Current Opinion in Immunology* 41: 18–22. https://doi.org/10.1016/j.coi.2016.05.008.

Vijayanathan, Veena, Thresia Thomas, Akira Shirahata, and T. J. Thomas. 2001. “DNA Condensation by Polyamines: A Laser Light Scattering Study of Structural Effects†.” *Biochemistry*. 40 (45): 13644-13651. https://doi.org/10.1021/BI010993T.

Viovy, Jean-Louis. 2000. “Electrophoresis of DNA and Other Polyelectrolytes: Physical Mechanisms.” *Reviews of Modern Physics* 72 (3): 813–72. https://doi.org/10.1103/RevModPhys.72.813.

Voytas, Daniel F., and Caixia Gao. 2014. “Precision Genome Engineering and Agriculture: Opportunities and Regulatory Challenges.” *PLoS Biology* 12 (6): 1–6. https://doi.org/10.1371/journal.pbio.1001877.

Wang, Tian, Hongyan Zhang, and Hongliang Zhu. 2019. “CRISPR Technology Is Revolutionizing the Improvement of Tomato and Other Fruit Crops.” *Horticulture Research*. 6: e77. https://doi.org/10.1038/s41438-019-0159-x.

Werner, Arne. 2011. “Predicting Translational Diffusion of Evolutionary Conserved RNA Structures by the Nucleotide Number.” *Nucleic Acids Research* 39 (3): e17. https://doi.org/10.1093/nar/gkq808.

Wessels, Hans Hermann, Alejandro Méndez-Mancilla, Xinyi Guo, Mateusz Legut, Zharko Daniloski, and Neville E. Sanjana. 2020. “Massively Parallel Cas13 Screens Reveal Principles for Guide RNA Design.” *Nature Biotechnology*. https://doi.org/10.1038/s41587-020-0456-9.

Wilson, Robert Wilfred, and Victor A. Bloomfield. 1979. “Counterion-Induced Condensation of Deoxyribonucleic Acid. A Light-Scattering Study.” *Biochemistry* 18 (11): 2192–96. https://doi.org/10.1021/bi00578a009.

Wittrup, Anders, and Judy Lieberman. 2015. “Knocking down Disease: A Progress Report on SiRNA Therapeutics.” *Nature Reviews Genetics* 16 (9): 543–52. https://doi.org/10.1038/nrg3978.

Wolter, Olga, and Günter Mayer. 2017. “Aptamers as Valuable Molecular Tools in Neurosciences.” *The Journal of Neuroscience* 37 (10): 2517 LP – 2523. https://doi.org/10.1523/JNEUROSCI.1969-16.2017.

Xu, Christine L., Merry Z.C. Ruan, Vinit B. Mahajan, and Stephen H. Tsang. 2019. “Viral Delivery Systems for Crispr.” *Viruses*. 11(1): 28. https://doi.org/10.3390/v11010028.

Yalcinkaya, Fatma, Evren Boyraz, Jiri Maryska, and Klara Kucerova. 2020. “A Review on Membrane Technology and Chemical Surface Modification for the Oily Wastewater Treatment.” *Materials* 13 (2): 493. https://doi.org/10.3390/ma13020493.

Yan, Fancheng, William Wang, and Jiaqiang Zhang. 2019. “CRISPR-Cas12 and Cas13: The Lesser

Known Siblings of CRISPR-Cas9." *Cell Biology and Toxicology*. 35: 489-492. https://doi.org/10.1007/s10565-019-09489-1.

Yin, Chaoran, Ting Zhang, Xiying Qu, Yonggang Zhang, Raj Putatunda, Xiao Xiao, Fang Li, et al. 2017. "In Vivo Excision of HIV-1 Provirus by SaCas9 and Multiplex Single-Guide RNAs in Animal Models." *Molecular Therapy* 25 (5): 1168–86. https://doi.org/10.1016/j.ymthe.2017.03.012.

Yu, Xianjun, Yuqing Zhang, Changyi Chen, Qizhi Yao, and Min Li. 2010. *Targeted Drug Delivery in Pancreatic Cancer*. *Biochimica et Biophysica Acta - Reviews on Cancer*. 1805(1): 97-104. https://doi.org/10.1016/j.bbcan.2009.10.001.

Zeman, Leos J, and Michael Wales. 1981. "Polymer Solute Rejection by Ultrafiltration Membranes." In *Synthetic Membranes: Volume II*, 411–34. https://doi.org/10.1021/bk-1981-0154.ch023.

Zeman, Leos J, and Andrew L Zydney. 1996. *Microfiltration and Ultrafiltration: Principles and Applications*. New York: Marcel Dekker.

Zhang, Baohong, Xiaoping Pan, George P. Cobb, and Todd A. Anderson. 2007. "MicroRNAs as Oncogenes and Tumor Suppressors." *Developmental Biology* 302 (1): 1–12. https://doi.org/10.1016/j.ydbio.2006.08.028.

Zhang, Hong, Huang-Tsu Chen, and Vladimir Glisin. 2003. "Isolation of DNA-Free RNA, DNA, and Proteins by Cesium Trifluoroacetate Centrifugation." *Biochemical and Biophysical Research Communications* 312 (1): 131–37. https://doi.org/10.1016/j.bbrc.2003.09.246.

Zor, Tsaffrir, and Zvi Selinger. 1996. "Linearization of the Bradford Protein Assay Increases Its Sensitivity: Theoretical and Experimental Studies." *Analytical Biochemistry* 236 (2): 302–8. https://doi.org/10.1006/abio.1996.0171.

Zydney, Andrew L. 1997. "Stagnant Film Model for Concentration Polarization in Membrane Systems." *Journal of Membrane Science* 130 (1–2): 275–81. https://doi.org/10.1016/S0376-

7388(97)00006-9.

Appendix A

RNA synthesis and purification

The *in vitro* synthesis of RNA is described in detail below, including DNA amplification using Phusion® DNA Polymerase (NEB #M0530) or a Q5® High fidelity DNA polymerase (NEB #M0515).

Mix the following reagents in a 0.2 mL 8-strip PCR tube, keeping all reagents in a bench top freezer box until used; return the reagents to freezer immediately after use.

Reagent mix for Phusion DNA polymerase

Reagent	Amount
Ultrapure DEPC treated water	To prepare 50 µL aliquot. $(50 - V_{\text{all reagents}})$
5 X Phusion Buffer	10 µL
10 µM ddNTPs	1 µL
100 µM F-Primer	0.25 µL
100 µM R-Primer	0.25 µL
Template DNA (gBlock)	5 ng ($V = 5\text{ ng} / C_{\text{template}}$)
Phusion DNA Polymerase (Add last, since Temp sensitive)	0.5 µL
Total Volume	50 µL

Reagent mix for Q5 High-Fidelity

Reagent	Amount
Ultrapure DEPC treated water	To prepare 50 µL aliquot. $(50 - V_{\text{all reagents}})$
Q5 High-Fidelity 2X Master Mix	25 µL
100 µM F-Primer	0.25 µL
100 µM R-Primer	0.25 µL
Template DNA (gBlock)	5 ng ($V = 5\text{ ng} / C_{\text{template}}$)
Total Volume	50 µL

Immediately after mixing, load samples into a preheated thermocycler at 98 °C. Run the following reaction cycle:

	Step	**Temperature**	**Time (Q5)**
30 cycles	Initial Denature	98 °C	15 s (30 s)
	Denature	98 °C	10 s
	Anneal	62.1 °C	30 s
	Extension	72 °C	30 s per kb
	Final Extension	72 °C	5 min (2 min)
	Hold	4 °C	∞

The amplified DNA is purified using Monarch® DNA Gel Extraction Kit (NEB #T1020). A pre-stained 1% agarose gel, with a final concentration of 0.2X of Gelstar® stain, is run at 100 V for 1 h. Visualize gel under UV light, and identify the band corresponding to the desired DNA

template. (Note that when dealing with new templates, it is useful to run the sample along with a MW marker).

Using an X-acto blade, cut the DNA band and load into a 5 mL tube. Add 4 volumes of Agarose Dissolving Buffer (e.g. 400 mL / 100 mg of agarose). Incubate in water bath at 55 °C until completely dissolved (~10 min). Next step is DNA purification using NEB's Monarch® DNA cleanup columns (Cat. #T1034)

Load solution into a spin column. Spin for 1 min and discard flow through. Add 300 µL of DNA wash buffer. Spin for 1 min, discard flow through. Repeat once. Using a new column, add 15 µL of ultrapure water. Incubate for 3 min, then spin for 1 min to elute the DNA.

T7 RNA polymerase in vitro reaction.

In an 8-strip PCR tube load the reagents shown in the Table below. All reagents should stay at 0 °C until use and then immediately returned to the cool box. Load the following reaction mix into a pre heated thermocycler and incubate overnight (a minimum of 4 h) at 37 °C.

Reagent mix using HiScribe™ T7 (NEB #E2040S) RNA Polymerase

Reagent	Amount
Ultrapure DEPC treated water	To prepare 30 µL aliquot. ($30 - V_{all\ reagents}$)
10 X Reaction Buffer	1.5 µL
100 µM UTP	1.5 µL
100 µM GTP	1.5 µL
100 µM ATP	1.5 µL
100 µM CTP	1.5 µL
10 mM DTT	0.3 µL
Template DNA	0.25 µL
100 µM R-Primer	110 ng ($V = 110\ ng / C_{template}$)
HiScribe™ T7 RNA Polymerase (Add last, since Temp sensitive)	1.5 µL
Total Volume	30 µL

Phenol:chloroform extraction and alcohol precipitation.

Prepare a master solution of 3 M sodium acetate at pH 5.2 in ultrapure DEPC treated water; 20 µL of the master solution are required per sample. If needed, prepare a 1:1 phenol:chloroform solution in a glass container and protect from light; 200 µL per sample are needed.

Transfer each RNA T7 reaction to a new 1.6 mL tube. Add 160 uL ultrapure DEPC treated water to each RNA T7 reaction. Add 20 µL of sodium acetate master solution, vortex and centrifuge for 10 s. Add 200 µL of phenol:chloroform mixture. Vortex 20 s and centrifuge for 1 min. Collect supernatant (Top layer). Transfer sample to a new tube.

Add 200 µL of chloroform. Vortex for 20 s and centrifuge for 1 min. Collect supernatant. Transfer sample to a new tube. Repeat and transfer to a new tube. Add 150 µL of cold 70% ethanol and incubate at -20 °C for 1 h (up to overnight). Centrifuge for 30 min at 4 °C and maximum speed using a refrigerated centrifuge. Carefully remove supernatant and keep pellet.

Wash pellet with 500 µL of cold 70% ethanol. Centrifuge for 5 min at 4 °C and maximum speed. Carefully remove supernatant. Incubate pellets for alcohol evaporation in open tubes at 37 °C until completely dry (~15 min). Tubes can be protected in aluminum foil previously sprayed with RNAse Away®. Resuspend RNA in 50 µL of ultrapure DEPC treated water or desired buffer.

Appendix B

Quant-it RiboGreen high range assay (0.02 – 1.0 µg/ml)

A volume of 100 uL of a working solution containing the RiboGreen dye is mixed with 100 uL of RNA samples. Concentration is determined from fluorescence intensity at Ex/Em 480/525. Concentrations are calculated from a calibration curve constructed with known samples. All samples should be assayed in duplicate.

Tip: Use an initial gain of 115 on the microplate reader. Adjust as needed

Working solution:

Use the following equation to determine the total volume needed of working solution (diluted dye):

V_{Dye} (uL) = 200*(N+S+1);

where N = Number of samples (total permeate, retentate, and feed) and S = Number of Standards (including blank).

The working solution is composed of a 20-fold dilution of 20X TE buffer and a 200-fold dilution of RiboGreen concentrated dye in DI water. This working solution can be now be added to our experimental and calibration samples.

For example, an experiment with 9 data points (9 bulk samples and 9 permeate samples) will require loading a total of 18 samples. A standard curve is typically made of 6 known concentrations including a blank. Thus, the total volume of working solution needed is:

V_{Dye} = 200*(18+6+1) = 5000 uL

TE 20X = 5000/20 = 250 uL

RiboGreen = 5000/200 = 25 uL

DI Water = 5000 – 250 – 25 = 4725 uL

Calibration curve and standards:

Prepare at least 300 µL of a 1 µg/mL RNA solution diluted in the same buffer as experimental samples. Tip: If the stock RNA has a concentration higher than 300 µg/mL, the sample should be diluted by mixing 1 µL with an appropriate volume of buffer.

Load the following volumes to a 96-wells microplate

RNA Standard	Tris Buffer	Concentration
µL	µL	µg/mL
0	100	0
2	98	0.020
6	94	0.060
20	80	0.200
35	65	0.350
50	50	0.500

	A	B	C	D	E	F	G	H
1	0/100							
2	0/100							
3	2/98							
4	2/98							
5	6/94							
6	6/94							
7	20/80							
8	20/80							
9	35/65							
10	35/65							
11	50/50							
12	50/50							

Appendix C

S. pyogenes Cas9 amino acid sequence

MDKKYSIGLD	IGTNSVGWAV	ITDEYKVPSK	KFKVLGNTDR	HSIKKNLIGA	50
LLFDSGETAE	ATRLKRTARR	RYTRRKNRIC	YLQEIFSNEM	AKVDDSFFHR	100
LEESFLVEED	KKHERHPIFG	NIVDEVAYHE	KYPTIYHLRK	KLVDSTDKAD	150
LRLIYLALAH	MIKFRGHFLI	EGDLNPDNSD	VDKLFIQLVQ	TYNQLFEENP	200
INASGVDAKA	ILSARLSKSR	RLENLIAQLP	GEKKNGLFGN	LIALSLGLTP	250
NFKSNFDLAE	DAKLQLSKDT	YDDDLDNLLA	QIGDQYADLF	LAAKNLSDAI	300
LLSDILRVNT	EITKAPLSAS	MIKRYDEHHQ	DLTLLKALVR	QQLPEKYKEI	350
FFDQSKNGYA	GYIDGGASQE	EFYKFIKPIL	EKMDGTEELL	VKLNREDLLR	400
KQRTFDNGSI	PHQIHLGELH	AILRRQEDFY	PFLKDNREK	IEKILTFRI	450
PYYVGPLARG	NSRFAWMTRK	SEETITPWNFE	EVVDKGASAQ	SFIERMTNF	500
DKNLPNEKVL	PKHSLLYEYF	TVYNELTKVK	YVTEGMRKPA	FLSGEQKKAI	550
VDLLFKTNRK	VTVKQLKEDY	FKKIECFDSV	EISGVEDRFN	ASLGTYHDLL	600
KIIKDKDFLD	NEENEDILEDI	VLTLTLFEDR	EMIEERLKTY	AHLFDDKVMK	650
QLKRRRYT	GWGRLSRKLI	NGIRDKQSGK	TILDFLKSDG	FANRNFMQLI	700
HDDSLTFKED	IQKAQVSGQG	DSLHEHIANL	AGSPAIKKGI	LQTVKVVDEL	750
VKVMGRHKPE	NIVIEMAREN	QTTQKGQKNS	RERMKRIEE	GIKELGSQIL	800
KEHPVENTQL	QNEKLYLYY	LQNGRDMYVD	QELDINRLSD	YDVDHIVPQS	850
FLKDDSIDNK	VLTRSDKNRG	KSDNVPSEEV	VKKMKNYWRQ	LLNAKLITQR	900
KFDNLTKAER	GGLSELDKAG	FIKRQLVETR	QITKHVAQIL	DSRMNTKYDE	950
NDKLIREVKV	ITLKSKLVSD	FRKDFQFYKV	REINNYHHAH	DAYLNAVVGT	1000
ALIKKYPKLE	SEFVYGDYKV	YDVRKMIAKS	EQEIGKATAK	YFFYSNIMNF	1050
FKTEITLANG	EIRKRPLIET	NGETGEIVWD	KGRDFATVRK	VLSMPQVNIV	1100
KKTEVQTGGF	SKESILPKRN	SDKLIARKKD	WDPKKYGGFD	SPTVAYSVLV	1150
VAKVEKGKSK	KLKSVKELLG	ITIMERSSFE	KNPIDFLEAK	GYKEVKKDLI	1200
IKLPKYSLFE	LENGRKRML	ASAGELQKGN	ELALPSKYVN	FLYLASHYEK	1250
LKGSPEDNEQ	KQLFVEQHKH	YLDEIIEQIS	EFSKRVILAD	ANLDKVLSAY	1300
NKHRDKPIRE	QAENIIHLFT	LTNLGAPAAF	KYFDTTIDRK	RYTSTKEVLD	1350
ATLIHQSITG	LYETRIDLSQ	LGGDGGSGPP	KKKRKVYPYD	VPDYA	1395

Appendix D

Akta Pure FPLC Nickel Affinity Chromatography method

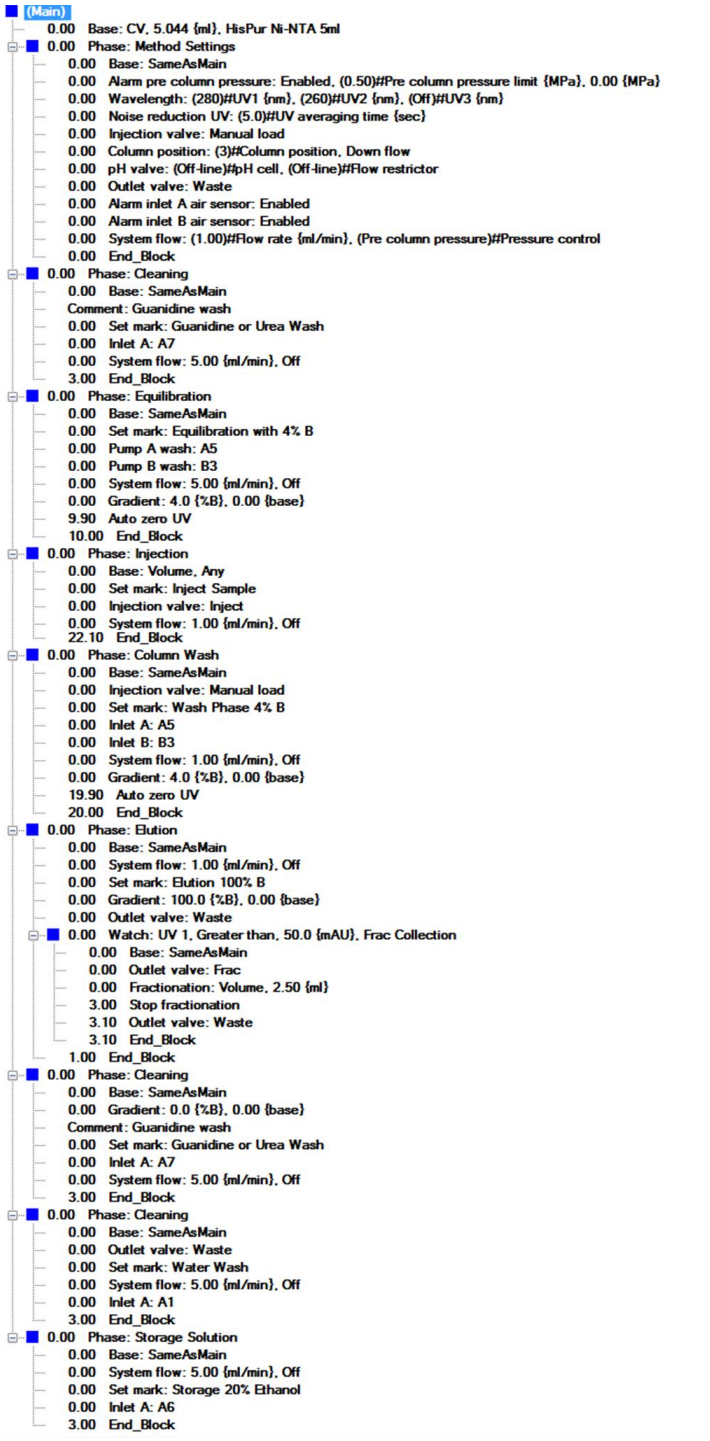

VITA

Jesus Ivan Manzano Garcia

Education

- Ph.D. Chemical Engineering, The Pennsylvania State University (June 2020)
- B.S. Chemical Engineering, University of Sonora (December 2012)

Employment

- Graduate research assistant, The Pennsylvania State University (August 2014 – present)
- Processing specialist (Technical Intern – Doctorate), Bristol-Myers Squibb (January – July 2019)
- Teaching Assistant (CHE 449: Bioseparations), The Pennsylvania State University (Spring 2018)
- Teaching Assistant (CHE 220: Thermodynamics), The Pennsylvania State University (Summers 2016 and 2018)
- Visiting Scholar, The Pennsylvania State University (October 2014 – March 2015)

Publications

- Ivan Manzano, et al., "RNA size and 3-dimensional structure determine ultrafiltration behavior of small RNA molecules", Separation and Purification Technology 237 (2020).
- Ying Li, Ivan Manzano, Andrew L. Zydney, "Effects of Polyamines on the Ultrafiltration of Plasmid DNA" Biotechnology Progress 35 (2019) 1-6.
- Ivan Manzano, Andrew L. Zydney, "Quantitative study of RNA transmission through ultrafiltration membranes" Journal of Membrane Science 544 (2017) 272-277.
- Ivan Manzano, et al., "Plasmid DNA pre-purification by tangential flow filtration" Biotechnology & Biotechnological Equipment, 29(3) (2015) 1-6.

Selected Graduate Presentations and Reunions

- "Ultrafiltration behavior of small RNA molecules: RNA size and ionic strength effect". Presentation in 257th ACS National Meeting, Orlando, FL, April 2019.
- "Ionic strength influence on RNA ultrafiltration behavior". Poster at Gordon Research Conference on Membranes: Materials and Processes, New Hampshire, August 2018
- "Use of polyamines for enhanced retention of plasmid DNA isoforms during ultrafiltration". Presentation at 254th ACS National Meeting, New Orleans, LA, March 2018.
- Selected participant in the 8th Workshop on Neutron Scattering Applications in Structural Biology. Oak Ridge National Laboratory, Tennessee, June 2017.
- "Ultrafiltration of Ribonucleic Acids". Presentation at AIChE Annual Meeting, San Francisco, CA, November 2016